



Pontifícia Universidade Católica do Rio Grande do Sul

FACULDADE DE ENGENHARIA

PROGRAMA DE PÓS-GRADUAÇÃO EM ENGENHARIA E TECNOLOGIA DE MATERIAIS

**OBTENÇÃO DE NANOCOMPÓSITOS MAGNÉTICOS DE  $Fe_3O_4$  -  
TALCO SINTÉTICO COM MATRIZES POLIURETÂNICAS BASE  
SOLVENTE E BASE ÁGUA**

Leonardo Moreira dos Santos

Químico Licenciado

Mestre em Engenharia e Tecnologia de Materiais

**TESE PARA A OBTENÇÃO DO TÍTULO DE DOUTOR EM ENGENHARIA E  
TECNOLOGIA DE MATERIAIS**

**Porto Alegre**

**Março, 2017**



Pontifícia Universidade Católica do Rio Grande do Sul

FACULDADE DE ENGENHARIA

PROGRAMA DE PÓS-GRADUAÇÃO EM ENGENHARIA E TECNOLOGIA DE MATERIAIS

# **OBTENÇÃO DE NANOCOMPÓSITOS MAGNÉTICOS DE $Fe_3O_4$ - TALCO SINTÉTICO COM MATRIZES POLIURETÂNICAS BASE SOLVENTE E BASE ÁGUA**

**Leonardo Moreira dos Santos**

Químico Licenciado

Mestre em Engenharia e Tecnologia de Materiais

ORIENTADOR: PROF(a). DR(a). Sandra Einloft

CO-ORIENTADOR: Prof(a). Dr(a). Rosane Ligabue

Tese realizada no Programa de Pós-Graduação em Engenharia e Tecnologia de Materiais (PGETEMA) da Pontifícia Universidade Católica do Rio Grande do Sul, como parte dos requisitos para a obtenção do título de Doutor em Engenharia e Tecnologia de Materiais.

**Porto Alegre  
Março, 2017**



**Pontifícia Universidade Católica do Rio Grande do Sul**  
 FACULDADE DE ENGENHARIA  
 PROGRAMA DE PÓS-GRADUAÇÃO EM ENGENHARIA E TECNOLOGIA DE MATERIAIS

## **OBTENÇÃO DE NANOCOMPÓSITOS MAGNÉTICOS DE FE<sub>3</sub>O<sub>4</sub> - TALCO SINTÉTICO COM MATRIZES POLIURETÂNICAS BASE SOLVENTE E BASE ÁGUA**

**CANDIDATO: LEONARDO MOREIRA DOS SANTOS**

Esta Tese de Doutorado foi julgada para obtenção do título de DOUTOR EM ENGENHARIA E TECNOLOGIA DE MATERIAIS e aprovada em sua forma final pelo Programa de Pós-Graduação em Engenharia e Tecnologia de Materiais da Pontifícia Universidade Católica do Rio Grande do Sul.

*Sandra Oliveira Einloft*

**DRA. SANDRA MARA OLIVEIRA EINLOFT - ORIENTADORA**

*Rosane Angélica Ligabue*

**DRA. ROSANE ANGÉLICA LIGABUE - CO-ORIENTADORA**

### **BANCA EXAMINADORA**

*Carlos Leonardo Pandolfo Carone*

**DR. CARLOS LEONARDO PANDOLFO CARONE - FEEVALE - UNIVERSIDADE FEEVALE**

*Katia Bernardo Gusmão*

**DRA. KATIA BERNARDO GUSMÃO - DO INSTITUTO DE QUÍMICA - UFRGS**

*Marcus Seferin*

**DR. MARCUS SEFERIN - DO PGETEMA/FENG - PUCRS**

“A tarefa não é tanto ver aquilo que ninguém viu, mas pensar o que ninguém ainda pensou sobre aquilo que todo mundo vê”.

Arthur Schopenhauer

## **DEDICATÓRIA**

A Deus e minha família.

## **AGRADECIMENTOS**

A todos que fizeram parte deste trabalho.

A professora Sandra Einloft, pela confiança, orientação e colaboração para o meu crescimento profissional.

A professor Rosane Ligabue pela co-orientação e apoio pela ajuda e incentivo nesta caminhada.

Aos meus amigos do Laboratório de Organometálicos e Resinas, por diversos momentos de felicidade. Em especial ao Wesley Formentin, Guilherme Dias, Franciele, Marisol Fernández, Marina Schwab, Evandro Pereira, Manoela Prado, Cristiane Valente, Marta, Juliana Holz, Fabiana Gonçalves, Daniela Maffi, Barbara Polesso, Patrícia, Brunas, Julius e Velma pela descontração e companhia em muitas paradas para saborear um café 12 molar.

Ao meus amigos e irmãos Vinícius Demétrio da Silva, Wagner Menezes, Wesley, Rafael Duczinski, Carmen Montoya pela amizade e ajuda nas horas boas e difíceis.

A professora Jeane Dullius por toda ajuda e apoio desde os trabalhos de iniciação científica.

Ao professor e amigo Vladimir Lavayen sempre disposto a ensinar e ajudar.

As secretárias da FAQUI (Luciana, Neiva e Nilza) e as do PGETEMA (Cláudia, Viviane e Anderson).

Ao pessoal do Almoxarifado (Betinho, Luciane, Paulo, Marcus e Fernando) sempre ajudando.

Ao vidreiro Nelson Goes, sempre socorrendo com materiais que precisamos para conseguir fazer um bom trabalho.

Ao pessoal da UNL/ FCT que me ajudaram de todas as formas, Carmen, Ana Diniz, Inês, Marta Corvo, Pedro Almeida, Micael, Thiago, Rita Craveiro, Ana Paninho, Filipe Oliveira, Marta Chaves.

Ao professor Eurico Cabrita, por me receber em seu laboratório.

A Capes (PDSE) pela bolsa sanduíche em Portugal (FCT/UNL) concedida.

## SUMÁRIO

<b>DEDICATÓRIA .....</b>	<b>5</b>
<b>AGRADECIMENTOS .....</b>	<b>6</b>
<b>SUMÁRIO .....</b>	<b>7</b>
<b>LISTA DE FIGURAS .....</b>	<b>8</b>
<b>LISTA DE SIGLAS E SÍMBOLOS .....</b>	<b>9</b>
<b>RESUMO .....</b>	<b>11</b>
<b>ABSTRACT .....</b>	<b>12</b>
<b>1. INTRODUÇÃO .....</b>	<b>13</b>
<b>2. OBJETIVOS .....</b>	<b>15</b>
<b>2.1. Objetivos Específicos .....</b>	<b>15</b>
<b>3. REVISÃO BIBLIOGRÁFICA.....</b>	<b>16</b>
<b>3.1. Poliuretanos.....</b>	<b>16</b>
<b>3.2. Silicatos Lamelares.....</b>	<b>20</b>
<b>3.3. Nanocompósitos poliméricos .....</b>	<b>23</b>
<b>3.3.1. Obtenção de nanocompósitos de Poliuretano com Diferentes Cargas</b>	<b>25</b>
<b>4. PROCEDIMENTOS EXPERIMENTAIS E RESULTADOS .....</b>	<b>32</b>
<b>4.1. Capítulo I: Poliuretano base solvente com Fe<sub>3</sub>O<sub>4</sub> talco sintético .....</b>	<b>33</b>
<b>4.2. Capítulo II: Poliuretano base água com Fe<sub>3</sub>O<sub>4</sub> talco sintético .....</b>	<b>46</b>
<b>5. CONCLUSÕES.....</b>	<b>68</b>
<b>6. REFERÊNCIAS BIBLIOGRÁFICAS .....</b>	<b>70</b>

## LISTA DE FIGURAS

Figura 3.1. Estrutura da cadeia do poliuretano Poliuretano. ....	16
Figura 3.2. Microdomínios existentes na cadeia do Poliuretano. ....	17
Figura 3.3. Representação da estrutura de um silicato lamelar 2:1 (Mittal <i>et al.</i> , 2009). ....	21
Figura 3.4. a) Talcos naturais e sintéticos têm a mesma estrutura cristalina. b) O talco é um recurso natural finito obtido sob a ação de fluidos hidrotermais durante vários milhões de anos e caracterizado por partículas de tamanho micrométrico. c) A síntese de fluxo hidrotérmico supercrítico é um novo processo para partículas de talco de tamanho nanométrico sintetizado com novas propriedades ( <sup>d</sup> Dumas <i>et al.</i> 2016). ....	22
Figura 3.5. I) Mistura simples dos componentes (por melt blending ou extrusão), II) Preparação de nanopartículas in situ (em solvente) e III) Polimerização da matriz in situ (modificado de Esteves <i>et al.</i> , 2004). ....	23
Figura 3.6. Representação esquemática dos diferentes graus de dispersão dos compósitos. (Adaptado de Paiva <i>et al.</i> , 2006). ....	24
Figura 3.7. Curvas de histerese para Fe <sub>3</sub> O <sub>4</sub> e OA-Fe <sub>3</sub> O <sub>4</sub> nanopartículas. ....	26
Figura 3.8. Cálculo de CSD dos nanocompósitos de Ni- talco sintético e talco natural (Prado <i>et al.</i> 2015). ....	27
Figura 3.9. <sup>29</sup> Si MAS NMR (a) PS/ Sílica híbrida e (b) PMMA/Sílica híbrida. ....	29
Figura 3.10. TGA NZFO e NZFO – IPTS nanopartículas (a), TGA curvas nanocompósitos de WPU/NZFO com diferentes quantidades de NZFO-IPTS (b), Curvas de módulo de armazenamentos (c) e curvas de fator de perda dos nanocompósitos de WPU/NZFO. ....	30
Figura 4.1. Esquema dos capítulos e síntese realizadas. ....	32



## LISTA DE SIGLAS E SÍMBOLOS

**PU:** Poliuretano

**PUBA:** Poliuretano Base Água

**WPU:** Waterborne polyuretane

**DBTDL:** dibutil dilaurato de estanho (IV)

**HDI:** 1,6 – hexametileno diisocianato

**DMPA:** 2,2-bis (hidroximetil) propiônico

**IPDI:** Isofornona diisocianato

**TEA:** trietilamina

**HDZ:** hidrazina

**FTIR:** Espectrôscopia de Infravermelho com Transformada de Fourier (do inglês, Fourier Transform Infrared Spectrometry)

**UATR:** Refletância atenuada total universal (do inglês, Universal Attenuated Total Reflectance)

**RMN:** Ressonância Magnética Nuclear

**MET:** Microscopia eletrônica de transmissão

**MEV:** Microscopia eletrônica de varredura

**AFM:** Microscopia de força atômica

**DSC:** Calorimetria Exploratória Diferencial (do inglês, Differential Scanning Calorimetry)

**TGA:** Análise termogravimétrica (do inglês, Thermogravimetric Analysis)

**DMPA:** Ácido dimetil propiônico

**DRX:** Difração de Raios- X

**GPC:** Cromatografia de Permeação em Gel (do inglês, and Gel Permeation Chromatography)

**M<sub>w</sub>:** Massa molar ponderal média

**M<sub>n</sub>:** Massa molar numérica média

**THF:** Tetrahidrofurano

**T<sub>g</sub>:** Temperatura transição vítrea

**T<sub>m</sub>:** Temperatura de fusão

**T<sub>c</sub>:** Temperatura de cristalização

**nm:** Nanômetro

**μm:** Micrômetro

**MMT:** Montmorilonita

**VSM:** Magnetômetro vibração de Amostra (do inglês *Vibrating sample Magnetometer*)

**emu/g:** Magnetização (do inglês magnetization)

**CSD:** Cambridge Structural Database

**SSMMP:** Partículas Minerais Silício – Metálicas

**rpm:** Rotação por minutos

**ΔH<sub>m</sub>:** Entalpia de fusão

**EDS:** Espectroscopia por Dispersão de Energia de Raios X

**mm:** milímetro

**<sup>29</sup> Si:** Silício

**2θ:** 2 Theta

**MPa:** Megapascal

**E':** Módulo de Armazenamento

**E'':** Módulo de Perda

## RESUMO

MOREIRA DOS SANTOS, Leonardo. **Obtenção de Nanocompósitos Magnéticos de Fe<sub>3</sub>O<sub>4</sub>-Talco Sintético Com Matrizes Poliuretânicas Base Solvente e Base Água.** Porto Alegre. 2016. Tese. Programa de Pós-Graduação em Engenharia e Tecnologia de Materiais, PONTIFÍCIA UNIVERSIDADE CATÓLICA DO RIO GRANDE DO SUL.

A obtenção de materiais com propriedades distintas e superiores quando comparados aos materiais existentes é um dos focos das pesquisas na área de materiais poliméricos. Os nanocompósitos vêm se destacando neste setor, pois utilizam a combinação de materiais que já tenham um bom desempenho visando obter novas características que possam ser utilizadas em diferentes nichos no mercado. Um polímero que tem uma ampla aplicação e é muito utilizado no meio industrial é o poliuretano. A inserção de cargas inorgânicas é uma alternativa muito usada para obter melhores propriedades destes materiais poliméricos. Desta forma, este trabalho tem como objetivo a incorporação de uma nova carga de Fe<sub>3</sub>O<sub>4</sub>-talco-sintético, em forma de pó e gel, em diferentes quantidades em relação a massa de poliuretano base solvente e base água. Nas amostras de nanocompósitos obtidos por mistura física com PU base solvente a carga ficou esfoliada/bem dispersa na matriz polimérica mesmo com altos teores de carga de 10% como mostrado pelas técnicas de DRX e MET. O comportamento magnético dos nanocompósitos foi confirmado por Mössbauer e medidas magnéticas, apresentando comportamento de ferromagnético em todas as temperaturas testadas. O uso do talco sintético para obter nanocompósitos magnéticos, produziu materiais com temperatura de cristalização e estabilidade térmica superior quando comparado com a matriz polimérica. O método se mostrou eficiente para evitar a atração dipolar da magnetita e, conseqüentemente a agregação da carga. Os nanocompósitos PUBA (poliuretano base água/Fe<sub>3</sub>O<sub>4</sub>-talco sintético) mostraram melhores propriedades no ensaio de tração quando comparados ao polímero puro. Por exemplo, o polímero puro apresentou um Módulo de Young de 29,3 MPa e passou para 70 MPa na amostra PUBA/ 40% Fe<sub>3</sub>O<sub>4</sub>-talco-sintético, mostrando que a adição de carga tende aumentar a resistência mecânica do material. As análises de DRX mostraram que há formação de uma estrutura intercalada entre a matriz polimérica e as nanopartículas. Análises de Ressonância Magnética Nuclear (RMN) mostraram que a carga interage com a matriz polimérica, corroborando os resultados de AFM. Mossbauer e curvas de magnetização, mostraram que as propriedades magnéticas variam com a temperatura, diferentemente ao observado nos nanocompósitos obtidos com PU base solvente.

Palavras-Chaves: talco sintético- Fe<sub>3</sub>O<sub>4</sub>, poliuretano, poliuretano base água.

## ABSTRACT

MOREIRA DOS SANTOS, Leonardo. **Syntheses of solvent and waterborne polyurethane based nanocomposites Fe<sub>3</sub>O<sub>4</sub> –synthetic talc.** Porto Alegre. 2016. PhD Thesis. Graduation Program in Materials Engineering and Technology, PONTIFICAL CATHOLIC UNIVERSITY OF RIO GRANDE DO SUL.

The obtaining of materials with different and superior properties when compared to existing materials is one of the main research focuses in polymeric materials field. Nanocomposites are important in this sector because they combine materials with good performance in order to obtain new features that can be used in different niches in the market. Polyurethane based materials finds a wide application and is widely used in industry. The insertion of an alternative inorganic filler is often used to obtain better properties of these polymeric materials. Thus, this work aims to incorporate different proportions of a new filler Fe<sub>3</sub>O<sub>4</sub>-synthetic talc, in powder and gel form, in solvent and waterborne polyurethane matrix. Nanocomposites PU solvent/ Fe<sub>3</sub>O<sub>4</sub>-synthetic talc obtained by physical mixture presented a good filler dispersion/exfoliation even at higher filler contents of 10% as corroborated by XRD and TEM techniques. Mössbauer and magnetic measurements confirmed the magnetic behavior of nanocomposites, being ferromagnetic in all tested temperatures. The use of synthetic talc to obtain magnetic nanocomposites produced materials with higher crystallization temperature and thermal stability compared with the polymeric matrix. This method is efficient to avoid attracting dipolar magnetite and therefore the charge aggregation. Nanocomposites WPU/ Fe<sub>3</sub>O<sub>4</sub>-synthetic talc presented better mechanical properties with higher filler contents compared to the pure polymer. The XRD analysis evidenced a formation of an intercalated structure between the polymer matrix and nanoparticles. Nuclear Magnetic Resonance (NMR) measurements evidenced the interaction filler/WPU corroborating the AFM analyses. Mössbauer and magnetization curves highlighted that the magnetic properties are temperature dependent unlike for nanocomposites obtained with solvent based PU.

Key-words: Fe<sub>3</sub>O<sub>4</sub>-synthetic talc; waterborne polyurethane, polyurethane, magnetic nanocomposites.

## 1. INTRODUÇÃO

Os poliuretanos (PU) são materiais que despertam grande interesse, tanto do ponto de vista acadêmico como no meio industrial, devido as inúmeras possibilidades de aplicações. Esses materiais podem ser utilizados na indústria, de revestimentos, adesivos, fibras, espumas, borrachas, elastômeros e compósitos (Zilg *et al.*, 1999). Suas propriedades mecânicas, térmicas e químicas podem ser modificadas pela reação entre diferentes tipos de polióis e diisocianatos. Nas últimas décadas vem tendo um crescente interesse no desenvolvimento de novas estruturas poliuretânicas aliadas a crescente preocupação em utilizar materiais menos agressivos ao meio ambiente. Na esteira da preocupação ambiental, as dispersões aquosas de PUs, a partir de polióis advindos de fontes renováveis, como óleos vegetais, vem ganhando espaço tanto na pesquisa acadêmica quanto em aplicações industriais (Chattopadhyay, 2007).

Mas não basta ser somente um material com propriedades menos agressivas ao meio ambiente, ele necessita também apresentar propriedades químicas, físicas e mecânicas adequadas para poder ser utilizado em diferentes nichos de aplicações. Uma das possibilidades de melhorar estas propriedades é pela incorporação de partículas (carga/reforço) em matrizes poliméricas, tais como partículas inorgânicas. O desempenho de um nanocompósito está diretamente relacionado com a morfologia e o tamanho da carga. As partículas nanométricas, mais utilizadas são talcos, argilas,  $\text{CaCO}_3$ ,  $\text{SiO}_2$  dentre outros (Zhang *et al.* 2003 e Dias *et al.* 2015). Os nanocompósitos poliméricos têm, na maioria das vezes, um desempenho térmico, mecânico e propriedades de barreira superiores as matrizes sem adição da partícula inorgânica (Thomas *et al.*, 2008).

O talco natural é uma carga bastante utilizada na indústria por ser um material de baixo custo. Porém apresentam alguns inconvenientes tais como, sua forma não é estável e homogênea abaixo de  $1\mu\text{m}$ , pois para ter a partícula nessas dimensões, é preciso um processo de moagem que afeta a estrutura da partícula deixando o material amorfo. A associação de outros minerais e a substituição de diferentes elementos no talco natural, também aparece como desvantagens. A composição química bem definida, a alta pureza e cristalinidade, tamanho de partícula definido e controle de espessura é possível de ser obtida por rota sintética (Yousfi *et al.* 2013, Dumas *et al.* 2013 e Dumas *et al.* 2013).

Diversos estudos já descrevem a aplicação de diferentes talcos sintéticos, com essas características, utilizados como carga em matrizes poliméricas tais como, poliuretano, polipropileno, poliamida, dentre outros (Dias *et al.* 2015, Beuguel *et al.* 2015, Yousfi *et al.* 2013, Monticelli *et al.* 2013).

As partículas de  $\text{Fe}_3\text{O}_4$  – talco sintético, podem ser utilizadas para produção de nanocompósitos poliméricos magnéticos e o talco sintético tem como função a melhora das propriedades quando é incorporado ao material. A incorporação de nanopartículas magnéticas de  $\text{Fe}_3\text{O}_4$  em matrizes poliméricas para fabricar nanocompósitos orgânico-inorgânicos tem atraído atenção em muitas áreas, tais como implantes biomédicos e dispositivos, administração de fármacos, blindagem por interferência eletromagnética (EMI), purificação de água, polímeros de memória de forma magnética (MSMP) (Mohammadi *et al.*, 2016).

Este trabalho visa sintetizar, pela primeira vez, nanocompósitos PU/  $\text{Fe}_3\text{O}_4$  – talco sintético com propriedades magnéticas. Os novos nanocompósitos foram obtidos por mistura física e utilizando diferentes concentrações de  $\text{Fe}_3\text{O}_4$  – sintético, bem como PU base solvente e base água. O material foi caracterizado quanto a sua morfologia, propriedades térmicas, mecânicas e magnéticas. Para as amostras de nanocompósitos obtidos com poliuretano base água foram realizados estudos da interação carga/polímero pela técnica de RMN.

## 2. OBJETIVOS

O objetivo principal deste trabalho é sintetizar e caracterizar nanocompósitos PU/  $\text{Fe}_3\text{O}_4$ -talco sintético com propriedades magnéticas usando poliuretanos base solvente e base água.

### 2.1. Objetivos Específicos

- Sintetizar nanocompósitos com propriedades magnéticas utilizando  $\text{Fe}_3\text{O}_4$ -talco sintético em Pó e em gel (base água);
- Avaliar o efeito da carga com o auxílio de técnicas como TEM, MEV, AFM, DSC, TGA, DMA, FTIR, DRX, Mössbauer;
- Estudar o mecanismo de interação entre polímero/carga usando técnicas de RMN;
- Verificar se a carga (talco) encontra-se esfoliada ou intercalada.

### 3. REVISÃO BIBLIOGRÁFICA

#### 3.1. Poliuretanos

Uma das matrizes poliméricas que mais se destacam entre as estudadas em compósitos é o PU, sendo um polímero de grande importância na indústria por ser base de muitos materiais. O PU consiste de uma sequência alternada de segmentos flexíveis (provenientes do polioliol) e rígidos (provenientes do diisocianato), como é ilustrado na figura 3.1. Assim as características deste material dependem diretamente da origem do isocianato e do polioliol utilizado na síntese, essas variações de parâmetros tais como: massa molar, distribuição de segmentos flexíveis e rígidos, e grau de ramificação das cadeias resultará como produto final, materiais preparados para aplicações específicas (Zhou *et al*, 2015).

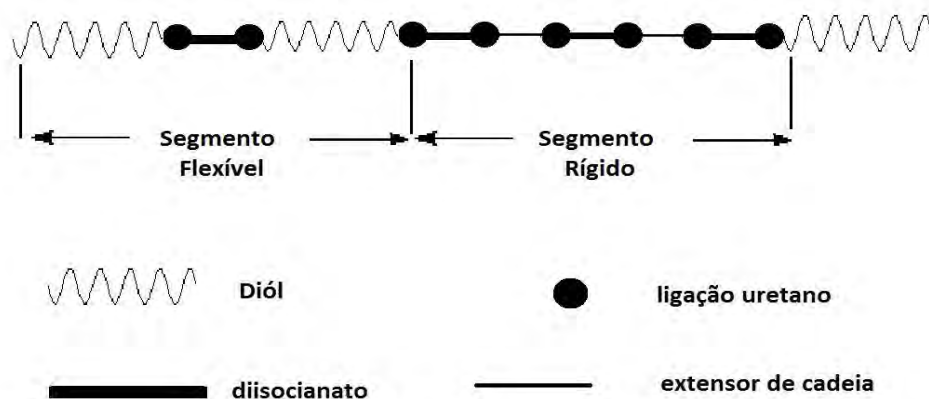


Figura 3.1. Estrutura da cadeia do poliuretano (Donge, 2003).



As propriedades mecânicas e de adesão destes materiais estão relacionadas a estes arranjos dos constituintes das cadeias poliméricas, tamanho dos segmentos flexíveis, a razão NCO/OH, o tipo de extensor e a presença ou não de solventes na síntese. No PU os segmentos flexíveis, atribuídos ao poliól, favorecem características elastoméricas ao polímero e os segmentos rígidos que, se atribui ao isocianato e ao extensor de cadeia, formam as ligações uretânicas altamente polares. Devido a estas ligações, os dois tipos de segmentos constituem microdomínios, figura 3.2. Assim o grau de separação de fases entre segmentos flexíveis e rígidos influi diretamente nas propriedades físicas, mecânicas e adesivas.

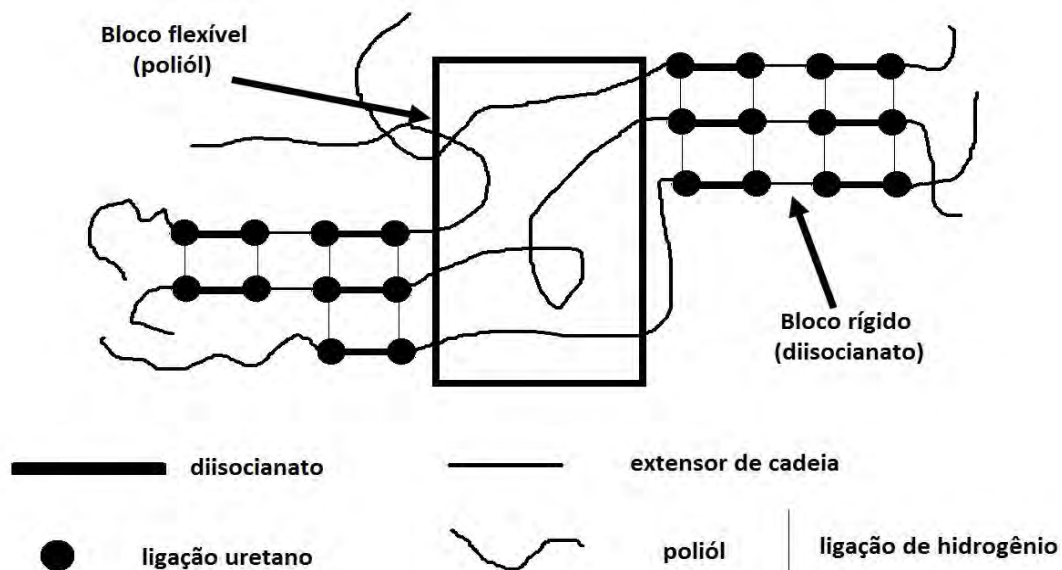


Figura 3.2. Microdomínios existentes na cadeia do Poliuretano (Donge, 2003).

Os poliuretanos formam uma classe ampla de materiais, encontrando aplicações em diversos nichos, tais como, elastômeros, fibras, adesivos, espumas e revestimentos de superfícies (Coutinho e Delpech, 1999; Riaz *et al.*, 2016).

No ano de 2012, o consumo brasileiro representou cerca de 4% do volume mundial de poliuretano. Estima-se que o Brasil consumiu aproximadamente 600 toneladas, o que é equivalente a 1,4 bilhão de reais naquele ano (Bain & Company). Estes dados evidenciam a importância deste material polimérico, bem

como a grande possibilidade de aumentar este mercado com o desenvolvimento de PUs com propriedades diferenciadas.

Com a crescente quantidade de compostos orgânicos voláteis (VOCs) liberados na atmosfera, produtos ecológicos estão sendo mais procurados pelas indústrias. E assim produtos com baixa quantidade de VOCs, vêm ganhando uma maior importância na indústria. Entre os produtos com baixo VOCs, a água é a melhor escolha para utilizar como meio na síntese e produção de produtos. A água foi considerada como segura, não tóxica, além de ser um solvente barato e benigno a saúde (Zhou *et al*, 2015).

O poliuretano base água (do inglês *waterborne polyurethane*- PUBA) tem sido estudado muito nesses últimos anos, principalmente pela demanda de indústrias que estão cada vez mais preocupadas com os VOCs (Marinho *et al*, 2013 and Zhou *et al*, 2015). A rota de síntese mais utilizada de PUBA é a mudança estrutural, isto é, mudando a cadeia principal do poliuretano hidrofóbico com inserção de grupos hidrofílicos (Coutinho *et al*, 2002). Em seguida é adicionada água para emulsionar e dispersar o pré-polímero hidrófilo com o processo de extensão da cadeia.

O PUBA vem sendo utilizado em diferentes frentes, pela sua diversificada aplicação, menos agressiva ao meio ambiente, além das características estruturais, que resultam em propriedades úteis e interessantes (Barboza *et al.*, 2014). O PUBA vem sendo utilizado em revestimentos para fibras, adesivos para substratos alternativos, na área biomédica, petroquímica, farmacêutica, corantes têxteis dentre outros. A matéria prima de maior importância na construção da estrutura de PUBA é o diisocianato e a fonte de poliols, onde corresponde aos segmentos rígidos e segmentos flexíveis, respectivamente. Os diisocianatos utilizados para a obtenção do PUBA, sendo alifático ou aromático, são responsáveis por algumas características do material, tais como a estabilidade à luz. Os polióis, mais utilizados são poliéteres, poliésteres, polidienos e poliolefinas (Yeh *et al.*, 2008 and Akbari *et al*, 2016). A aplicação de polióis de origem vegetal (fonte renovável) vem sendo estudada (Engels *et al*. 2013). O esquema 1, mostra um comparativo entre métodos tradicionais e novos para a síntese de PUBA (Zhou *et al*, 2015).



Esquema 1. Principais processos de obtenção de poliuretano base água (Zhou *et al.*, 2015).

Em seu trabalho de revisão de PUBA's, Zhou e co-autores descrevem alguns métodos já existentes e citam novos processos que estão sendo desenvolvidos para a síntese de novos PUBA, tais como, polimerização homogênea em solução (HSP) (Wang *et al.* 2008), processo de polimerização em miniemulsão (MEPP) (Tiarks *et al.*, 2001, Zang *et al.* 2012), processo de polimerização de transferência reversível de cadeia por adição - fragmentação (RAFT) e polimerização radicalar via transferência de átomo (ATRP).

Existem duas técnicas para síntese de poliuretanos: método de etapa única e método em duas etapas. A sequência de adição de reagentes, faz a diferença entre os dois processos. Neste trabalho utilizou-se as duas técnicas, a de uma etapa, onde o isocianato, o extensor da cadeia, os polióis, e aditivos são

misturados todos ao mesmo tempo, visando a obtenção do PU base solvente. Já a técnica de duas etapas, envolve a pré-reação de um isocianato com um diól (1000-4000 g/mol), para formar um produto intermediário (pré-polímero) contendo baixa concentração de grupos NCO, cerca de 3% a 10% da massa, aproximadamente. Numa segunda etapa, o pré-polímero reage com um extensor de cadeia para produzir o polímero final. Esta técnica foi utilizada para obtenção do PUBA.

### 3.2. Silicatos Lamelares

As argilas vêm sendo utilizadas em diferentes aplicações, tais como, fertilizantes, catalisadores, adsorventes e tintas. Também, vários estudos descrevem seu uso como carga em polímeros e elastômeros, entre outras matrizes (Dias *et al.* 2015, Prado *et al.* 2014). O crescente aumento na utilização é devido a diversidade de argilas existentes e pela melhoria nas propriedades térmicas, mecânicas, inchamento, adsorção, reológicas e plastificante que esta carga proporciona. Nanocompósitos, tendo como matriz polímeros e carga filossilicatos, vêm sendo publicados em grande número, e em geral as matrizes são, poliéster, poliéter, poliuretano, poliamida, polipropileno, resinas epóxis, etc. (Paiva *et al.*, 2008; Yeh *et al.*, 2008).

Os silicatos lamelares utilizados na síntese de nanocompósitos podem ser naturais ou sintéticos, consistindo em camadas muito finas, as quais estão normalmente ligadas entre si por contra-íons (Dumas *et al.*, 2013). Blocos são criados e sua construção básica é constituída de folhas tetraédricas em que o silício é cercado por quatro átomos de oxigênio e folhas octaédricas em que um metal, como o alumínio, é cercado por oito átomos de oxigênio. Portanto, em estruturas 1:1 em camadas (por exemplo, a caulinita) uma folha tetraédrica é ligada a uma folha octaédrica, em que os átomos de oxigênio são compartilhados (Coelho *et al.*, 2007 e Pavlidou e Papasrydes, 2008).

Na estrutura 2:1 silicatos/filossilicatos são constituídos por camadas bidimensionais, onde uma folha octaédrica central de alumina está fundida com dois tetraédros de sílica externos, de certa forma que os íons da folha octaédrica também

pertencem às folhas tetraédricas (Figura 3.3). A espessura da camada é de aproximadamente 1 nm e as laterais podem ser de 300 Å e podem chegar a vários micras (Dumas *et al.*, 2013).

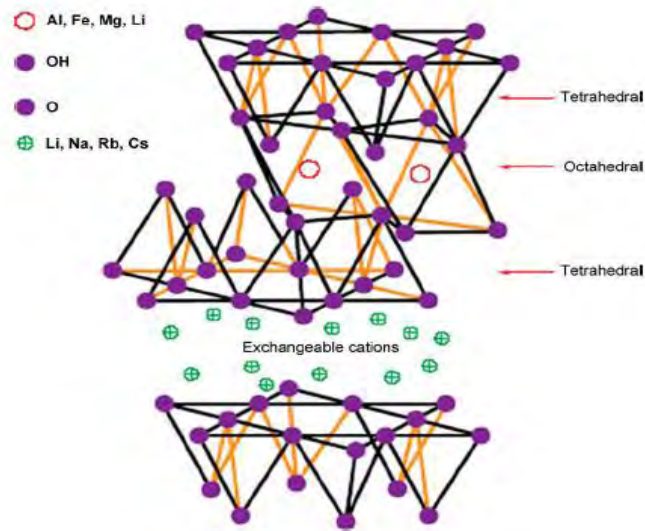


Figura 3.3. Representação da estrutura de um silicato lamelar 2:1 (Mittal *et al.*, 2009).

Talco é um mineral em camadas de silicato de magnésio com a fórmula  $Mg_3Si_4O_{10}(OH)_2$ , é utilizado como material de enchimento em compósitos para reduzir os seus custos de produção, propriedades físicas e químicas, e/ou oferecer novas funcionalidades. Em estudos de Martin *et al.* (2002) foi evidenciado que o tamanho de partícula de talco é extremamente importante. Mas partículas de talco natural, não podem ser moídas homogeneamente abaixo de um micron, sem destruir a sua estrutura. Esta limitação foi revelada quando talco natural foi introduzido na indústria aeronáutica, em uma matriz de metal feita de Zn/Ni e Ni/P, para aumentar as suas propriedades lubrificantes.

A partir do estudo de um processo experimental dos pesquisadores Decarreau *et al.*, (1989) e Lebre (2004, 2007), onde trabalharam em um processo para obter um talco sintético com uma pureza controlada e uma escala abaixo de um micron, Martin *et al.* (2006 b,c e 2008 a,b) obtiveram talco sintético, mas seus resultados revelaram defeitos estruturais ocorridos durante o processo.

Mais recentemente, este processo foi melhorado e patentado (<sup>a</sup>Dumas et al., 2012, b, 2013a, b) alterando as fontes de reagentes, bem como o procedimento de mistura. Além de controlar o tamanho de partícula e a pureza do talco (figura 3.4), o novo processo reduz o tempo necessário para o tratamento hidrotérmico e conduz a um produto monofásico.

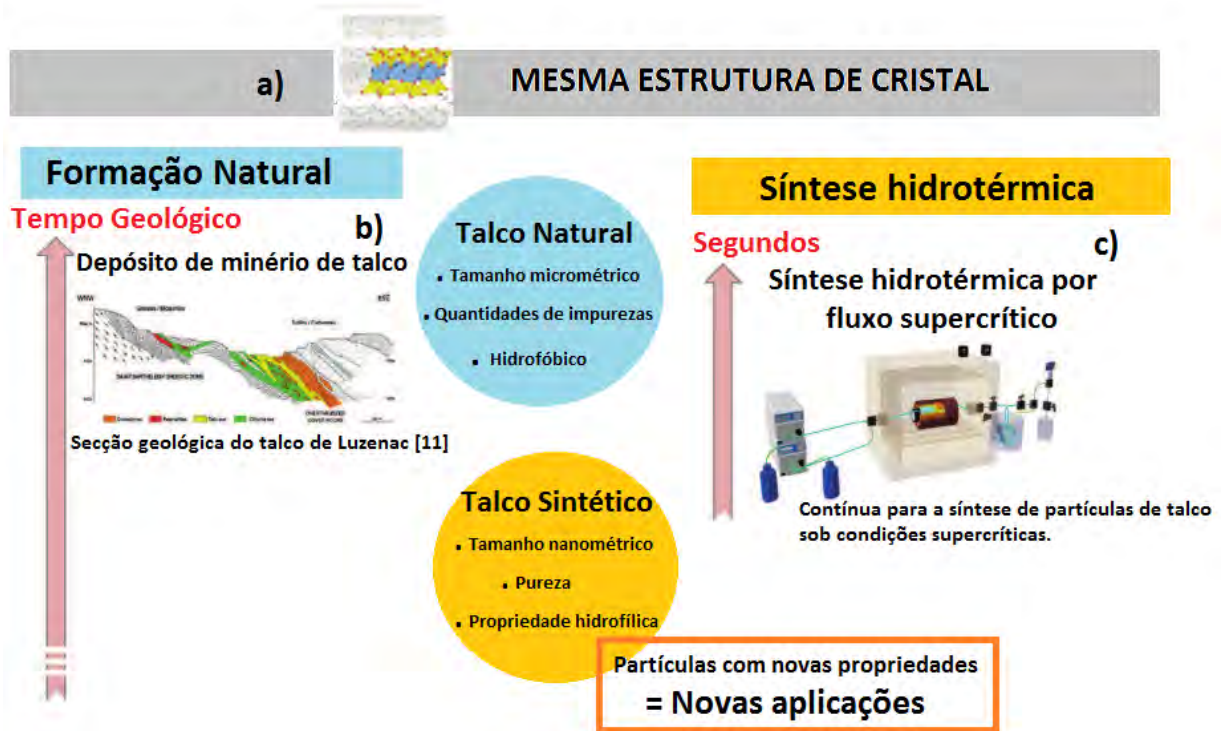


Figura 3.4. a) Talcos naturais e sintéticos têm a mesma estrutura cristalina. b) O talco é um recurso natural finito obtido sob a ação de fluidos hidrotermais durante vários milhões de anos e caracterizado por partículas de tamanho micrométrico. c) A síntese de fluxo hidrotérmico supercrítico é um novo processo para partículas de talco de tamanho nanométrico sintetizado com novas propriedades (<sup>d</sup>Dumas et al. 2016).

A utilização de talco sintético permite obter amostras com uma composição química definida, além de uma elevada pureza, controle do tamanho da partícula e também a espessura da camada. Os talcos nanométricos sintéticos possuem novas propriedades para novas aplicações (Figura 3.4). Entre estas propriedades salienta-se o caráter hidrofílico resultante das inúmeras arestas (Si-O e Mg-O) e grupos hidroxilas, pois permite que estas cargas, sejam pela primeira vez, usadas como carga fluida. O uso de nano-talco em suspensão é muito importante pois combina a estrutura lamelar do talco (T-O-T) com um forte caráter hidrofílico.

Estes materiais podem facilmente formar ligações de hidrogênio e interações polares com a água. (Dumas *et al.*, 2016)

### 3.3. Nanocompósitos poliméricos

Nanocompósitos fazem parte de uma classe de materiais formados por híbridos de materiais orgânico e inorgânico, onde a fase inorgânica está dispersa em escala nanométrica na matriz polimérica, como demonstrado na figura 3.5 (Paiva *et al.*, 2006). Dentre as nanocargas inorgânicas mais utilizadas, podem ser citados os carbonatos, sulfatos, alumino-silicatos, talcos e argilas, que são as mais estudadas atualmente (Esteves *et al.*, 2004; Viana *et al.*, 2012).

Os nanocompósitos podem ser obtidos por três diferentes processos, sendo eles: mistura no estado fundido, em solução e em polimerização *in situ*. Na mistura no estado fundido ou *melt blending*, os materiais são misturados mecanicamente por extrusão em temperaturas elevadas, sendo este método mais utilizado (Rodrigues, 2012; Viana, 2012). No processo em solução, a matriz (polímero) é dissolvida em solventes e após é adicionado carga (carga/reforço). E no processo de polimerização *in situ*, a formação do nanocompósito do tipo poliuretano é feita pela adição dos reagentes de partida em uma reação de policondensação, onde a carga/reforço é adicionada desde o início (Fang *et al.*, 2013).

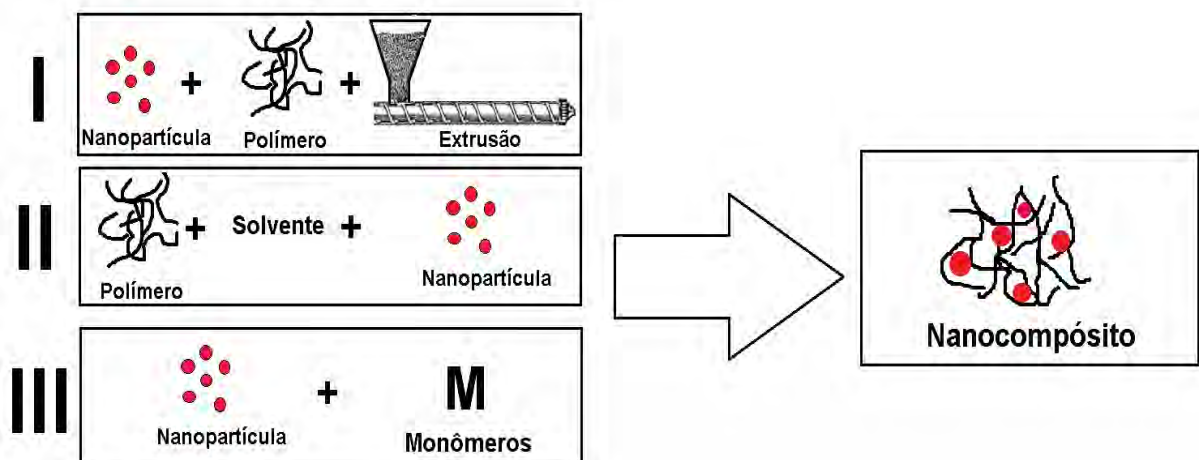


Figura 3.5. I) Mistura simples dos componentes (por *melt blending* ou extrusão), II) Preparação em



solução e III) Polimerização da matriz *in situ* (modificado de Esteves *et al*, 2004).

Os nanocompósitos poliméricos com base de silicatos lamelares têm sido o foco de grande interesse. A ampla utilização de silicatos é devido a sua potencialidade de dispersão na matriz polimérica. Dentre as formas de silicato em camadas ou lamelares, também conhecidos como filossilicatos, destacam-se mica, talco, montmorilonita (MMT), vermicolita, hectorita, saponita, entre outras. Dentre todas essas formas de filossilicatos, se destacam a MMT, hectorita, saponita tendo dois tipos de estruturas, tetraédro-substituído e o octaédro- substituído. No caso dos tetraédricos, as cargas negativas estão na superfície das lamelas e assim ficando mais fácil de reagir com o polímero do que os octaédros (Sinha, Ray e Okamoto, 2003).

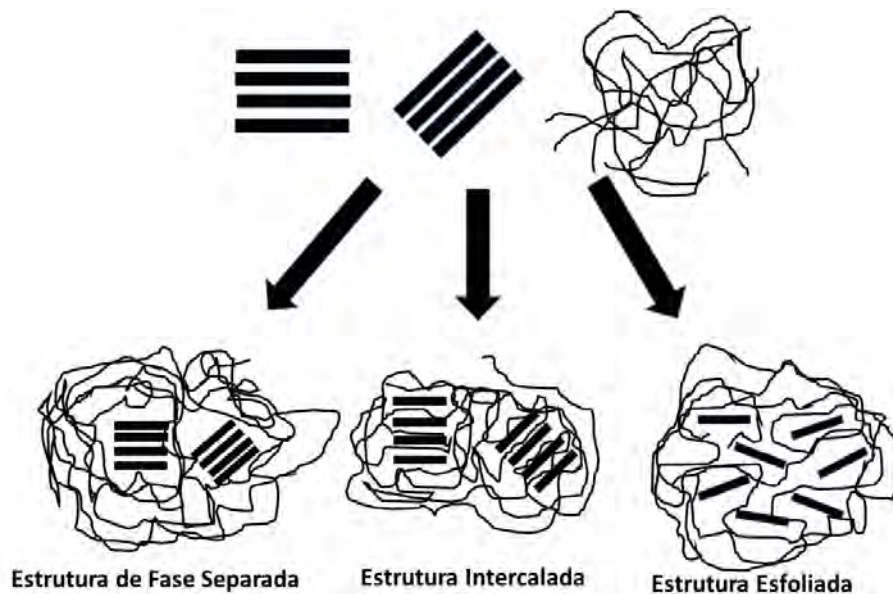


Figura 3.6. Representação esquemática dos diferentes graus de dispersão dos compósitos.

(Adaptado de Paiva *et al.*, 2006).

Dependendo da força de interação interfaciais da matriz com o silicato lamelar, têm-se três diferentes tipos de nanocompósitos que são termodinamicamente possíveis: fase separada, intercalada e esfoliada (figura 3.6).



Em nanocompósitos intercalados, as cadeias simples do polímero são intercaladas nas camadas do silicato tendo uma regularidade na sua alternância (polímero/silicato/polímero). No modo intercalado, acontece por uma interação com as pontas hidroxiladas e assim tende-se uma aglomeração. E por fim nanocompósitos esfoliados, onde o silicato é totalmente esfoliado na matriz polimérica, onde se perde a estrutura ordenada. Normalmente o teor de carga em um material intercalado é maior do que um material esfoliado (Sinha, Ray e Okamoto, 2003).

Pode-se dizer que a miscibilidade limitada é maior nos nanocompositos intercalados, enquanto a miscibilidade é total em nanocompósitos esfoliados (Ray *et al.* 2003). A representação ilustrada na Figura a 3.6 mostra diferentes situações, porém estas estruturas híbridas podem coexistir no mesmo nanocompósito.

### **3.3.1. Obtenção de nanocompósitos de Poliuretano com Diferentes Cargas**

Zhang e colaboradores (2003) investigaram em seu trabalho a interação da nanosílica quando adicionada na matriz polimérica PUBA. Os pesquisadores utilizaram o método de sol-gel, onde incorporam diferentes quantidades de carga (5, 10 e 15% em relação a quantidade de massa de polímero puro). Foi usado o método *in situ* para se obtenção dos nanocompósitos. Como caracterização foi usada a técnica de MEV (Microscopia Eletrônica de Varredura). As amostras analisadas estavam na forma de filmes, onde foi possível verificar a distribuição da carga na matriz e se observou que a medida que se aumenta a quantidade de carga na matriz cresce a agregação de carga, evidenciando a interação carga-carga e não mais carga-polímero.

Nos trabalhos de Zhang, as nanocargas de  $\text{Fe}_3\text{O}_4$  foram adicionadas a uma matriz de PUBA nas proporções de 0,5 a 4,0% em massa em relação a massa de polímero. Mas antes de adicioná-las a matriz polimérica, as cargas passaram por um pré-tratamento com ácido oleico, visando uma maior afinidade com os monômeros. Após esse tratamento com ácido oleico, a mesma foi colocada com os demais reagentes. O nanocompósito foi preparado *in situ* e a carga foi adicionada

por último, depois do pré-polímero. Após o ensaio de VSM (do inglês *Vibrating sample Magnetometer*), observou-se que as nanocargas de  $\text{Fe}_3\text{O}_4$  revestidas com ácido oleico, quando comparada com as não revestidas, apresentaram resultados superiores de saturação magnética, tendo 58,9 emu/g (puro) e 52,1 emu/g (revestida com ácido Oleico) (figura 3.7). Não foi detectado coercividade e nem valores remanescentes. E assim, confirmando as suas propriedades paramagnéticas em temperatura ambiente. Nas curvas de histerese obtidas por VSM a temperatura ambiente, os nanocompósitos de PUBA, exibiram comportamento superparamagnético. Os valores de magnetização de saturação medidos em PUBA/ $\text{Fe}_3\text{O}_4$  - 2.0 não revestido (2,17 emu/g), são menores que do PUBA/ $\text{Fe}_3\text{O}_4$  - 2.0 revestido (19,1 emu/g). Os valores de magnetização de saturação dos nanocompósitos crescem com o aumento do teor de ácido oleico.

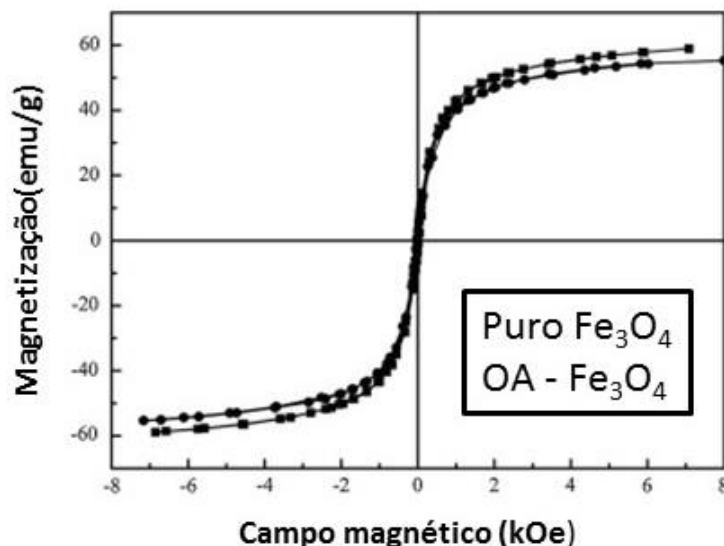


Figura 3.7. Curvas de histerese para  $\text{Fe}_3\text{O}_4$  e OA- $\text{Fe}_3\text{O}_4$  nanopartículas.

Resultados de análise térmica para os nanocompósito PUBA/ $\text{Fe}_3\text{O}_4$  - 4,0 com 4% de carga mostraram que a resistência térmica teve um aumento de 15°C em relação ao PUBA puro. O resíduo obtido no final da análise térmica também teve um aumento de aproximadamente 20% para o PUBA/ $\text{Fe}_3\text{O}_4$  - 4,0 quando comparado ao PUBA.

Prado *et al.* (2015) realizaram estudos de síntese *in situ* de poliuretano com adição de talco sintético com níquel em diferentes proporções de 0,5 a 5% de talco (massa/massa) em relação ao polímero puro e comparou com talco natural. As análises de DRX foram usadas para observar a estrutura cristalina dos nanocompósitos de talco-níquel como também dos obtidos com talco natural. Para os nanocompósitos de PU/talco natural e PU/talco sintético, se observaram que quando comparados tinham os mesmos picos do talco natural.

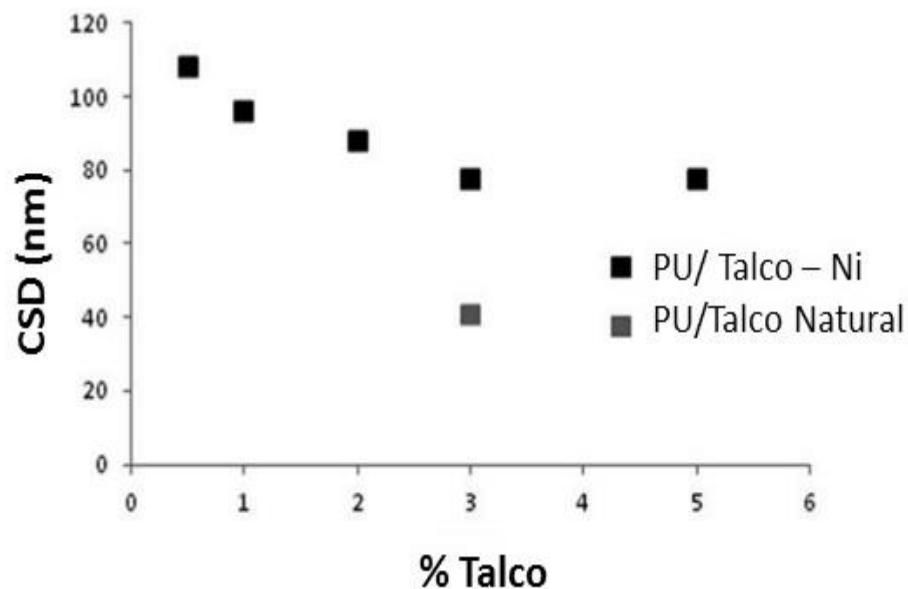


Figura 3.8. Cálculo de CSD dos nanocompósitos de Ni- talco sintético e talco natural (Prado *et al.* 2015).

Quando feito os cálculos de CSD (figura 3.8), onde os valores dão uma noção da ordem de empilhamento (distância de uma lamela para outra), foi evidenciado que a distância da camada do talco sintético (31 nm) é menor quando comparada com a camada do talco natural (85,2 nm). Os autores observaram um aumento na temperatura de degradação do compósito com quantidades maiores de talco/Ni no polímero.

O trabalho de Dias *et al.*, 2015, descreve a incorporação da carga em uma matriz de poliuretano em uma reação *in situ*, onde a carga teve dois diferentes tratamentos (tempo de reação 7 e 24 horas) denominados SSMMP. Os resultados de TGA mostraram valores de temperatura de degradação inicial com a quantidade

de 3% de talco, superiores quando comparado com o PU puro. Onde a degradação inicial do PU puro foi em 301°C enquanto que as temperaturas para os nanocompósitos SSMMP 7 e 24 horas foram 340 e 337°C, respectivamente. Por DTG, observou-se que houve um aumento no pico que corresponde aos seguimentos flexíveis, pelo aumento de adição de SSMMP. Onde os autores justificam que pode ter ocorrido uma formação de estrutura de rede, pelos grupos hidroxilas na superfície da nanopartícula através de ligações de hidrogênio com a cadeia polimérica.

Em outro trabalho de Dias *et al.*, 2016, incorporou talco sintético em uma matriz de poliuretano em uma reação *in situ*. As cargas talco – Ni, talco – Mg foram comparados com talco natural. Sendo que a área específica dos talcos sintéticos são de 135 e 329 m<sup>2</sup>/g para o Talco Ni e para o talco Mg, respectivamente. Foi observado nas análises de DRX que talcos sintéticos apresentam picos mais largos e não tão intensos, o que indica que os talcos são formados por domínios com pequenos números de camadas. Os espectros de DRX dos compósitos de talco - Mg evidenciaram que a carga esfoliada foi incorporada ao polímero (matriz), o mesmo não aconteceu com os nanocompósitos que têm como carga o talco – Ni. Os autores relatam que pode ter tido uma interação do Ni com as ligações uretanas, que foi corroborada com os resultados do FTIR. E ainda foi possível ver a diferença morfológica nas imagens de fratura e dos filmes.

O trabalho de Zhao *et al.* (2012) descreve a obtenção de compósitos de poliuretano-talco em uma reação *in situ*. Os ensaios de resistência a tração em temperatura ambiente, mostram que obtiveram melhorias nas propriedades mecânicas, até a quantidade de 9% de carga, em quantidade maiores as propriedades diminuíram. Concluíram que até 9% de carga os nanocompósitos ficaram homogêneos.

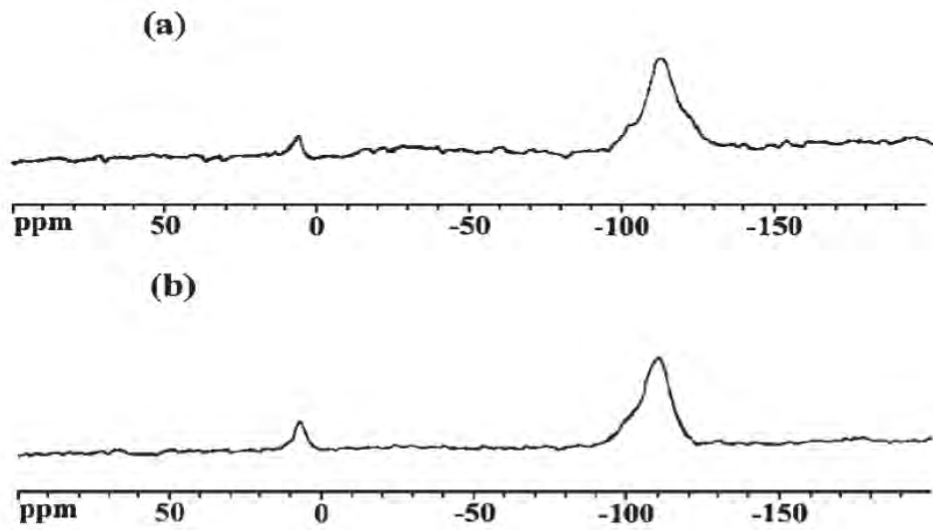


Figura 3.9.  $^{29}\text{Si}$  MAS RMN (a) PS/ Sílica híbrida e (b) PMMA/Sílica híbrida.

No trabalho de Wang, et al 2008 onde adicionaram nanopartículas de sílica em PS e PMMA e utilizaram a técnica de RMN de  $^{29}\text{Si}$  de estado sólido para verificar a incorporação da carga na matriz. Na Figura 3.9 (a), é visto um pico a 7,1 ppm relacionado com  $-\text{CH}_2\text{Si}(\text{CH}_3)_2\text{O}-$ , que é atribuído à ressonância do núcleo de silício do iniciador ligado à superfície. Além disso, podem ser observados os picos de  $Q_2$ ,  $Q_3$  e  $Q_4$  por volta de 100 ppm. É visto que a área total de  $Q_2$  e  $Q_3$  diminui enquanto a área de  $Q_4$  aumenta, quando comparada com a partícula de nanosílica pura, indicando a reação de silanóis de superfície. Um fenômeno semelhante é observado para o PMMA/sílica híbrida (Fig. 3.9 (b)). O pico a 9,1 ppm também está relacionado com  $-\text{CH}_2\text{Si}(\text{CH}_3)_2\text{O}-$ , com um desvio relativamente pequeno em comparação com o do híbrido PS / sílica.

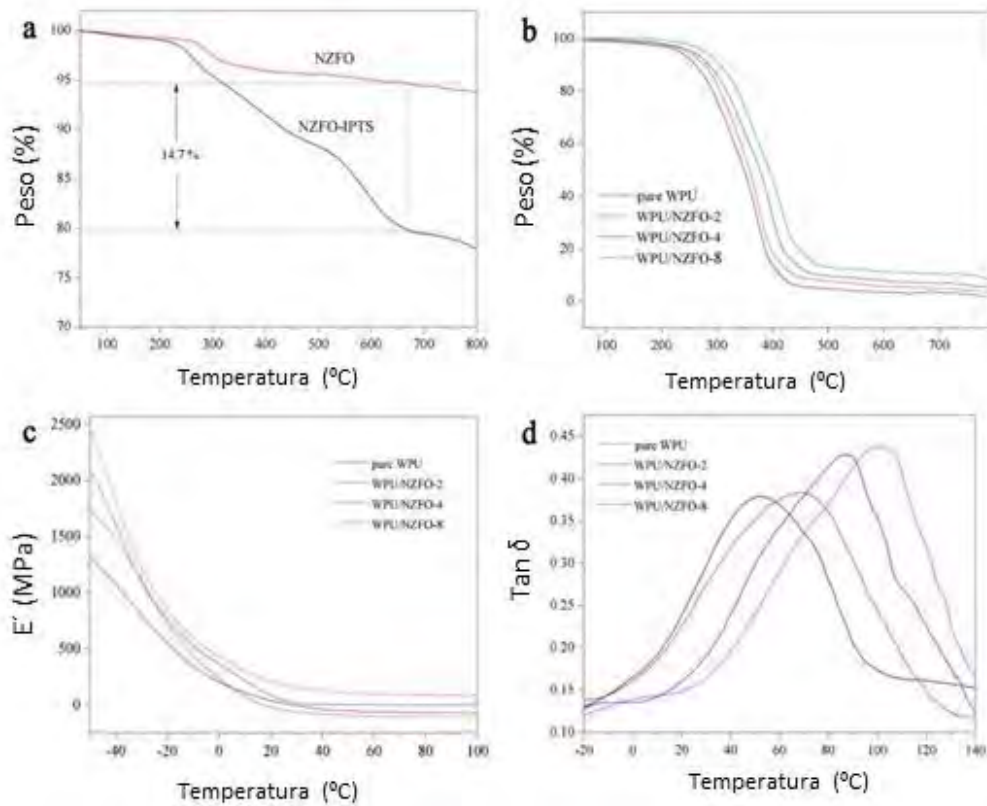


Figura 3.10. TGA NZFO e NZFO – IPTS nanopartículas (a), TGA curvas nanocompósitos de WPU/NZFO com diferentes quantidades de NZFO-IPTS (b), Curvas de módulo de armazenamentos (c) e curvas de fator de perda dos nanocompósitos de WPU/NZFO.

Nanocompósitos superparamagnéticos com matriz poliuretano base água (WPU) foram sintetizados por Chen *et al.*, 2015, ligados covalentemente a nanoesferas de ferrita  $\text{Ni}_{0.3}\text{Zn}_{0.7}\text{Fe}_2\text{O}_4$  (NZFO) usando o método de polimerização *in situ*. As nanopartículas  $\text{Ni}_{0.3}\text{Zn}_{0.7}\text{Fe}_2\text{O}_4$  (NZFO) foram modificadas com isocianato de 3-(trietoxisilil)propilo(IPTS) para melhorar a compatibilidade com monômeros. Resultados de estabilidade térmica foram observados por TGA. Curvas de TGA (figura 3.10.b) dos nanocompósitos WPU / NZFO com diferentes quantidades de NZFO-IPTS mostraram dois estágios de perda de massa, para todas as amostras, atribuídos aos seguimentos rígidos e flexíveis. A Temperatura de degradação na fase dos segmentos flexíveis aumentou quanto maior a funcionalização dos conteúdos NZFO.

Os autores (Chen *et al.*,2015) ainda descrevem que a técnica de DMA foi realizada para investigar o comportamento viscoelástico dos polímeros. Figura 3.10.c e d mostram o módulo de armazenamento ( $E'$ ) e as curvas do fator de perda ( $\tan \delta$ ) dos filmes WPU e nanocompósitos WPU/NZFO. O módulo de armazenamento ( $E'$ ) pode fornecer informação relativamente ao grau de reticulação. A temperatura associada à posição de pico da curva  $\tan \delta$  é definida como a temperatura de transição vítrea ( $T_g$ ). Como visto na Fig. 3.10.d, os valores de  $T_g$  dos nanocompósitos aumentaram à medida que o teor de NZFO-IPTS aumentou. Isto indicou que a introdução de nanopartículas de NZFO-IPTS teve um efeito favorável nos valores de  $T_g$  dos nanocompósitos, bem como as demais caracterizações.

## 4. PROCEDIMENTOS EXPERIMENTAIS E RESULTADOS

Neste trabalho foram sintetizados dois tipos de nanocompósitos de poliuretano. Sendo um poliuretano base solvente, que foi incorporado talco sintético- $\text{Fe}_3\text{O}_4$  (na forma de pó) e outro poliuretano base água, onde foi incorporado talco sintético- $\text{Fe}_3\text{O}_4$  (na forma de gel). Ambos nanocompositos de poliuretano foram obtidos por mistura física com auxílio de ultraturrax. Visou-se neste estudo, correlacionar as técnicas espectroscópica, morfológica, propriedades térmicas, mecânicas e magnéticas nos nanocompósitos sintetizados. Além de estudar a interação do polímero/carga por RMN. Tendo como objetivo obter nanocompósitos com propriedades magnéticas e boas características térmicas e mecânicas.

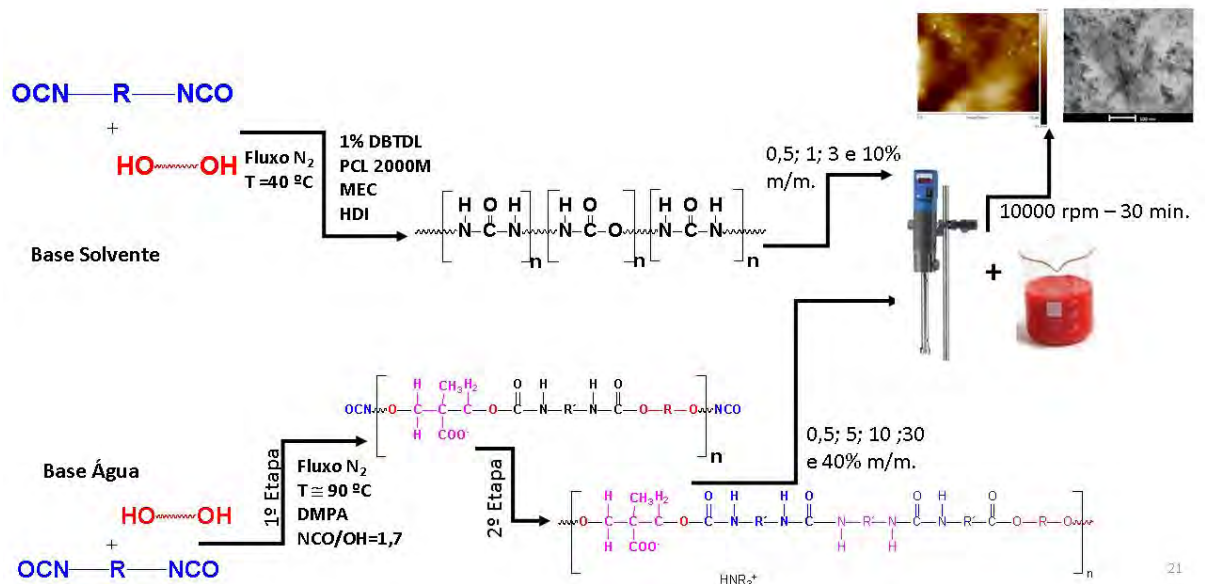


Figura 4.1. Esquema dos capítulos e síntese realizadas.

Nesta secção, em forma de artigos, serão apresentados os métodos, resultados e discussões fundamentais a esta tese, divididos da seguinte forma:



poliuretano base solvente com  $\text{Fe}_3\text{O}_4$  talco sintético (capítulo I) e poliuretano base água com  $\text{Fe}_3\text{O}_4$  talco sintético (capítulo II). A figura 4.1, mostra uma representação esquemática dos dois trabalhos abordados nesta tese. Secção 5, será apresentado um comparativo dos principais resultados obtidos de cada capítulo.

#### **4.1. Capítulo I: Poliuretano base solvente com $\text{Fe}_3\text{O}_4$ talco sintético**

Este capítulo descreve a síntese e caracterização de PU/ $\text{Fe}_3\text{O}_4$  talco sintético (em pó) disperso em poliuretano base solvente, por meio do artigo intitulado de “New magnetic nanocomposites: Polyurethane/ $\text{Fe}_3\text{O}_4$  – synthetic talc” publicado na European Polymer Journal. Foi sintetizado poliuretano base solvente e posteriormente foram adicionados diferentes quantidade de talco sintético- $\text{Fe}_3\text{O}_4$  na forma de pó (0,5; 1; 3 e 10% m/m). Os nanocompositos sintetizados foram caracterizados por FTIR, DRX, SEC, TEM, MEV, AFM, TGA, DSC, DMTA e propriedades magnéticas (Mössbauer, curvas de magnetização e magnetização vs temperatura). Os resultados demonstraram que há uma interação da carga/polímero. As microscopias corroboram com os espectros de DRX, mostrando a carga dispersa completamente na matriz polimérica e por DRX é visto o desaparecimento do pico característico no talco sintético. Podendo ainda ressaltar que o talco demonstrou ser um ótimo material para potencializar as propriedades do polímero puro.



ELSEVIER

Contents lists available at ScienceDirect

European Polymer Journal

journal homepage: [www.elsevier.com/locate/europolj](http://www.elsevier.com/locate/europolj)

Macromolecular Nanotechnology

## New magnetic nanocomposites: Polyurethane/ Fe<sub>3</sub>O<sub>4</sub>-synthetic talc



Leonardo M. dos Santos<sup>a</sup>, Rosane Ligabue<sup>a,b</sup>, Angela Dumas<sup>c</sup>, Christophe Le Roux<sup>c</sup>,  
Pierre Micoud<sup>c</sup>, Jean-François Meunier<sup>d</sup>, François Martin<sup>c</sup>, Sandra Einloft<sup>a,b,\*</sup>

<sup>a</sup> Programa de Pós-Graduação em Engenharia e Tecnologia de Materiais (PGETEMA), Pontifícia Universidade Católica do Rio Grande do Sul (PUCRS), Porto Alegre, Brazil

<sup>b</sup> Faculdade de Química (FAQUI), Pontifícia Universidade Católica do Rio Grande do Sul (PUCRS), Porto Alegre, Brazil

<sup>c</sup> ERT 1074 Géomatériaux, GET UMR 5563 CNRS, Université de Toulouse, Toulouse, France

<sup>d</sup> Laboratoire de Chimie de Coordination, Université de Toulouse, Toulouse, France

### ARTICLE INFO

#### Article history:

Received 17 April 2015

Received in revised form 19 May 2015

Accepted 24 May 2015

Available online 27 May 2015

#### Keywords:

Polyurethane

Nanocomposites

Synthetic Fe<sub>3</sub>O<sub>4</sub>-talc

Physical mixture

### ABSTRACT

New Fe<sub>3</sub>O<sub>4</sub>-synthetic talc was used as filler in the synthesis of PU/Fe<sub>3</sub>O<sub>4</sub>-synthetic talc nanocomposites obtained by physical mixture. The Fe<sub>3</sub>O<sub>4</sub>-synthetic talc-nanofillers were exfoliated/well dispersed into the polyurethane matrix even at high filler content of 10 wt.% as supported by XRD and TEM analyses. The SEM micrographs corroborated the good distribution of the fillers and evidenced an important morphology change with the increase of the filler content. These morphological changes caused by the balance between the hydrogen bonding among polymer/polymer, polymer/filler and filler/filler were also confirmed by topological changes as well as in the roughness values evaluated by AFM. The magnetic behavior of the nanocomposites was confirmed by means of Mossbauer transmission and magnetic measurements. The use of Fe<sub>3</sub>O<sub>4</sub>-synthetic talc for obtaining magnetic nanocomposites resulted in improved materials with superior crystallization temperature and thermal stability proving to be a simple way of avoiding dipolar attraction of magnetite and consequently the filler aggregation.

© 2015 Elsevier Ltd. All rights reserved.

### 1. Introduction

Magnetic materials can find a great number of applications in different niches such as data storage, biomedicine, nanoabsorbent materials, biosensor, drug delivery agent, and magnetic resonance imaging devices, among others [1–4]. Polymeric materials are a potential matrix for magnetic particle incorporation allowing the obtainment of materials with improved mechanical properties beyond the appearance of interesting magnetic characteristics [5,6]. Despite the incorporation of nanosized particles into a polymeric matrix is a well-known subject, the obtainment of homogeneous distribution of the filler into the polymeric matrix is still a challenge [7]. The filler dispersion plays an important role in determining the nanocomposites behavior and when achieved produces materials with properties often superior to the constituents [6]. The magnetic dipolar attraction of magnetite induces aggregation and usually these particles are encapsulated into polymers to avoid this phenomenon and improve their chemical stability [1]. Another possibility to overpass these problems is to produce synthetic talc containing magnetic particles in their composition as obtained by the ERT 1074 Géomatériaux (Toulouse,

\* Corresponding author at: Programa de Pós-Graduação em Engenharia e Tecnologia de Materiais (PGETEMA), Pontifícia Universidade Católica do Rio Grande do Sul (PUCRS), Porto Alegre, Brazil.

E-mail address: [einloft@pucrs.br](mailto:einloft@pucrs.br) (S. Einloft).

<http://dx.doi.org/10.1016/j.eurpolymj.2015.05.026>

0014-3057/© 2015 Elsevier Ltd. All rights reserved.



France) [8,9]. These new synthetic talc- $\text{Fe}_3\text{O}_4$  nanoparticles can be used as filler for producing magnetic polymeric nanocomposites allying the good properties provided by synthetic talc with magnetic properties of this filler. Despite their good performance as filler and low price, natural talc presents some drawbacks. One of the main limitations is the impossibility of being homogeneously grounded below  $1\ \mu\text{m}$  without becoming amorphous and having their structure destroyed [10–12]. The association of other minerals and the substitution for different elements into the structure of natural talc also appears as disadvantages [10–14]. Talc samples with a well-defined chemical composition, high purity, the crystallinity, particle size and the layer thickness control can be obtained by synthetic way [10–12]. The literature describe the use of new synthetic talc as nanofillers reinforcement for polyurethane [15,16] polypropylene and polyamide 6 systems [10] and polypropylene/polyamide 6 blends [17]. When the matrix is polyurethane (PU) a good compatibility of both phases filler/polymer is achieved mainly due to the OH groups interaction of the filler, by hydrogen bonding, with the polymeric chain [15,16].

The main goal of this work is to present the obtainment and characterizations of PU/ $\text{Fe}_3\text{O}_4$ -synthetic talc nanocomposites. The new magnetic nanocomposites materials were obtained by physical mixture of polymer and filler and characterized regarding the nanocomposites formation, morphology, thermal, mechanical and magnetic properties.

## 2. Experimental

### 2.1. Polyurethane synthesis

The PU synthesis was performed at School of Chemistry/PUCRS and was performed from the reaction between poly (caprolactone) diol (PCL, MM = 2000 g/mol, Sigma–Aldrich) and 1,6-hexamethylene diisocyanate (HDI, for synthesis, Merck) using a molar ratio of NCO/OH of 1:1. Dibutyl tin dilaurate (DBTDL, Miracema-Nuodex Ind.) was used as catalyst (0.1% w/w) and methyl ethyl ketone (MEK, P.A., Merck) as solvent (about 50 mL).

### 2.2. Synthesis of the filler $\text{Fe}_3\text{O}_4$ -synthetic talc

Magnetic-talc fillers were synthesized in the GET laboratory by the ERT 1074 Géomatériaux group (Toulouse, France) according the patents [8,9]. An aqueous solution (300 mL) of iron chloride (0.65 M) is prepared by dissolving in air atmosphere 35.02 g (129.57 mmole) iron (III) chloride hexahydrate ( $\text{FeCl}_3 \cdot 6\text{H}_2\text{O}$ ) and 12.88 g (64.78 mmole) of iron (II) chloride tetrahydrate ( $\text{FeCl}_2 \cdot 4\text{H}_2\text{O}$ ) in a molar ratio identical to magnetite ( $\text{Fe}^{2+}:\text{Fe}^{3+} = 1:2$ ). Then, under mechanical stirring, the solution of the aqueous solution of iron chlorides is added to a suspension of synthetic talc (corresponding to 30 g of dry talc in 1 l of distilled water) – product referred as 6H in [12] – and the yellow-orange suspension is heated to  $70\ ^\circ\text{C}$ . Then, 80 ml of aqueous ammonia is added carefully in order to precipitate the magnetite particles, a reaction visually monitored since the color of the suspension turns to black. After homogenization, the suspension is centrifuged (three times) to separate the talc particles and magnetite from the ammonium chloride solution. The magnetic-talc particles obtained are then air-dried at  $120\ ^\circ\text{C}$ . The iron oxide content of the final composition is 33% wt/wt with respect to synthetic talc. The synthesized magnetic particles are composed of magnetite [18].

### 2.3. Nanocomposites syntheses

The PU/ $\text{Fe}_3\text{O}_4$ -synthetic talc nanocomposites were prepared using 20 g of pure polyurethane solubilised in MEK. After that the different filler content were added (0.5 wt.%, 1 wt.%, 3 wt.% and 10 wt.%) in relation to pure PU. After that the mixtures were placed in an ultraturrax mixer (IKA T18 Basic) during 30 min at 10,000 rpm. At the end of this time films of  $70\ \mu\text{m}$  of thickness were produced by casting.

### 2.4. Characterization methods

#### 2.4.1. Fourier transform infrared spectroscopy (FTIR)

The progress of the reactions were followed by Fourier transform infrared spectroscopy (FTIR-Perkin Elmer FTIR spectrometer model Spectrum100) as well as the incorporation of  $\text{Fe}_3\text{O}_4$ -synthetic talc, which was confirmed by the changes in the area of the characteristics bands in relation to pure PU (School of Chemistry/PUCRS).

#### 2.4.2. X-ray diffraction (XRD)

The XRD patterns were recorded on an INEL CPS 120 powder diffractometer with  $\text{Co K}\alpha_{1+2}$  radiations between  $0.334$  and  $127.206^\circ 2\theta$  with a step size of  $0.032$  (GET, University of Toulouse).

#### 2.4.3. Transmission electron microscopy (TEM)

Transmission electron microscopy (TEM) was used to determine the particle size, morphology of  $\text{Fe}_3\text{O}_4$ -talc and  $\text{Fe}_3\text{O}_4$ -talc nanocomposites. The samples were cryomicrotomed and analyzed in a Tecnai G2 T20 FEI operating at 200 kV. The medium particle size of the  $\text{Fe}_3\text{O}_4$ -synthetic talc and the  $\text{Fe}_3\text{O}_4$ -synthetic talc into the nanocomposites were measured using the Image J software (LabCEMM/PUCRS).



#### 2.4.4. Size exclusion chromatography (SEC)

The number average molecular weight ( $M_n$ ), weight average molecular weight ( $M_w$ ) and molecular weight distribution were obtained by size exclusion chromatography using a liquid chromatograph equipped with an isocratic pump-1515 (eluant: tetrahydrofuran (THF), flow: 1 mL/min) and refractive index detector-2414 Waters Instruments with styragel column set (45 °C) (School of Chemistry/PUCRS).

#### 2.4.5. Differential scanning calorimetry (DSC)

Differential scanning calorimetry (DSC) (TA Instruments model Q20 equipment) was used to measure the material's melting temperature ( $T_m$ ) and crystallization temperature ( $T_c$ ). The DSC analyses were performed in triplicate in two heating-cooling cycles, where the second heating run was used to collect the  $T_m$  data. The tests were carried out under  $N_2$  in a temperature range from  $-80$  °C to 200 °C with a heating rate of 20 °C  $min^{-1}$  (School of Chemistry/PUCRS).

#### 2.4.6. Thermogravimetric analyses (TGA)

The thermogravimetric analyses were performed in a SDT equipment (TA Instruments model Q600). The tests were carried out in a temperature range from 25 °C to 800 °C with a heating rate of 20 °C/min under constant  $N_2$  flow. The TGA were performed in triplicate and the results were repeatable (School of Chemistry/PUCRS).

#### 2.4.7. Magnetic properties

The magnetic properties were measured in a magnetometer Quantum design MPMS5 with a sensibility of  $10^{-8}$  emu. Samples PU/3 wt.%  $Fe_3O_4$ -synthetic talc and PU/10 wt.%  $Fe_3O_4$  – synthetic talc were weighted and disposed inside a magnetic capsule. For zero-field-cooled/field cooled ZFC/FC measurements first the sample was cooled until 2 K without magnetic field. After that a field of 10 Oe was applied and the measurements carried out at a rate of 1 K/min from 2 K to 300 K and from 300 K to 2 K. The magnetization cycles were performed at  $\pm 50,000$  Oe (5 T) at 2 K, 100 K, 200 K and 300 K. A  $^{57}Fe$  Mössbauer spectrum was collected at room temperature on a constant-acceleration conventional spectrometer with a 1.85 GBq source of  $^{57}Co$  (Rh matrix), and recorded over the range  $\pm 12$  mm/s with 512 channels. The Mössbauer spectrometer is composed of a compact detector  $\gamma$ -system for high count-rates and a conventional constant-acceleration Mössbauer device (WISSEL). The spectra were obtained at 300 K, and were recorded with a Canberra multichannel analyzer, coupled to a computer. The isomer shift was recorded with respect to  $\alpha$ -Fe metal. Lorentzian line-shapes were assumed for deconvolutions based on least-squares fitting procedures in Recoil Mossbauer Analysis Software 1.05 from Ken Lagarec & Denis Rancourt (Ottawa University, Canada). The  $\chi^2$  (2.90462) and misfit values were used to measure the goodness of the computer fit (Laboratoire de Chimie de Coordination/ University of Toulouse).

#### 2.4.8. Tensile strength analysis

Stress  $\times$  strain tests were carried out at 25 °C with rectangular shape films with a thickness close to 0.15 mm, length 12 mm and a width of approximately 7.0 mm on a DMTA equipment (model Q800, TA Instruments) with 1 N/min. The Young moduli of the materials were determined according to ASTM D638. The analyses were carried out in triplicate (School of Chemistry/PUCRS)

#### 2.4.9. Field emission scanning electron microscopy (FESEM)

The field emission scanning electron microscopy (FESEM) analyses were performed in a FEI Inspect F50 equipment in secondary electrons (SE) mode and used for assessment of the fillers distribution in the polymer matrix. The samples in a form of a film of 200  $\mu m$  were placed in a stub and covered with a thin gold layer (LabCEMM/PUCRS).

#### 2.4.10. Atomic force microscopy (AFM)

The Atomic force microscopy (AFM) was used to collect roughness, elastic mode as well as surface adhesion data of the pure PU and the nanocomposites. The analyses were performed in Peak force tapping mode using a Bruker Dimension Icon PT equipped with a TAP150A probe (Bruker, resonance frequency of 150 kHz and 5 N  $m^{-1}$  spring constant). The equipment was calibrated prior to samples measurements. The scanned area of the images was  $5 \times 5 \mu m^2$  with a resolution of 512 frames per area (LabCEMM/PUCRS).

### 3. Results and discussions

#### 3.1. FTIR analysis

Fig. 1((A)–(C)) shows the comparison of the pure PU(I), PU/10 wt.%  $Fe_3O_4$ -synthetic talc (II) and  $Fe_3O_4$  synthetic talc (III) spectra in different wavenumbers. The assignments of the bands are in agreement with those described in literature [15,18,19].

For pure PU and the nanocomposite PU/10 wt.%  $Fe_3O_4$ -synthetic talc (Fig. 1(A)), the bands in the region of 2939 and 2864  $cm^{-1}$  can be assigned to the different vibrational modes of  $CH_2$  group. The band at 1727  $cm^{-1}$  is characteristic of the C=O group of the urethane bond. The CO–O group bond appears at 1235  $cm^{-1}$ . In the regions of 1096, 1065 and 1042  $cm^{-1}$  the bands relatives of N–CO–O and C–O–C groups are observed [15]. In the  $Fe_3O_4$ -synthetic talc spectrum



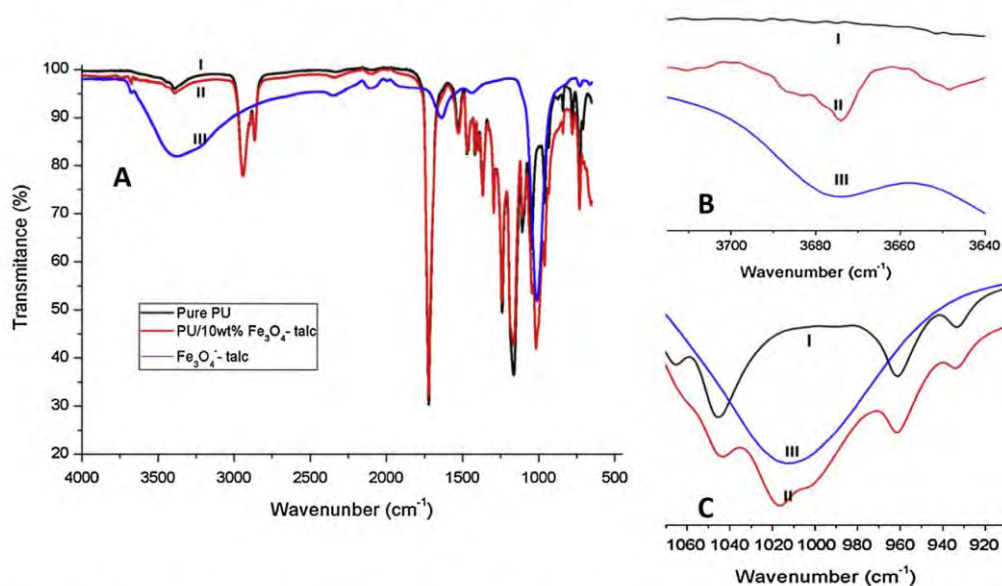


**Fig. 1.** FT-IR spectra of (I) pure PU; (II) PU/10 wt.% Fe<sub>3</sub>O<sub>4</sub>-synthetic talc and (III) Fe<sub>2</sub>O<sub>3</sub>-synthetic talc in different wavenumber A (4000–500 cm<sup>-1</sup>), B (3720–3640 cm<sup>-1</sup>) and C (1060–920 cm<sup>-1</sup>).

the band at 3677 cm<sup>-1</sup> is characteristic of the Mg<sub>3</sub>OH vibrations of the synthetic talc [11]. The bands around 3340 cm<sup>-1</sup> and 1630 cm<sup>-1</sup> are assigned to the O–H vibrations of the OH adsorbed on the Fe<sub>3</sub>O<sub>4</sub> nanoparticles present on the talc [3,18]. The band at 1040 cm<sup>-1</sup> is characteristic of Si–O bond and the band at 1014 cm<sup>-1</sup> is attributed to Si–O–Si bonds [14,15,20]. The incorporation of the Fe<sub>3</sub>O<sub>4</sub>-synthetic talc into the polymeric matrix is evidenced by the characteristic bands of the filler that appears in the nanocomposite PU/10 wt.% Fe<sub>3</sub>O<sub>4</sub>-talc when compared to pure PU, as for example the band around 1000 cm<sup>-1</sup> related with the Si–O–Si bonds (Fig. 1(C)) as well as the band at 3340 cm<sup>-1</sup> characteristic of the OH of the Fe<sub>3</sub>O<sub>4</sub> vibrations of the synthetic talc (Fig. 1(B)).

### 3.2. X-ray diffraction (XRD) and transmission electron microscopy (TEM)

The crystalline structure of the Fe<sub>3</sub>O<sub>4</sub>-talc as well as the PU/Fe<sub>3</sub>O<sub>4</sub>-synthetic talc nanocomposites were evaluated by XRD. The TEM images of the Fe<sub>3</sub>O<sub>4</sub>-synthetic talc sample and the PU/10% Fe<sub>3</sub>O<sub>4</sub>-talc nanocomposite are also presented aiming to corroborate the XRD findings.

The synthesized Fe<sub>3</sub>O<sub>4</sub>-talc present the most characteristics peaks of natural talc [11,12] with broader and less intense peaks as well as the Fe<sub>3</sub>O<sub>4</sub> characteristic peaks as depicted in Fig. 2 [21]. The literature describes [22] that the disappearance, in the nanocomposite materials, of the characteristic X-ray diffraction peak associated to the filler indicate a delamination of the silicate layers. Fig. 2 shows the diffractograms of the Fe<sub>3</sub>O<sub>4</sub>-synthetic talc and the nanocomposites with different filler content evidencing that the peak associated to the filler is not present in the nanocomposites diffractograms. Also the diffraction peak associated to the PU crystalline phase decreases when the Fe<sub>3</sub>O<sub>4</sub>-synthetic talc content increases indicating the good filler dispersion into the polymeric matrix achieved by the interaction filler–polymeric chain.

Fig. 2 also presents the TEM images for Fe<sub>3</sub>O<sub>4</sub>-synthetic talc and the nanocomposite PU/10% Fe<sub>3</sub>O<sub>4</sub>-synthetic talc corroborating the XRD results. As shown in Fig. 2(F) the TEM image for Fe<sub>3</sub>O<sub>4</sub>-synthetic talc present agglomerated particles while the nanocomposite Fig. 2(G) even with a high filler content of 10% shows that the filler is well dispersed into the polymeric matrix presenting small agglomerations points and an average particle size of 11 ± 0.6 nm. Similar results are presented for PP/PA6 blends and polyurethane filled with synthetic talc [16,17]. Another point to emphasize is the good compatibility of the polyurethane matrix and the talc achieved even when the nanocomposites are obtained by physical mixture. This behavior is probably due to the interaction of the OH of the filler with the polymeric chain [15].

### 3.3. Molecular weight analysis

The results of size exclusion chromatography are presented in Table 1. As it can be seen the molecular weight presents a tendency to increase with the increase of the filler content. This behavior probably is due to the presence of the iron (III), which is a well-known catalyst for polyurethane reaction formation [23]. The time of 30 min and temperature of 45 °C during the nanocomposite preparation through physical mixture must be the responsible for new bond formation and the increase of the molecular weight.

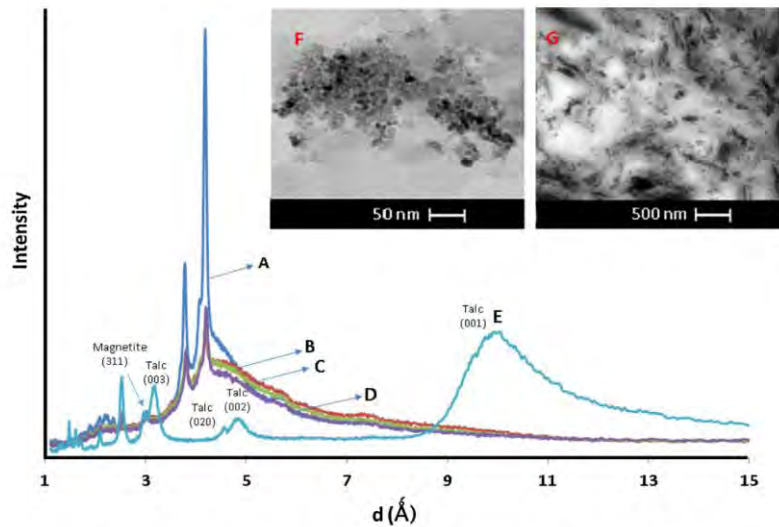


**Fig. 2.** XRD diffractogram patterns (A) PU pure, (B) PU/0.5 wt.%  $\text{Fe}_3\text{O}_4$ -synthetic talc, (C) PU/3 wt.%  $\text{Fe}_3\text{O}_4$ -synthetic talc, (D) PU/10 wt.%  $\text{Fe}_3\text{O}_4$ -synthetic talc, (E)  $\text{Fe}_3\text{O}_4$ -synthetic talc and TEM micrographs, (F)  $\text{Fe}_3\text{O}_4$ -synthetic talc, and (G) PU/10 wt.%  $\text{Fe}_3\text{O}_4$ -synthetic talc.

**Table 1**  
Results obtained by SEC analysis for the nanocomposites.

% Filler	Mn	Mw	Mn/Mw
0.0	39,962	70,133	1.8
0.5	70,735	103,197	1.5
3.0	79,318	124,155	1.6
10.0	65,761	97,936	1.5

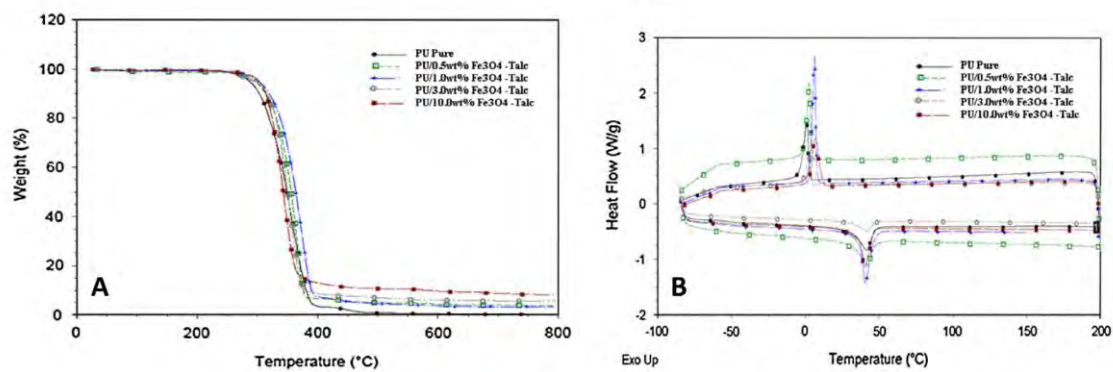


**Fig. 3.** TGA (A) and DSC (B) curves for pure PU and the nanocomposites  $\text{Fe}_3\text{O}_4$ -synthetic talc.

The use of fillers with OH available on the surface can result in a decrease in molecular weight of the nanocomposite when compared to the polyurethane matrix without filler addition. This behavior was observed for polyurethane based nanocomposites with titanium dioxide as filler as well as synthetic talc when obtained by *in-situ* polymerization [15,16,24]. The increase of the molecular weight with the increase of the filler addition must be highlighted because the molecular weight value is an important parameter for polymer applications [25]. Narrow molecular weight distribution values were obtained for the pristine PU as well as for the nanocomposites.



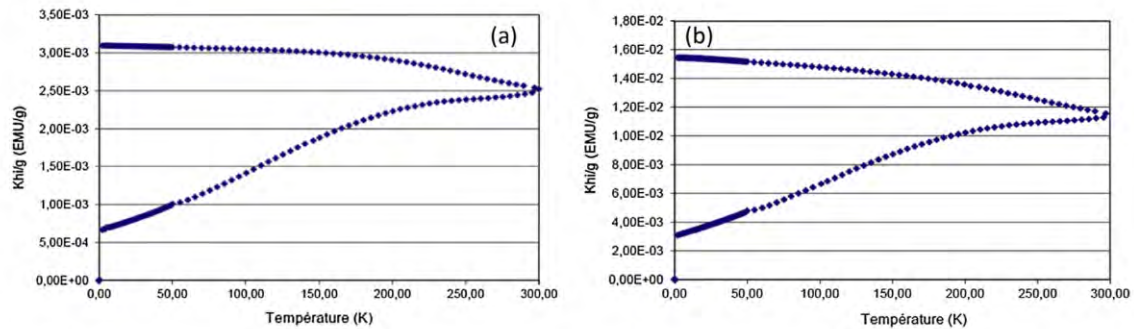


Fig. 4. Magnetization vs temperature for the nanocomposites: (a) PU/3 wt.%  $\text{Fe}_3\text{O}_4$ -synthetic talc, and (b) PU/10 wt.%  $\text{Fe}_3\text{O}_4$ -synthetic talc.

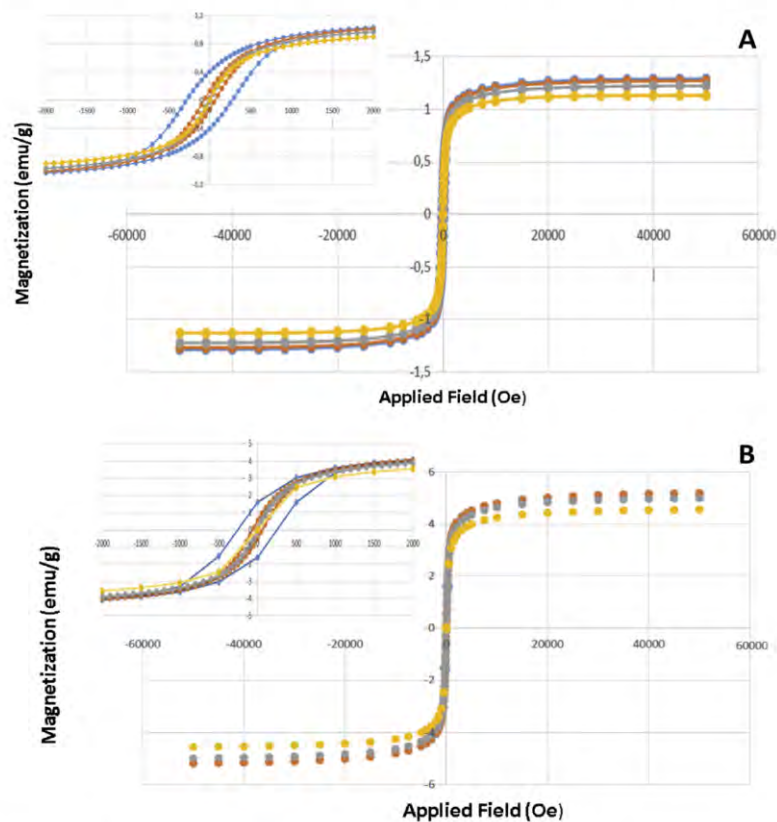


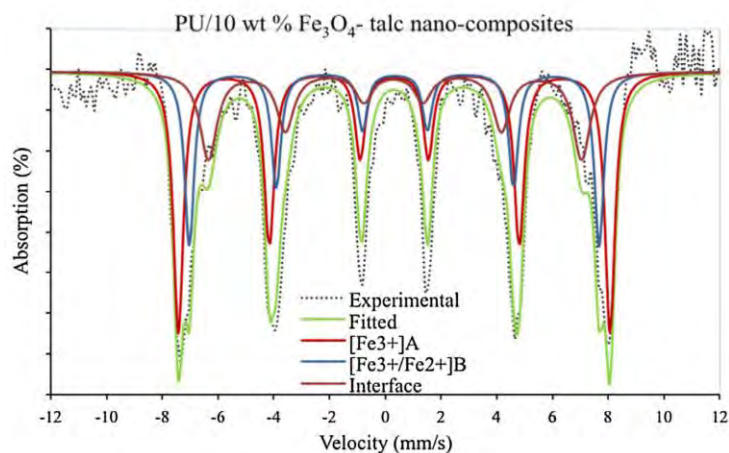
Fig. 5. Magnetization curves for (A) PU/3 wt.%  $\text{Fe}_3\text{O}_4$ -synthetic talc and (B) PU/10 wt.%  $\text{Fe}_3\text{O}_4$ -synthetic talc nanocomposites at different temperatures.

### 3.4. Thermal properties

In order to evaluate the thermal properties of the nanocomposites when compared to pure PU the TG measurements were performed. The TGA measurements are presented in Fig. 3(A). As it can be seen the nanocomposites  $\text{Fe}_3\text{O}_4$ -synthetic talc present a higher initial thermal decomposition temperature when compared to pure PU increasing from around 314 °C to 337 °C for the nanocomposite PU/1 wt.%  $\text{Fe}_3\text{O}_4$ -synthetic talc. The increase of the thermal stability was also described in literature for waterborne polyurethane filled with nano- $\text{Fe}_3\text{O}_4$  nanocomposites [19] as well as for polyurethane filled with synthetic talc-Ni nanocomposites [15]. For the samples with higher filler content the initial degradation temperature was lower when compared to the nanocomposite with PU/1 wt.%  $\text{Fe}_3\text{O}_4$ -synthetic talc of filler and can be attributed to a higher interaction filler-filler [15,24].

**Table 2**Magnetic properties of PU/3 wt.% Fe<sub>3</sub>O<sub>4</sub>-synthetic talc and PU/10 wt.% Fe<sub>3</sub>O<sub>4</sub>-synthetic talc nanocomposites at different temperatures.

Property	PU/3 wt.% Fe <sub>3</sub> O <sub>4</sub> -synthetic talc				PU/10 wt.% Fe <sub>3</sub> O <sub>4</sub> -synthetic talc			
	2 K	100 K	200 K	300 K	2 K	100 K	200 K	300 K
Saturation magnetization (emu/g)	1.25	1.25	1.22	1.12	5.18	5.14	4.95	4.5
Remanent magnetization (emu/g)	0.40	0.13	0.03	0	1.6	0.55	0.124	0
Coercivity (Oe)	275	74	12	0	250	60	13	0

**Fig. 6.** Mössbauer spectrum at 300 K of PU/10 wt.% Fe<sub>3</sub>O<sub>4</sub>-talc nano-composites.

The DSC curves are presented in Fig. 3(B). The crystallization temperature increased with the increase of the filler content. For pure PU the T<sub>c</sub> was of 0.8 °C and for the nanocomposite PU/10 wt.% Fe<sub>3</sub>O<sub>4</sub>-synthetic talc of 6.8 °C, corroborating with literature that synthetic talc acts as a nucleating agent [15]. The melting temperature values of the nanocomposites were similar to the pristine PU.

### 3.5. Magnetic properties

Magnetic properties were investigated by magnetization taken in the ZFC and FC processes and Mossbauer spectroscopy. Fig. 4 shows the temperature dependence of the magnetization carried out by ZFC and FC processes (in temperature range of 2–300 K) measured at 10 Oe for the PU/3 wt.% Fe<sub>3</sub>O<sub>4</sub>-synthetic talc and PU/10 wt.% Fe<sub>3</sub>O<sub>4</sub>-synthetic talc nanocomposites. For both samples, inside the range of 2–300 K it can be seen a typical ferromagnetic behavior with a blocking temperature higher than 300 K. The blocking temperature is field dependent and increases as temperature increases [26]. At this field (10 Oe) and temperature range (2–300 K) the nanocomposites present a ferromagnetic behavior.

The magnetization curves in function of the applied field at different temperatures (2 K, 100 K, 200 K and 300 K) for the PU/3 wt.% Fe<sub>3</sub>O<sub>4</sub>-synthetic talc and PU/10 wt.% Fe<sub>3</sub>O<sub>4</sub>-synthetic talc nanocomposites are presented in Fig. 5 and the magnetic properties in Table 2. The insert in Fig. 5 shows a magnification of the central area of the magnetization loops at these temperatures.

The hysteresis loops for the PU/3 wt.% Fe<sub>3</sub>O<sub>4</sub>-synthetic talc and PU/10 wt.% Fe<sub>3</sub>O<sub>4</sub>-synthetic talc for different temperatures presented similar saturation magnetization values with the temperature variation. For sample PU/3 wt.% Fe<sub>3</sub>O<sub>4</sub>-synthetic talc the values varied from 1.25 emu g<sup>-1</sup> at 2 K to 1.12 emu g<sup>-1</sup> at 300 K and for the sample PU/10 wt.% Fe<sub>3</sub>O<sub>4</sub>-synthetic talc the values varied from 5.18 emu g<sup>-1</sup> at 2 K to 4.5 emu g<sup>-1</sup> at 300 K. For nanocomposites PMMA/magnetite a value of 13 emu g<sup>-1</sup> at room temperature was found for a sample with 32 wt.% of iron oxide and a value of 3 emu g<sup>-1</sup> for a sample with 6 wt.% iron oxide [6]. Our results were slight higher once the sample PU/10 wt.% Fe<sub>3</sub>O<sub>4</sub>-synthetic talc which contains 3.3 wt.% of iron oxide presented a value of 4.5 emu g<sup>-1</sup> at 300 K. Very low coercivity values were observed for both nanocomposites varying from 275 Oe at 2 K to 0 Oe at 300 K for the sample PU/3 wt.% Fe<sub>3</sub>O<sub>4</sub>-synthetic talc and from 250 Oe at 2 K to 0 Oe at 300 K for the sample PU/10 wt.% Fe<sub>3</sub>O<sub>4</sub>-synthetic talc. For the nanocomposites PMMA/magnetite 32 and 6 wt.% values of 240 and 220 Oe respectively were found at room temperature [6].

The Mossbauer spectrum at 300 K for the sample PU/10 wt.% Fe<sub>3</sub>O<sub>4</sub>-synthetic talc presented in Fig. 6 and Table 3 corroborates that the obtained nanocomposites behavior as a ferromagnetic material. The spectrum is decomposed in 3 sextets, two sextet components corresponding to [Fe<sup>3+</sup>]A and [Fe<sup>3+</sup>/Fe<sup>2+</sup>]B in site of nanomagnetite (size of particles around



**Table 3**  
Mössbauer parameters at 300 K of PU/10 wt.% Fe<sub>3</sub>O<sub>4</sub>-synthetic talc nano-composites.

	$\delta$ (mm/s)	$\Delta$ (mm/s)	$H$ (kOe)	$\Gamma$ site populations (mm/s)	(%)
Sextet 1	0.308(10)	-0.001(10)	480.2(12)	0.218(23)	45.5(68)
Sextet 2	0.320(15)	-0.011(15)	456.0(16)	0.206(44)	28.7(85)
Sextet 3	0.308(40)	0.028(39)	415.4(39)	0.370(75)	25.9(61)

$\delta$ : isomer shift to respect of  $\alpha$ -Fe metal in mm/s;  $\Delta$  quadrupole splitting in mm/s;  $H$  magnetic field kOe;  $\Gamma$  width at half height in mm/s; site populations in %.

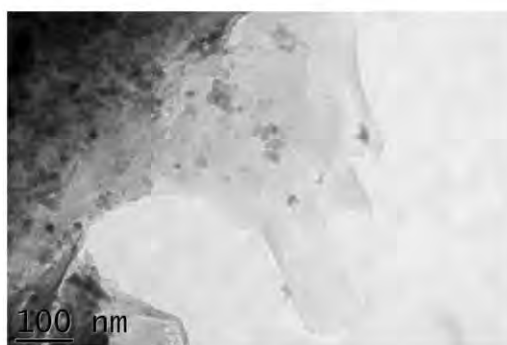


**Fig. 7.** Transmission electron microscopy image of Fe<sub>3</sub>O<sub>4</sub>33%-Talc66% - w/w. The small black particles are nanomagnetite and talc appears with in gray form.

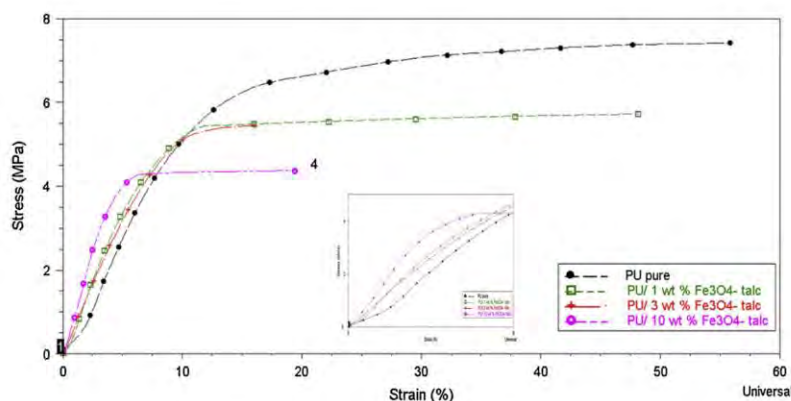


**Fig. 8.** Stress/strain curves of nanocomposites and pure PU.

10 nm) and the third component with a broad distribution corresponding to interface, where the diffusion of Mg and Fe cations can take place, as suggested by Handke et al. [27]. The result indicates clearly that the interface between nanomagnetite and talc is on the edge of talc particle. This indirect observation is corroborated by the TEM image presented in Fig. 7. In transmission electron microscopy, magnetite nano-particles appear with a size around 10 nm and they are positioned preferentially on the edges of the synthetic talc particles.

### 3.6. Mechanical properties

The stress/strain properties of Pure PU and the nanocomposites are presented in Fig. 8 and Table 4. The stress at break and the deformation values decreases with the filler content probably caused by the new fracture mechanisms involved, rigidity augmentation and also due to the filler–filler interaction instead of filler–polymer interaction with the increase of the filler content [15,18,19,24].

**Table 4**  
Mechanical properties of the nanocomposites and pure PU.

% Filler	Stress at break (MPa)	Strain at break (%)	Young modulus (MPa)
0.0	7.1 ± 0.6	52 ± 10	0.5 ± 0.1
1.0	6 ± 1	47 ± 7	0.6 ± 0.1
3.0	4.7 ± 0.6	12 ± 4	0.6 ± 0.0
10.0	4 ± 1	16.5 ± 5	0.9 ± 0.1

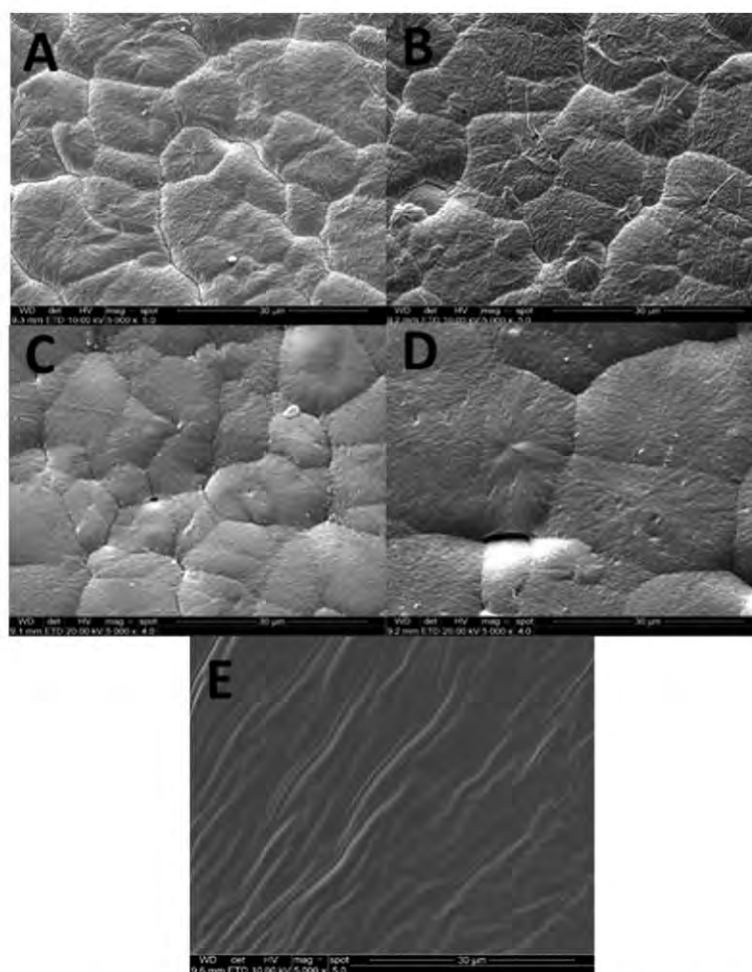


**Fig. 9.** Micrographs, mode SE, of the materials at magnification of 5000 × (A) PU pure, (B) PU/0.5 wt.%  $\text{Fe}_3\text{O}_4$ -synthetic talc, (C) PU/1 wt.%  $\text{Fe}_3\text{O}_4$ -synthetic talc, (D) PU/3 wt.%  $\text{Fe}_3\text{O}_4$ -synthetic talc, (E) PU/ 10 wt.%  $\text{Fe}_3\text{O}_4$  - synthetic talc.

As it can be seen from [Table 4](#) the increase in the filler content does not alter the elastic modulus of the polymer except for the nanocomposite PU/10 wt.%  $\text{Fe}_3\text{O}_4$ -synthetic talc where a small increase was observed.

This behavior can be associated with a more important cohesive energy among the polymer structure and the filler through hydrogen bonding. These inter-associated structures (polymer–filler) are also responsible by the increase of the crystallinity and  $T_c$  of the polyurethane and as a consequence a decrease in the mechanical strength as well as in the polymer deformability.

### 3.7. Scanning electron microscopy

[Fig. 9](#) shows the SEM images of PU pure and the nanocomposites PU/0.5 wt.%  $\text{Fe}_3\text{O}_4$ -synthetic talc, PU/1 wt.%  $\text{Fe}_3\text{O}_4$ -synthetic talc, PU/3 wt.%  $\text{Fe}_3\text{O}_4$ -synthetic talc and PU/10 wt.%  $\text{Fe}_3\text{O}_4$ -synthetic talc. It could be highlighted that the

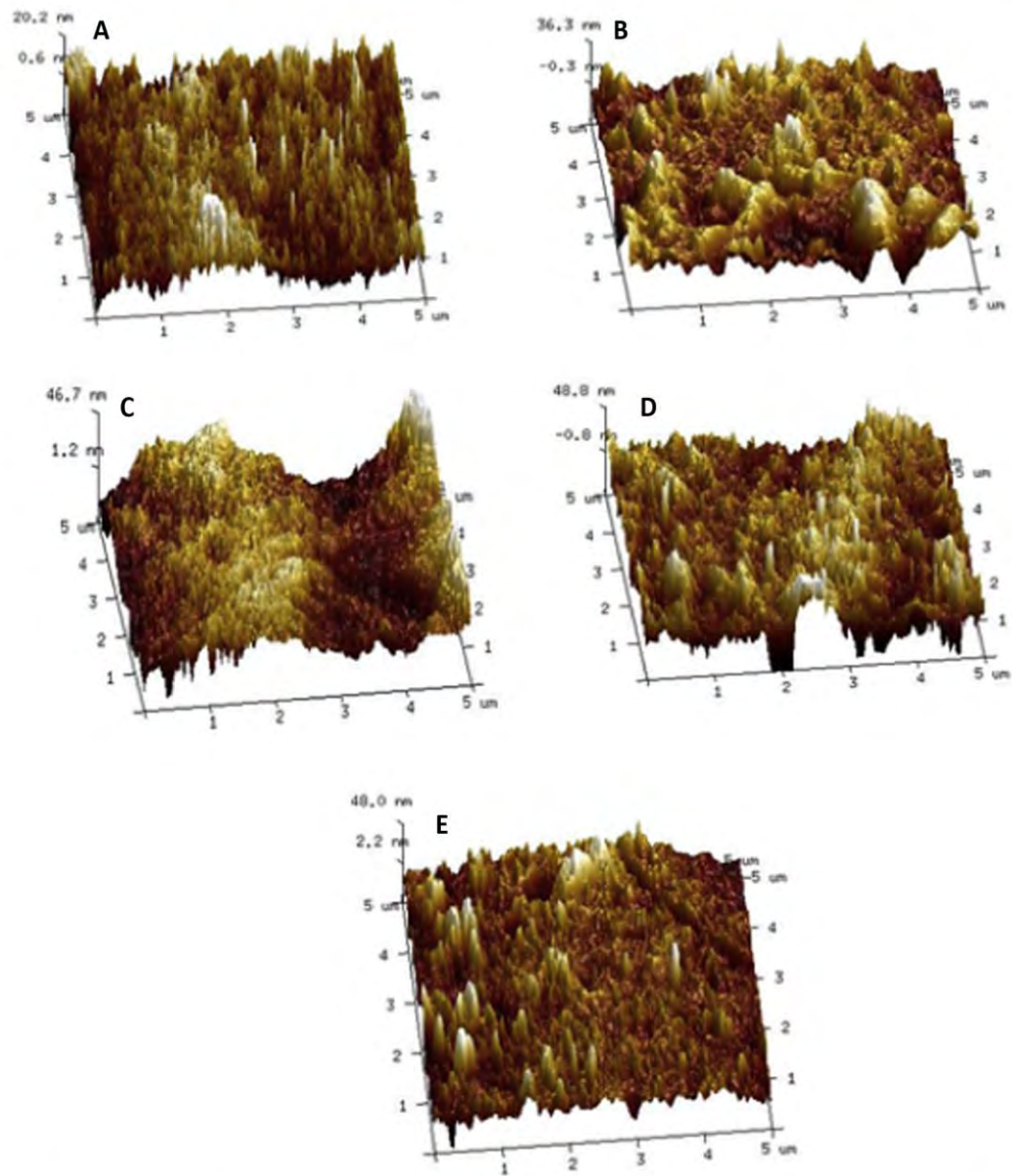


**Fig. 10.** AFM images (height) (A) PU pure, (B) PU/0.5 wt.%  $\text{Fe}_3\text{O}_4$ -synthetic talc, (C) PU/1 wt.%  $\text{Fe}_3\text{O}_4$ -synthetic talc, (D) PU/3 wt.%  $\text{Fe}_3\text{O}_4$ -synthetic talc, and (E) PU/10 wt.%  $\text{Fe}_3\text{O}_4$ -synthetic talc.

**Table 5**

Average roughness (Ra); root mean square roughness (Rq); maximum height roughness (Rmax); adhesion (Adh) for the nanocomposites PU/ $\text{Fe}_3\text{O}_4$ -synthetic talc with different filler content.

% Filler	Ra (nm)	Rq (nm)	Rmax (nm)	Adh (nN)
0.0	4.2	5.4	55	11
0.5	7.3	9.7	86	14
1.0	11.4	14	105	13.9
3.0	10.3	13.8	213	16.8
10.0	7.3	10.8	171	17.3



SEM images displayed in Fig. 9 corroborates that the fillers are well dispersed into the polyurethane matrix suggesting a good compatibility of talc with the polymeric matrix. The talc fillers can interact with the polyurethane chain through the Mg—OH and Si—OH groups on the edges of the talc layers allowing a good dispersion of the filler without the addition of coupling agents [15,16]. The filler Fe<sub>3</sub>O<sub>4</sub>-synthetic talc also can interact with the Fe—OH present in the Fe<sub>3</sub>O<sub>4</sub> surface. The same behavior was related for PVA/talc, PVA/CaCO<sub>3</sub>, PU/synthetic Ni-talc composites evidencing the important role of the OH present in talc and CaCO<sub>3</sub> nanocomposites allowing a good dispersion of the fillers [28,15].

In SEM images of the nanocomposites until 1% of filler content a very similar PU microstructure are observed. In the nanocomposite with 3 wt.% of filler addition can be observed a more important change in the morphology with the increase of the size of the spherulites and for the nanocomposite with 10 wt.% of filler the spherulites disappeared given place to fibrils. This change indicates the reorganization of the polyurethane in presence of higher filler content. The crystallization and the hydrogen bonding strongly affect the morphology and properties of polymers [29]. For the nanocomposites Fe<sub>3</sub>O<sub>4</sub>-synthetic talc the morphological changes are probably related with the balance of the interaction hard-soft segments of polyurethane, filler-polymer and filler-filler being the latter more important with higher filler content. The higher density of the interaction of the PU soft segments-filler can difficult the crystallization of the soft segments in the spherulitic form. These morphological changes allied to a good dispersion of the filler and the interaction filler-polymer affect directly the thermal and mechanical properties [20,30,31] as discussed earlier. These morphological changes also affect the roughness as will be discussed using the results obtained by AFM.

### 3.8. Atomic force microscopy-AFM

Fig. 10 and Table 5 present the AFM topographs showing the average roughness (Ra), root mean square roughness (Rq), maximum height roughness (Rmax), adhesion (Adh) and Young moduli for the nanocomposites PU/Fe<sub>3</sub>O<sub>4</sub>-synthetic talc with different filler content. These results indicates that the addition of the filler improves the roughness until 1% and starts to decrease in agreement with the change observed in the nanocomposites morphology by SEM and topography by AFM. In nanocomposites WPU/Fe<sub>3</sub>O<sub>4</sub> Zhang and co-workers observed a smooth of the surface until 1% of Fe<sub>3</sub>O<sub>4</sub> and an increase after 2% of Fe<sub>3</sub>O<sub>4</sub> addition probably due to the particles aggregation [19].

We observed by AFM that in pure PU, PU/0.5 wt.% Fe<sub>3</sub>O<sub>4</sub>-synthetic talc and PU/1 wt.% Fe<sub>3</sub>O<sub>4</sub>-synthetic talc the hard domains of PU (lighter regions) present some connectivity or continuity associated with them. This behavior is probably due to the hydrogen bonding between hard/hard segments and hard/soft segments being more important than the polymer/filler interaction. When higher filler content are added in the nanocomposites, PU/3 wt.% Fe<sub>3</sub>O<sub>4</sub>-synthetic talc and PU/10 wt.% Fe<sub>3</sub>O<sub>4</sub>-synthetic talc, the polymer/filler and filler/filler interaction became more important. In this case the hard and soft segments start to reorganize increasing the miscibility between them due to the new hydrogen bond among the filler and polymeric chain. With 10% of filler content we have a complete different morphology and topography as evidenced by SEM and AFM. The adhesion increases with the filler content until 3% and can be related to the roughness increasing as presented in Table 4.

## 4. Conclusions

Magnetic properties are important for the design of new polymeric devices for different applications. X-ray diffraction allied to microscopy (TEM, SEM, AFM) showed the good dispersion of the filler into the polymeric matrix resulting in nanocomposites PU/Fe<sub>3</sub>O<sub>4</sub>-synthetic talc with improved thermal stability and magnetic properties. These results evidenced that the synthetic talc is interesting material, to be used as mineral filler improving the polymer properties, as noticed before. It also must be highlighted that these synthetic talcs can be produced with different functionalization allowing the obtainment of polymeric nanocomposites with diverse properties.

## Acknowledgements

The authors would like to thank PRONEX/FAPERGS for financial support. SE and RL acknowledge CNPq for DT grant.

## References

- [1] F. Yan, J. Li, J. Zhang, F. Liu, W. Yang, J. Nanopart. Res. 11 (2009) 289–296.
- [2] S. Balakrishnan, M.J. Bonder, G. Hadjipanayis, Magn. Magn. Mater. (2009) 117–122.
- [3] S.K. Giri, G.C. Pradhan, N.J. Das, Polym. Res. 21 (2014) 446.
- [4] S. Kalia, S. Kango, A. Kumar, Y. Haldorai, B. Kumari, R. Kumar, Colloid Polym. Sci. 292 (2014) 2025–2052.
- [5] A.A. NovaKova, V.Y. Lanchinskaya, A.V. Volkov, T.S. Gendler, T.Y. Kiseleva, S.B. Moskvina, S.B. Zevin, Magn. Magn. Mater. (2003) 354–357.
- [6] P. Dallas, V. Georgakilas, D. Niarchos, P. Komninou, T. Kehagias, D. Petridis, Nanotechnology (2006) 2046–2053.
- [7] S. Kirchberg, M. Rudolph, G. Ziegmann, U.A. Peuker, J. Nanomater. (2012) 1–8.
- [8] A. Dumas, E. Gardes, C. Le Roux, F. Martin, P. Micoud, Process for preparing a magnetic talcous composition and magnetic talcous composition. PCT Int. Pat. Appl. WO 2013093376 A1 June 27 2013 Fr. Pat. Appl. FR 2984872 A1 June 28 2013.
- [9] A. Dumas, C. Le Roux, F. Martin, P. Micoud, Process for preparing a composition comprising synthetic mineral particles and composition. PCT Int. Pat. Appl. WO 2013004979 A1 Jan 10 2013 Fr. Pat. FR 2977580 B1 August 16 2013.
- [10] M. Yousfi, S. Livia, A. Dumas, C. Le Roux, J. Crépin-Leblond, M. Greenhill-Hooper, J. Duchet-Rumeau, J. Colloid Interface Sci. 403 (2013) 29–42.

- [11] A. Dumas, F. Martin, E. Ferrage, P. Micoud, C. Le Roux, S. Petit, *Appl. Clay Sci.* 85 (2013) 8–18.
- [12] A. Dumas, F. Martin, C. Le Roux, P. Micoud, S. Petit, E. Ferrage, J. Brendlé, O. Grauby, M. Greenhill-Hooper, *Phys. Chem. Miner.* 40 (2013) 361–373.
- [13] K. Chabrol, M. Gressier, N. Pebere, M.J. Menu, F. Martin, J.P. Bonino, C. Marichal, J. Brendlé, *J. Mater. Chem.* 20 (2010) 9695–9706.
- [14] F. Martin, P. Micoud, L. Delmotte, C. Marichal, R. Le Dred, P. De Parseval, A. Mari, J.P. Fortuné, S. Salvi, D. Béziat, O. Grauby, *J. Ferret, Can. Mineral.* 37 (1999) 997–1006.
- [15] M. Prado, G. Dias, C. Carone, R. Ligabue, A. Dumas, C. Roux, P. Micoud, F. Martin, S. Einloft, *J. Appl. Polym. Sci.* 2015 (1854) 4.
- [16] G. Dias, M. Prado, C. Carone, R. Ligabue, A. Dumas, F. Martin, C. Roux, P. Micoud, S. Einloft, *Polym. Bull.* 2015 (In press).
- [17] M. Yousfi, S. Livi, A. Dumas, J. Crépin-Leblond, M. Greenhill-Hooper, J. Duchet-Rumeau, *J. Appl. Polym. Sci.* 131 (2014) 40453.
- [18] C. Meiorin, D. Muraca, K. Pirota, M. Aranguren, M. Mosiewicki, *Eur. Polym. J.* 53 (2014) 90–99.
- [19] S. Zhang, Y. Li, L. Peng, Q. Li, S. Chen, K. Hou, *Composites Part A* 55 (2013) 94–101.
- [20] M.G. Fonseca, C.R. Silva, J.S. Barone, C. Airoidi, *Mater. Chem.* 10 (2000) 789.
- [21] Angela Dumas, *Elaboration de Nouveaux procédés de Synthèse et Caractérisation de Talcs Sub-Microniques: de la Recherche Fondamentale vers des Applications Industrielles*. Toulouse. 2013. Thesis. Sciences de la Terre et des Planètes Solides, Université Toulouse III-Paul Sabatier.
- [22] S. Ray, M. Okamoto, *Prog. Polym. Sci.* 28 (2003) 1539–1641.
- [23] V. De Lima, N. Pelissoli, J. Dullius, R. Ligabue, S. Einloft, *J. Appl. Polym. Sci.* 115 (2010) 1797.
- [24] V. Da Silva, L. Dos Santos, S. Subda, R. Ligabue, M. Seferin, C. Carone, S. Einloft, *Polym. Bull.* 70 (2013) 1819–1833.
- [25] M. Rogers, T. Long, *Synthetic Methods in Step-Growth Polymers*. John Wiley & Sons Inc, 2003.
- [26] E. Choi, Y. Ahn, E. Hahn, *J. Korean Phys. Soc.* 53 (2008) 2090–2094.
- [27] B. Handke, T. Slezak, M. Kubik, J. Korecki, *Radioanal. Nucl. Chem.* 246 (1) (2000) 27–32.
- [28] G.K. Latinwo, D.S. Aribike, A.A. Susu, S.A. Kareem, *Nat. Sci.* 8 (2010) 23.
- [29] J. Sheth, D. Klinedinst, G. Wilkes, I. Yilgor, E. Yilgor, *Polymer* 46 (2005) 7317–7322.
- [30] L.A. Castillo, S.E. Barbosa, N.J. Capiati, *J. Polym. Res.* 20 (2013) 152.
- [31] S. Jain, M. Misra, A.K. Mohanty, A.K. Ghosh, *J. Polym. Environ.* 20 (2012) 1027–1037.


## 4.2. Capítulo II: Poliuretano base água com Fe<sub>3</sub>O<sub>4</sub> talco sintético

Este capítulo descreve a síntese e caracterização de WPU/Fe<sub>3</sub>O<sub>4</sub> - talco sintético (em gel) disperso em poliuretano base aquosa, por meio do artigo intitulado de "Waterborne polyurethane/Fe<sub>3</sub>O<sub>4</sub> – synthetic talc composites: synthesis, characterization and magnetic properties" publicado na Polymer Bulletin. Foi sintetizado poliuretano base água e posteriormente foram adicionadas diferentes quantidades de talco sintético-Fe<sub>3</sub>O<sub>4</sub> na forma de gel (0,5; 5;10; 30 e 40% m/m). Os nanocompositos sintetizados foram caracterizados por FTIR, RMN, DRX, TEM, MEV, AFM, TGA, DSC, DMTA e propriedades magnéticas (Mössbauer, curvas de magnetização e magnetização vs temperatura). A técnica de RMN, foi fundamental para avaliar a interação polímero/carga. Os resultados demonstraram que há uma interação da carga/polímero. Foi utilizado Mössbauer para observar a características magnéticas do material quando submetidas a diferentes temperaturas. Os nanocompositos apresentam um comportamento ferromagnético a baixo da temperatura de Curie (aproximadamente 120K) e um comportamento superparamagnético acima de 120K.





## Waterborne polyurethane/Fe<sub>3</sub>O<sub>4</sub>-synthetic talc composites: synthesis, characterization, and magnetic properties

Leonardo M. dos Santos<sup>1</sup> · Rosane Ligabue<sup>1,2</sup> · Angela Dumas<sup>3</sup> ·  
Christophe Le Roux<sup>3</sup> · Pierre Micoud<sup>3</sup> · Jean-François Meunier<sup>4</sup> ·  
François Martin<sup>3</sup> · Marta Corvo<sup>5</sup> · Pedro Almeida<sup>5,6</sup> ·  
Sandra Einloft<sup>1,2</sup> 

Received: 6 March 2017 / Revised: 26 June 2017 / Accepted: 14 July 2017  
© Springer-Verlag GmbH Germany 2017

**Abstract** Nano-Fe<sub>3</sub>O<sub>4</sub>-synthetic talc gel was used as filler in the synthesis of waterborne polyurethane/Fe<sub>3</sub>O<sub>4</sub>-synthetic talc nanocomposites. This filler presents numerous edges (Si–O and Mg–O) and OH groups easily forming hydrogen bonds and polar interaction with water conferring hydrophilic character, consequently improving filler dispersion within a water-based matrix. Yet, the use of waterborne polyurethane (WPU) as matrix must be highlighted due to its environmentally friendly characteristics and low toxicity compared to solvent-based product. Fe<sub>3</sub>O<sub>4</sub>-synthetic talc-nanofillers were well dispersed into the polyurethane matrix even at high filler content as supported by XRD and TEM analyses. NMR indicates the interaction of filler OH groups with the matrix. For all nanocomposites, one can see a typical ferromagnetic behavior below Curie temperature (about 120 K) and a superparamagnetic behavior above this temperature. The use of Fe<sub>3</sub>O<sub>4</sub>-synthetic talc for obtaining magnetic nanocomposites resulted in improved materials with superior mechanical properties compared to solvent-based nanocomposites.

**Electronic supplementary material** The online version of this article (doi:[10.1007/s00289-017-2133-9](https://doi.org/10.1007/s00289-017-2133-9)) contains supplementary material, which is available to authorized users.

✉ Sandra Einloft  
einloft@pucrs.br

<sup>1</sup> Post-Graduation Program in Materials Engineering and Technology, Pontifical Catholic University of Rio Grande do Sul-PUCRS, Porto Alegre, Brazil

<sup>2</sup> School of Chemistry, Pontifical Catholic University of Rio Grande do Sul-PUCRS, Porto Alegre, Brazil

<sup>3</sup> ERT 1074 Géomatériaux-GET UMR 5563 CNRS-Université de Toulouse, Toulouse, France

<sup>4</sup> Laboratoire de Chimie de Coordination, Université de Toulouse, Toulouse, France

<sup>5</sup> CENIMAT/I3N, Universidade Nova de Lisboa, 2829-516 Caparica, Portugal

<sup>6</sup> Área Departamental de Física, Instituto Superior de Engenharia de Lisboa, Instituto Politécnico de Lisboa, 1959-007 Lisbon, Portugal

**Keywords** Waterborne polyurethane · Nanocomposites · Synthetic  $\text{Fe}_3\text{O}_4$ -talc · Physical mixture

## Introduction

Magnetic nanoparticles, in particular  $\text{Fe}_3\text{O}_4$ , can be used in electromagnetic screening devices, magnetic sensing, biotechnology, biomedicine, biomedical application, drug delivery, etc [1–4]. A significant effort has been made to develop new strategies for obtaining magnetic materials. The myriad of possible application of magnetic materials corroborates the importance of having a platform of materials combining magnetic properties with specific needs for each application field. Magnetic nanoparticles tend to aggregation limiting their utilization [3, 5]. Development of strategies to avoid agglomeration is very important to broaden the use of magnetic nanoparticles. Magnetic nanoparticles can be encapsulated into polymeric material to avoid this phenomenon and improve their chemical stability [3]. The incorporation of nanosized particles into a polymeric matrix is a well-known subject. However, homogeneous distribution of filler into the polymeric matrix is crucial for the obtainment of nanocomposites with superior properties relative to the neat constituents [1, 6]. To overcome these issues, we developed the usage of a synthetic talc containing magnetic particles in their composition [7, 8] to obtain magnetic nanocomposites polyurethane/ $\text{Fe}_3\text{O}_4$ -synthetic talc [9]. We also described the usage of different synthetic talcs as nanofillers reinforcement for polyurethane [10–12]. The usage of synthetic talc as filler for other polymeric matrix was also reported, namely polypropylene and polyamide 6 systems [13] and polypropylene/polyamide 6 blends [14]. Synthetic talc presents numerous edges (Si–O and Mg–O) and OH groups easily forming hydrogen bonds and polar interaction with water [15]. It can be produced in the form of nano-synthetic talc gel suspension with a hydrophilic character (unlike natural talc which is hydrophobic) which can improve filler dispersion within matrix [15]. Water-based materials are environmentally and friendly materials due to their low toxicity as compared to solvent-based products [16–18]. Waterborne polyurethane (WPU) is a generation of polyurethanes (PU), whereas water is used as solvent largely reducing volatile organic compounds release [17, 18]. WPU has been used in different fields, such as adhesives, coatings, membranes, and biological products [16–18]. WPU presents advantages relative to organic solvent-based polyurethane, including good process abilities, versatile structure–property, low viscosity, high molecular weight and high adhesion, etc [16–18]. However, the films present lower thermal stability, mechanical properties, and solvent resistance than solvent-based products [16, 17]. To our knowledge, the obtainment of WPU/ $\text{Fe}_3\text{O}_4$ -synthetic talc nanocomposites is a new strategy to obtain environmental friendly magnetic materials.



In this work, WPU/Fe<sub>3</sub>O<sub>4</sub>-synthetic talc nanocomposites were obtained with different filler contents. Furthermore, we evaluated the filler content in nanocomposites formation, morphology, thermal, mechanical, and magnetic properties.

## Experimental

### Polyurethane synthesis

Synthesis of WPU was carried out by pre-polymer method as described elsewhere [19]. Initially, the NCO-terminated PU pre-polymer was synthesized in five-necked flask at 80–100 °C during 60 min using excess of isophorone diisocyanate (IPDI, for synthesis, Merck), diol (MM = 1000 g/mol), dimethylol propionic acid (DMPA, 99%, Perstorp), and dibutyl tin dilaurate [DBTDL Miracema-Nuodex Ind (0.1wt%)] as catalyst. The NCO/OH ratio of 1.7 was used. The carboxylic acid of DMPA was neutralized with trimethylamine (Perstorp). The free NCO content was monitored by titration with dibutylamine (Bayer) until reach 3.5%. At the next step, the NCO residual of the pre-polymer was reacted with hydrazine and used as chain extender, in water. The solid content of final dispersion was 35 wt%.

### Synthesis of the filler Fe<sub>3</sub>O<sub>4</sub>-synthetic talc

Magnetic-talc fillers were synthesized according to process described elsewhere [7, 8]. An aqueous solution (300 mL) of iron chloride (0.65 M) was prepared by dissolving 35.02 g (129.57 mmol) iron(III) chloride hexahydrate (FeCl<sub>3</sub>·6H<sub>2</sub>O) and 12.88 g (64.78 mmol) of iron(II) chloride tetrahydrate (FeCl<sub>2</sub>·4H<sub>2</sub>O) in a molar ratio identical to magnetite (Fe<sup>2+</sup>:Fe<sup>3+</sup> = 1:2). Then, under mechanical stirring, the aqueous solution of iron chlorides is added to a suspension of synthetic talc [with structural formulae Si<sub>4</sub>Mg<sub>3</sub>O<sub>10</sub>(OH)<sub>2</sub>, corresponding to 30 g of dry talc in 1 L of distilled water]—product referred as 6H [20]—the resulting yellow–orange suspension is heated up to 70 °C. Then, 80 mL of aqueous ammonia is added carefully to precipitate the magnetite particles, a reaction visually monitored, since the color of the suspension turns to black. After homogenization, the suspension is centrifuged (3×) to separate the talc particles and magnetite from the ammonium chloride solution.

### Nanocomposites syntheses

The PU/Fe<sub>3</sub>O<sub>4</sub>-synthetic talc nanocomposites were prepared by adding the filler Fe<sub>3</sub>O<sub>4</sub>-nano-talc gel suspension (solid content 33%) into the WPU dispersion (previously synthesized) to obtain nanocomposites containing 0.5, 5.0, 10.0, 30.0, and 40.0% of filler relative to neat polymer matrix. In the next step, mixtures were placed in Ultraturrax mixer (IKA T18 Basic) during 30 min at 10,000 rpm. At the end of this time, films of 70 μm of thickness were produced by casting.

## Characterization methods

### *Fourier transform infrared spectroscopy (FTIR)*

The films were characterized by Fourier transform infrared spectroscopy (FTIR-Perkin Elmer spectrometer model Spectrum100, using UATR from 4000 at  $650\text{ cm}^{-1}$ ) to evaluate  $\text{Fe}_3\text{O}_4$ -synthetic talc incorporation into the polymeric matrix, confirmed by the changes in the characteristic band area of nanocomposites relative to neat WPU.

### *X-ray diffraction (XRD)*

XRD analyses were performed by INEL CPS 120 powder diffractometer with  $\text{Cu K}\alpha_{1+2}$  radiations between  $0.334$  and  $127.206^\circ 2\theta$  with a step size of  $0.032$ .

### *Transmission electron microscopy (TEM)*

Particle size, and morphology of  $\text{Fe}_3\text{O}_4$ -talc and  $\text{Fe}_3\text{O}_4$ -talc nanocomposites were achieved by transmission electron microscopy (TEM). Samples were cryomicrotomed and analyzed on Tecnai G2 T20 FEI operating at  $200\text{ kV}$ . Image J software was used to assess medium particle size of  $\text{Fe}_3\text{O}_4$ -synthetic talc and  $\text{Fe}_3\text{O}_4$ -synthetic talc into nanocomposites.

### *Differential scanning calorimetry (DSC)*

Melting temperature ( $T_m$ ) was assessed by differential scanning calorimetry (DSC) (TA Instruments model Q20 equipment). Analyses were performed in triplicate in two heating-cooling cycles. Temperature range from  $-80$  to  $200\text{ }^\circ\text{C}$  with a heating rate of  $20\text{ }^\circ\text{C min}^{-1}$  was used under  $\text{N}_2$  atmosphere.

### *Thermogravimetric analyses (TGA)*

Thermogravimetric analyses were performed by SDT equipment (TA Instruments model Q600). Temperature range from  $25$  to  $800\text{ }^\circ\text{C}$  with a heating rate of  $20\text{ }^\circ\text{C/min}$  under constant  $\text{N}_2$  flow was used for all samples. TGA were performed in triplicate and the results were repeatable. TGA was used to calculate the  $\text{Fe}_3\text{O}_4$ -synthetic talc content incorporated in nanocomposites using the formula used by Tang et al. [21]:  $(\text{wt}\% \text{WPU}_{25-600\text{ }^\circ\text{C}} - \text{wt}\% \text{WPU/Fe}_3\text{O}_4\text{-synthetic talc}_{200-600\text{ }^\circ\text{C}})$ .

### *Magnetic properties*

Magnetometer Quantum design MPMS5 with a sensibility of  $10^{-8}\text{ emu}$  was used to assess the magnetic properties. Samples WPU/0.5, 5, 10, 30, and 40 wt%  $\text{Fe}_3\text{O}_4$ -synthetic talc were weighted and disposed inside a magnetic capsule. For zero-field-cooled/field cooled ZFC/FC measurements, first, the sample was cooled until  $2\text{ K}$  without magnetic field. In the next step, a field of  $10\text{ Oe}$  was applied and the



measurements performed at a rate of 1 K/min from 2 to 300 K and from 300 to 2 K. Magnetization cycles were performed at  $\pm 50,000$  Oe (5 T) at 2, 100, 200, and 300 K. A  $^{57}\text{Fe}$  Mössbauer spectrum was performed at room temperature on constant-acceleration conventional spectrometer with a 1.85 GBq source of  $^{57}\text{Cu}$  (Rh matrix). Mössbauer spectra were recorded over the range  $\pm 12$  mm/s with 512 channels. Mössbauer spectrometer is composed of a compact detector  $\gamma$ -system for high count-rates and a conventional constant-acceleration Mössbauer device (WISSEL). The spectra were obtained at 80 and 300 K, and recorded with a Canberra multichannel analyser, coupled to a computer. The isomer shift was recorded with respect to  $\alpha$ -Fe metal. Lorentzian line shapes were assumed for deconvolutions based on least-squares fitting procedures in Recoil Mossbauer Analysis Software 1.05 from Ken Lagarec and Denis Rancourt (Ottawa University, Canada) with five parameters IS (isomer shift),  $\Delta$  (quadrupole splitting),  $\Gamma$  (line width),  $H$  (magnetic field), and % of site population. The  $\chi^2$  and misfit values were used to measure the goodness of the computer fit.

#### *Dynamic mechanical thermal analysis (DMTA) for thermo-mechanical tests*

Rectangular shape films with a thickness close to 0.15 mm, length 12 mm, and a width of approximately 7.0 mm were used to perform the stress  $\times$  strain tests. All tests were carried out at 25 °C with on DMTA equipment (model Q800, TA Instruments) with 1 N/min. Young moduli of materials were determined according to procedure described elsewhere (ASTM D638). The analyses were carried out in triplicate.

#### *Field emission scanning electron microscopy (FESEM)*

FEI Inspect F50 equipment in secondary electrons (SE) mode was used to perform emission scanning electron microscopy (FESEM) analyses. Samples in a film form of 200  $\mu\text{m}$  were placed in a stub and covered with a thin gold layer.

#### *Atomic force microscopy (AFM)*

Roughness data of pure PU and nanocomposites were assessed by atomic force microscopy (AFM). Analyses were performed in peak force tapping mode using Bruker Dimension Icon PT equipped with a TAP150A probe (Bruker, resonance frequency of 150 kHz and  $5 \text{ Nm}^{-1}$  spring constant). The scanned area of the images was  $5 \times 5 \mu\text{m}^2$  with resolution 512 frames per area and the equipment was calibrated prior to samples measurements.

#### *Nuclear magnetic resonance spectroscopy (NMR)*

Solid-state  $^{29}\text{Si}$  MAS-NMR spectra were acquired in a 7 T (300 MHz) AVANCE III Bruker spectrometer equipped with a BBO probe head. The samples were spun at the magic angle at a frequency of 10 kHz in 4 mm-diameter rotors at room

temperature. The  $^{29}\text{Si}$  MAS-NMR spectra were obtained by a single-pulse sequence with a  $90^\circ$  pulse of  $4.5 \mu\text{s}$  at a power of 40 W, and a relaxation delay of 10.0 s.

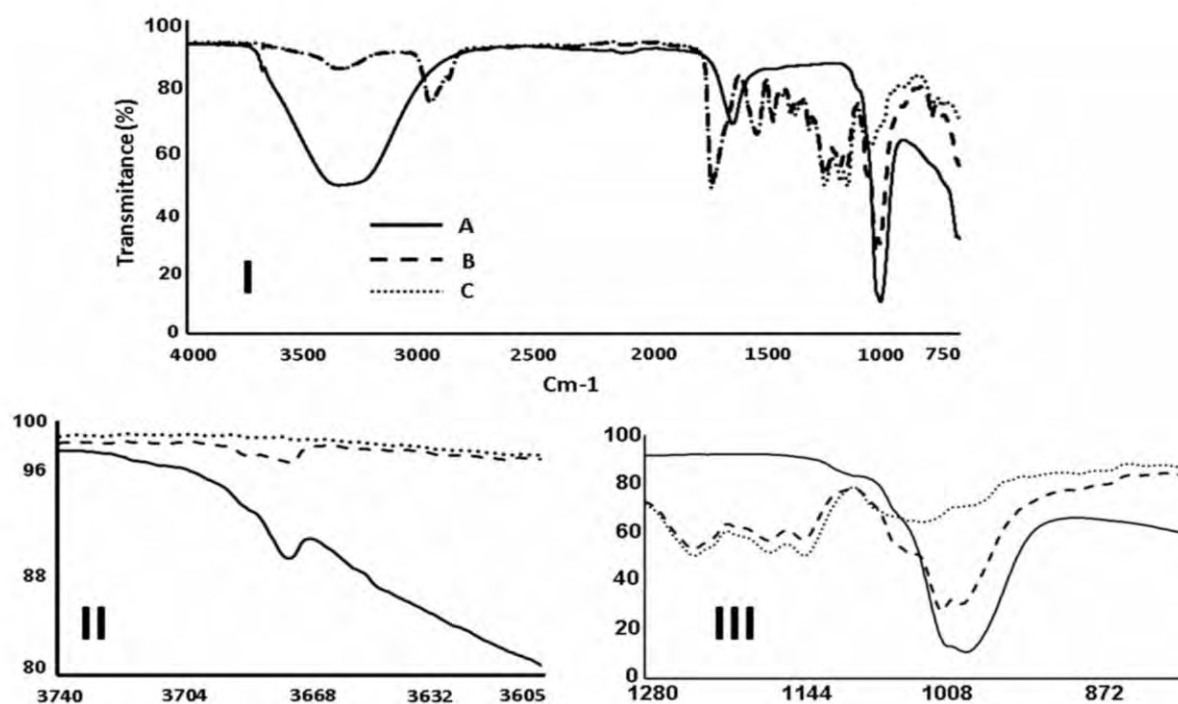
## Results and discussion

### FTIR analysis

Figure 1 shows FTIR spectra of the WPU and the nanocomposite WPU/40%  $\text{Fe}_3\text{O}_4$ -synthetic talc as well the neat  $\text{Fe}_3\text{O}_4$ -synthetic talc. The bands at  $1014\text{--}1000 \text{ cm}^{-1}$  (III) are attributed to Si–O–Si present in the composite and neat filler spectra. Therefore, the filler was successfully introduced into the WPU matrix. New bands at  $\sim 1040 \text{ cm}^{-1}$  (III) (Si–O)<sup>9, 12</sup> and  $\sim 3700 \text{ cm}^{-1}$  (II) (Fe–OH) also corroborate the nanocomposite formation. The FTIR spectra (Fig. 1I, II) also reveal urethane-specific bands at  $2936 \text{ cm}^{-1}$  attributed to C–H stretching of  $\text{CH}_3$  and  $\text{CH}_2$  groups; at  $1532 \text{ cm}^{-1}$  corresponding to deformation vibration of H–N group; at  $1245 \text{ cm}^{-1}$  attributed to N–C stretching vibration [9, 10, 12, 22].

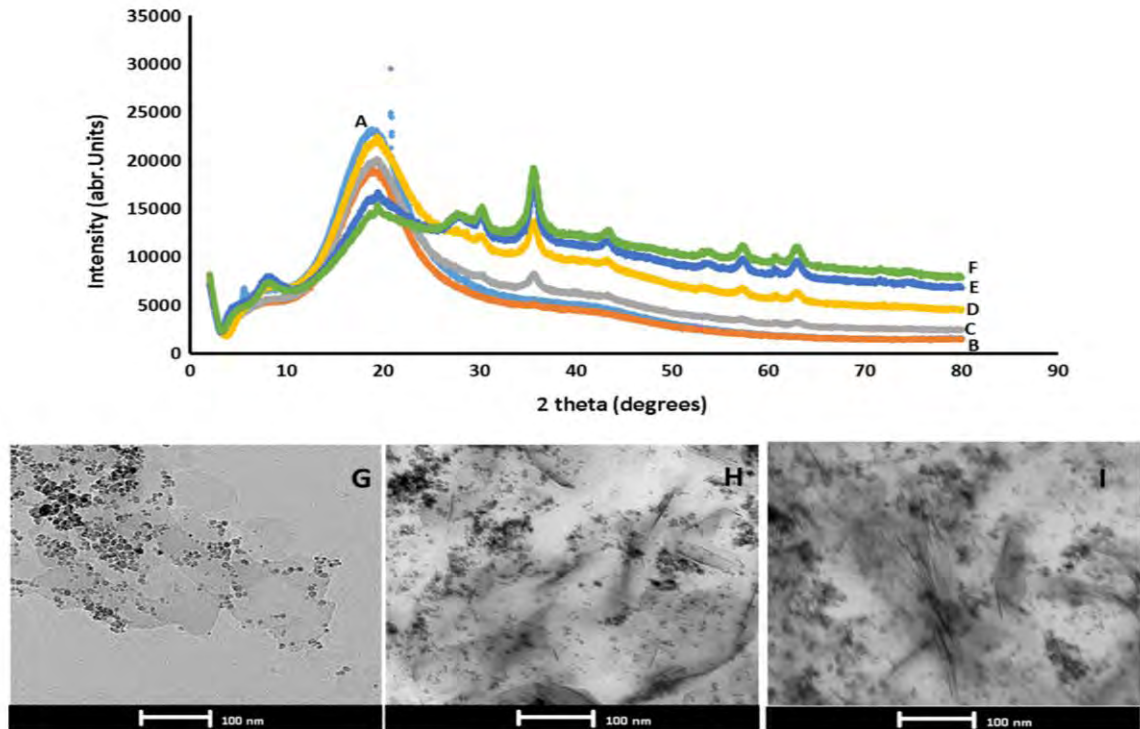
### X-ray diffraction (XRD) and transmission electron microscopy (TEM)

Figure 2 presents the crystalline structure of  $\text{Fe}_3\text{O}_4$ -talc, WPU as well as for WPU/ $\text{Fe}_3\text{O}_4$ -synthetic talc nanocomposites assessed by XRD. TEM images of  $\text{Fe}_3\text{O}_4$ -synthetic talc and WPU/30%  $\text{Fe}_3\text{O}_4$ -synthetic talc and WPU/40%  $\text{Fe}_3\text{O}_4$ -synthetic talc nanocomposites are also presented aiming to corroborate the XRD findings.



**Fig. 1** FTIR spectra  $4000\text{--}650 \text{ cm}^{-1}$  (I), around  $3700 \text{ cm}^{-1}$  (II), around  $1000 \text{ cm}^{-1}$  (III) of  $\text{Fe}_3\text{O}_4$ -synthetic talc (A), WPU/40% $\text{Fe}_3\text{O}_4$ -synthetic talc (B) and WPU (C)





**Fig. 2** XRD of *A* WPU pure, *B* WPU/0.5%  $\text{Fe}_3\text{O}_4$ -synthetic talc, *C* WPU/10%  $\text{Fe}_3\text{O}_4$ -synthetic talc, *D* WPU/30%  $\text{Fe}_3\text{O}_4$ -synthetic talc, *E* WPU/40%  $\text{Fe}_3\text{O}_4$ -synthetic talc, *F*  $\text{Fe}_3\text{O}_4$ - $\text{Fe}_3\text{O}_4$ -synthetic talc and TEM micrographs of *g*  $\text{Fe}_3\text{O}_4$ -synthetic talc, *h* WPU/30%  $\text{Fe}_3\text{O}_4$ -synthetic talc, and *i* WPU/40%  $\text{Fe}_3\text{O}_4$ -synthetic talc

Diffraction peak associated with WPU phase WPU ( $2\theta \cong 14^\circ$ – $24^\circ$ ) tends to decrease with growing  $\text{Fe}_3\text{O}_4$ -synthetic talc content. The same behavior was observed for nanocomposites WPU/silica nanocomposites [16]. Yet, with the growing filler content, an increase in peak at  $2\theta = 10^\circ$  and  $2\theta = 35^\circ$  corresponding to 9.4 and 3.13 Å, characteristic of the filler, is observed.

The same behavior was observed for nanocomposites PU–Ni-synthetic talc [12] indicating a good filler distribution into the polymeric matrix. TEM images (Fig. 2h WPU/30%  $\text{Fe}_3\text{O}_4$ -synthetic talc and i WPU/40%  $\text{Fe}_3\text{O}_4$ -synthetic talc) show a good filler distribution. Surprisingly, even at 30 and 40 wt%, one can see the fillers are intercalated and exfoliated into the WPU matrix. The good dispersion is probably related to the interaction filler/polymeric chain [9, 12]. The talc OH groups of the filler can easily form hydrogen bonds with water [15]. This is probably the main reason to obtain WPU/ $\text{Fe}_3\text{O}_4$ -synthetic talc with good dispersion even at high filler content.

### $^{29}\text{Si}$ CP-MAS NMR

The analysis of the  $^{29}\text{Si}$  NMR spectra allowed us to evaluate the silicon environment in the present nanocomposites. It is well known that the presence of ferromagnetic impurities causes severe broadening and poor resolution, and the  $^{29}\text{Si}$  NMR

chemical shift in solid silicates is strongly influenced by the chemical environment of the silicon nucleus and is highly correlated with the degree of  $\text{SiO}_4$  tetrahedral polymerization [23].  $^{29}\text{Si}$  NMR spectra are thus characterized by the presence of  $Q^n$  peaks, where  $Q^n$  indicates the  $\text{SiO}$  unit corresponding to  $\text{Si}(\text{OSi})_n(\text{OH})_{4-n}$ . These materials are usually characterized by the presence of  $Q^2$ ,  $Q^3$ , and  $Q^4$  bands at  $-93$ ,  $-96$ , and  $-115$  ppm, respectively [21]. The  $^{29}\text{Si}$  MAS-NMR spectra of WPU/0.5, 5, and 10%  $\text{Fe}_3\text{O}_4$ -synthetic talc nanocomposites display a single peak in the  $-110$  to  $-115$  ppm region (Fig. 3), which correspond to a  $Q^4$  environment. The predominance of  $Q^4$  bands is an indication of the absence of free silanol units which indicates the interaction between silicon and the WPU. The increase of  $Q^4$  peaks over  $Q^2$  and  $Q^3$  was reported earlier by Wang et al. [24] when preparing PMMA and PS nanocomposites with functionalised silicon. The authors indicated that the reaction of surface silanols is responsible for  $Q^2$  plus  $Q^3$  peaks decrease and  $Q^4$  increase when compared to those of pristine nanosilica. The WPU nanocomposites exhibit predominantly  $Q^4$  peaks which should be an evidence of surface modification as well, corroborating the XRD and TEM findings.

The  $^{13}\text{C}$  CP/MAS NMR of the nanocomposites WPU/0.5, 5.0, and 10.0%  $\text{Fe}_3\text{O}_4$ -synthetic talc was performed (Fig S1 and Table S1). A peak at 173 ppm observed at the carbonyl region is attributed to  $\text{COO}^-$ . The resonance at 160 ppm is attributed to carbons of the urethane group. A peak at 66 ppm is associated with soft-segments carbons. The peaks at 45–20 and 10 ppm are attributed to CH,  $\text{CH}_2$ , and  $\text{CH}_3$ , respectively.

### Thermal properties

Thermogravimetric analysis (TGA) was performed to assess thermal stability of the synthesized materials (Fig S1 and Table 1). Samples until 5.0% of filler content

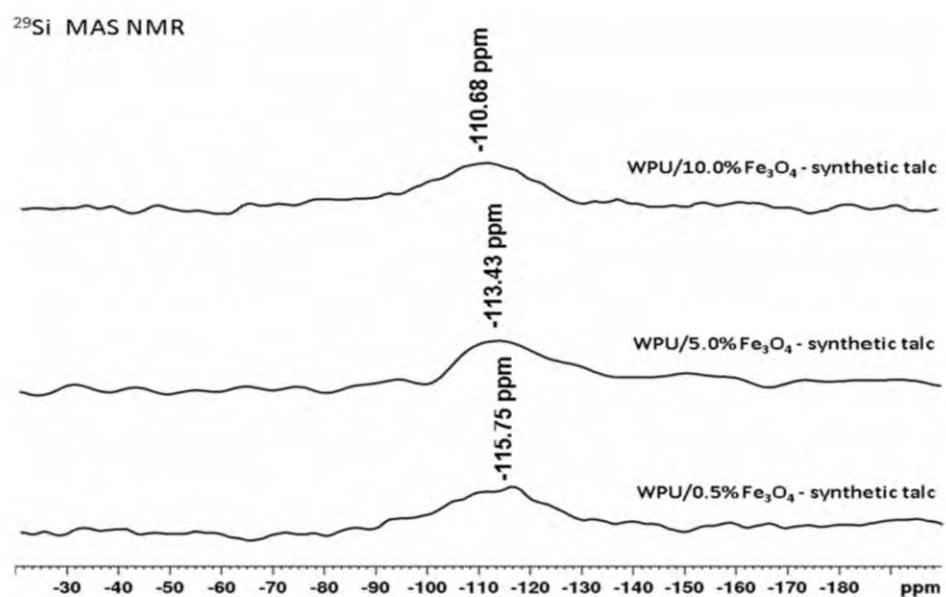


**Fig. 3**  $^{29}\text{Si}$  MAS-NMR WPU/0.5, 5.0, and 10.0%  $\text{Fe}_3\text{O}_4$ -synthetic talc



**Table 1** Results of thermal analyses of neat WPU and the corresponding nanocomposites 0.5, 5.0, 10.0, 30.0, and 40.0% of Fe<sub>3</sub>O<sub>4</sub>-synthetic talc

Filler (%)	$T_{\text{onset}}$ (°C)	$T_{200-600}$ °C (%)	$T_{25-600}$ °C (%)	Wt% remaining at 600 °C	Filler content calculated (%)	$T_{\text{endset}}$
0.0	311	*	96.37%	3.0	–	350/389
0.5	327	90.58		3.1	*	370
5.0	322	90.73		4.8	5.64	343
10.0	299	85.86		6.8	10.5	347
30.0	295	74.47		16.6	21.9	336
40.0	298	70.40		25.2	26.0	335
Talc	32	–		77	–	194

\* Due to low filler content, it was impossible to calculate

showed a higher initial thermal degradation temperature relative to neat WPU. Compare 311 °C for neat WPU to 327 and 322 °C for nanocomposites with 0.5 and 5.0 wt% of filler addition, respectively. Nanocomposites PU/Ni-synthetic talc [12] and PU/SSMMP [10] also showed an improvement in thermal stability for filler content up to 3.0 wt%. The degradation temperatures decrease somewhat with increasing of filler content being 298 °C for the sample with 40.0 wt% of filler content. The same behavior was observed for nanocomposites PU/Fe<sub>3</sub>O<sub>4</sub>-synthetic talc for filler content higher than 1.0 wt% and PU/Ni-synthetic talc with 5.0 wt% [9, 12]. This behavior can be related with higher interaction filler/filler and induced by the high thermal stability of synthetic talc (850 °C), which does not influence the degradation of the composite [9, 12, 22].

The degradation temperatures increase somewhat at the higher filler content until reach 5%. Compare 311 and 322 °C for neat WPU and WPU/5.0% Fe<sub>3</sub>O<sub>4</sub>-synthetic talc, respectively (see Fig. S1 and Table 1). For higher filler contents, degradation temperatures decrease when compared to neat WPU. The residue consists of an inorganic content of the material [25, 26]. The residue content increases as the filler content increases. Table 1 shows the filler content calculated using the formula described in experimental section as well as the residue (wt%) remaining at 600 °C. As we can see, the calculated values are for most nanocomposites slightly different from the remaining values [21]. For higher filler values, one can see that the incorporated filler content into the WPU matrix was lower than the added. Compared for 30 wt%, we really incorporated 21.9 wt%, and for 40 wt%, the filler content was 26.0 wt%. These results suggest that we probably approached the higher filler content possible to be incorporated into the WPU matrix. DSC analysis shows that glass transition temperature ( $T_g$ ) was slightly affected with filler addition being for neat  $-33.8$  °C and around  $-33.0$  °C for nanocomposites.

### Magnetic properties

Magnetic properties were investigated by magnetization carried out in ZFC and FC processes and Mössbauer spectroscopy. Temperature dependence of magnetization performed by ZFC and FC processes (temperature range 2–300 K) measured at 10



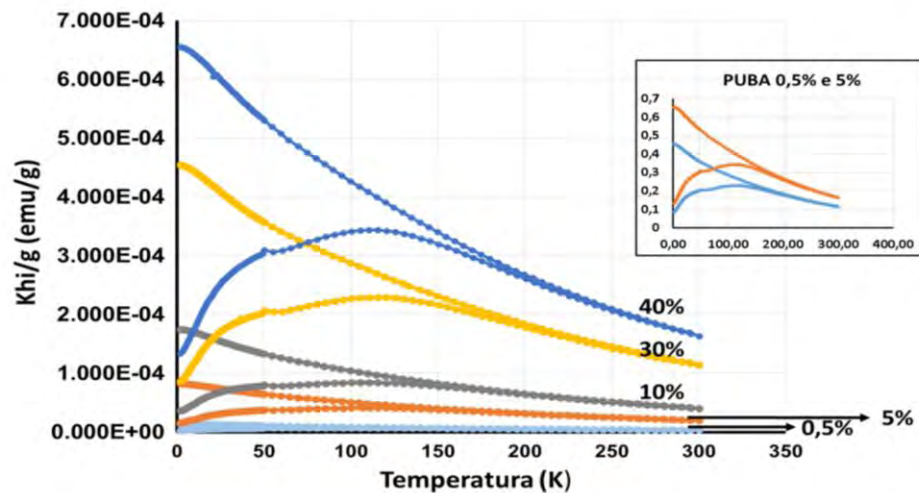


**Fig. 4** Magnetization vs temperature for the nanocomposites: WPU 0.5 wt%  $\text{Fe}_3\text{O}_4$ -synthetic talc and WPU/5 wt%  $\text{Fe}_3\text{O}_4$ -synthetic talc, WPU/10 wt%  $\text{Fe}_3\text{O}_4$ -synthetic talc, WPU/30 wt%  $\text{Fe}_3\text{O}_4$ -synthetic talc, WPU/40 wt%  $\text{Fe}_3\text{O}_4$ -synthetic talc

Oe for nanocomposites is shown in Fig. 4. For all samples, inside the range of 2–300 K, one can see a typical ferromagnetic behavior below blocking temperature (about 120 K) and a superparamagnetic behavior above this temperature. The blocking temperature is field-dependent growing with the temperature increase [9, 27, 28]. Surprisingly, nanocomposites using the same filler ( $\text{Fe}_3\text{O}_4$ -synthetic talc) but obtained using as matrix a conventional solvent-based PU [9] presented ferromagnetic behavior in all temperature intervals. Besides the different matrix, also the filler was used in a form of powder unlike in this work that was used in a gel form. These changes resulted in composites with different magnetic behavior.

Field-dependent magnetization curves at different temperatures (2, 100, 200, and 300 K) for all nanocomposites are presented in Fig S2. Magnetic properties are shown in Table S1. Magnification of magnetization loops is shown in an insert in Fig. S2 highlighting nanocomposites hysteresis loops with different filler content at different temperatures. Saturation magnetization values are similar with increasing temperature for nanocomposites with low filler content. Compare 0.153 emu/g (2 K) with 0.123 emu/g (300 K) in WPU/0.5 wt%  $\text{Fe}_3\text{O}_4$ -synthetic talc. For higher filler content, the variation on saturation magnetization with temperature is more important. Compare 7.4 emu/g (2 K) with 6.14 emu/g (300 K) in WPU/40.0 wt%  $\text{Fe}_3\text{O}_4$ -synthetic talc. Santos et al. [9] described coercivity values of 275 Oe (2 K) and 0 Oe (300 K) for nanocomposites PU/0.5wt%  $\text{Fe}_3\text{O}_4$ -synthetic talc and 250 Oe (2 K) and 0 Oe (300 K) for PU/10 wt%  $\text{Fe}_3\text{O}_4$ -synthetic talc. Our results show coercivity values of 239 Oe (2 K) and 20 Oe (300 K) for 0.5% of filler content and for 10% of filler content 229 Oe (2 K) and 25 Oe (300 K). Here, also one can observe the influence of nanocomposites obtainment in magnetic properties. This behavior was also corroborated by Mössbauer results.

Mössbauer spectra recorded at 80 and 293 K for WPU/40 wt%  $\text{Fe}_3\text{O}_4$ -synthetic talc are shown in Fig. 5a, b and Table 2. As can be seen, the particles are able to reverse its magnetic moment by thermal activation. This behavior indicates the presence of small superparamagnetic particles [6]. Two well-defined sextuplet is

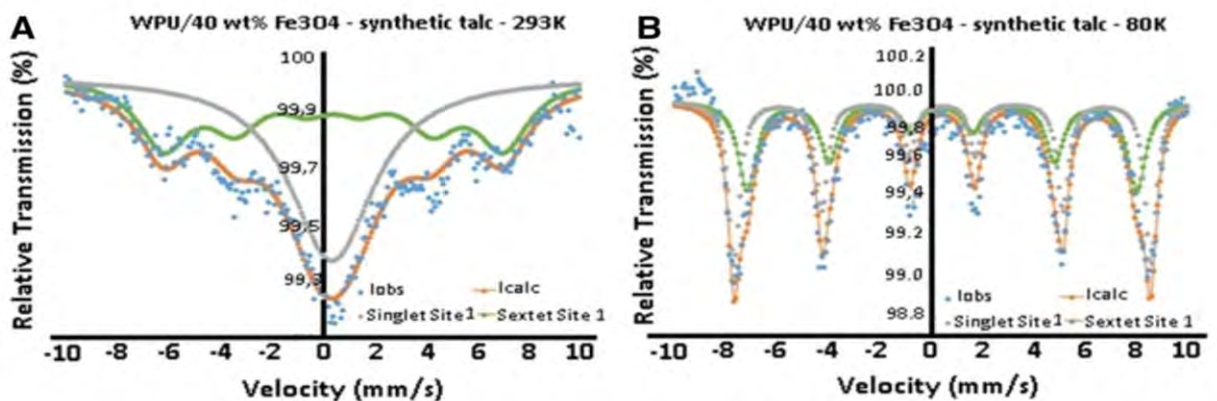


**Table 2** Mössbauer parameters for WPU/40 wt% Fe<sub>3</sub>O<sub>4</sub>-synthetic talc nanocomposite at 293 K at 80 K

	IS (mm/s)	$\Delta$ (mm/s)	$H$ (kOe)	$\Gamma$ (mm/s)	Site populations (%)
WPU/40 wt% Fe <sub>3</sub> O <sub>4</sub> -synthetic talc—293 K					
Single site t1	0.357 ( $\pm 0.064$ )	–	–	1.99 ( $\pm 0.15$ )	53.20 ( $\pm 0.39$ )
Sextet site 1	0.42 ( $\pm 0.11$ )	–0.002 ( $\pm 0.082$ )	408.90 ( $\pm 0.72$ )	1.20 ( $\pm 0.19$ )	46.80 ( $\pm 0.83$ )
WPU/40 wt% Fe <sub>3</sub> O <sub>4</sub> -synthetic talc—80 K					
Sextet site 1	0.442 ( $\pm 0.013$ )	0*	503.30 ( $\pm 0.15$ )	0.271 ( $\pm 0.035$ )	54 (11)
Sextet site 2	0.426 ( $\pm 0.029$ )	0*	470.30 ( $\pm 0.48$ )	0.427 ( $\pm 0.075$ )	46 (14)

Fitting procedures include five parameters  $IS$  isomer shift with respect to the  $\alpha$ -Fe metal,  $\Delta$  quadrupole splitting,  $H$  magnetic field,  $\Gamma$  line width, and % of site populations

\* Fixed value

**Fig. 5** Mössbauer spectrum at 80 K (a) and 293 K (b) of WPU/40 wt% Fe<sub>3</sub>O<sub>4</sub>-synthetic talc nanocomposite

observed until 80 K temperature (Fig. 5b; Table 2). At 293 K, the sextuplets are partially replaced by a broad paramagnetic singlet (Fig. 5a; Table 2). Yet, one can observe a perturbation in spectrum indicating the presence of both superparamagnetic/ferromagnetic forms at this temperature.

### Mechanical properties

Tensile properties and Young moduli (Fig. 6; Table 3) indicate that the higher filler content leads to the larger Young moduli  $29 \pm 2$  MPa in neat WPU and  $70 \pm 2$  MPa in WPU/40 wt% Fe<sub>3</sub>O<sub>4</sub>-synthetic talc. Therefore, higher content of filler is desirable to obtain nanocomposites with competitive mechanical strengths and improved rigidity of the films. Nanocomposites exhibit superior mechanical properties relative to neat WPU. An increase in stress and stress values is observed for all nanocomposites (Fig. 6). Films obtained with neat WPU and 0.5% of filler did not break at the test condition.

Storage modulus ( $E'$ ) increases with the augmentation of filler content indicating the filler incorporation into the WPU matrix. Compare (1689 MPa) and

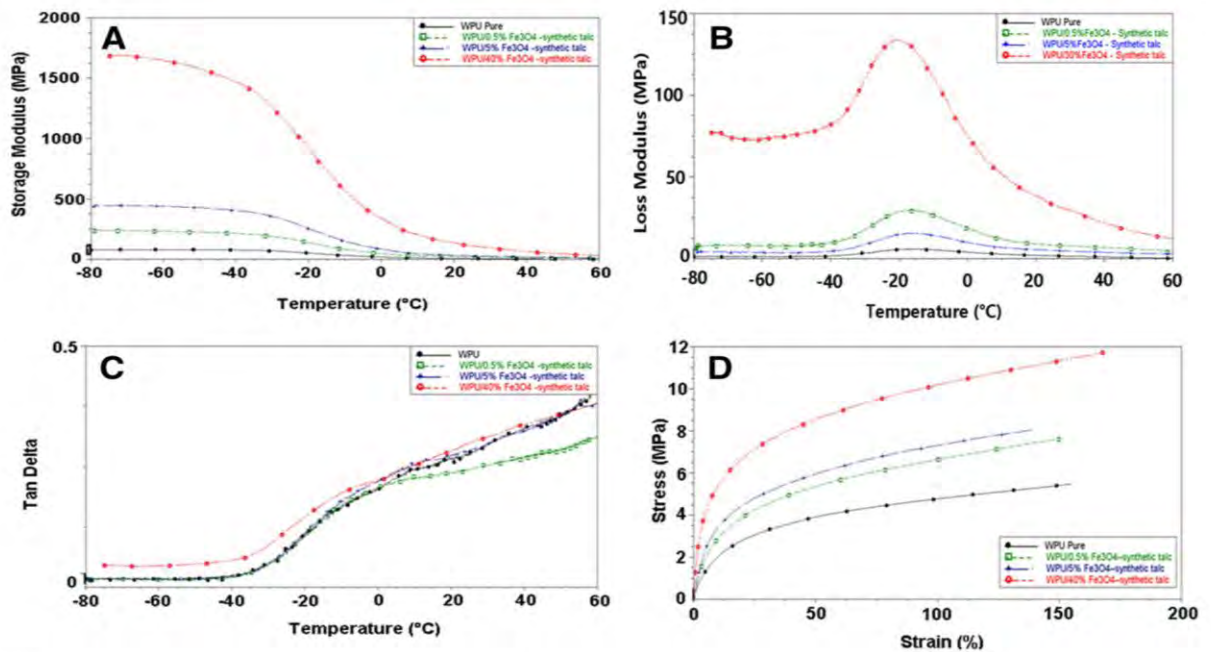


**Fig. 6** Temperature dependence of **a** storage modulus, **b** loss modulus, and **c** loss factor  $\tan \delta$  and stress/strain curves of WPU pure and its nanocomposites

**Table 3** Mechanical properties of WPU/Fe<sub>3</sub>O<sub>4</sub>-synthetic talc nanocomposites and for neat WPU

Filler (%)	Stress (Mpa)	Strain (%)	Young moduli (MPa)
0.0	5.7 ± 0.1	143 ± 3	29 ± 2
0.5	7.5 ± 0.3	154 ± 1	34 ± 2
5.0	8.0 ± 0.4	140 ± 2	45 ± 2
40.0	7.8 ± 0.2	159 ± 8	70 ± 2

(79.83 MPa) for 40% Fe<sub>3</sub>O<sub>4</sub>-synthetic talc and neat WPU, respectively. Lei et al. [29] observed the same behavior for nanocomposites WPU/graphene obtaining a value of (2694 MPa) for 0.5% of graphene addition. This is an advantage of these nanocomposites which is capable of maintaining high modulus even at temperatures above  $T_g$  [30]. The glass transition temperature was determined at maximum  $\tan \delta$  value [31]. Figure 6b, c shows a single peak for nanocomposites WPU/0.5, 5, and 40% Fe<sub>3</sub>O<sub>4</sub>-synthetic talc, as well as for neat WPU corresponding to the  $T_g$  of these materials. The loss modulus ( $E''$ ) values are also higher for nanocomposites relative to neat WPU. Compare the loss modulus of neat WPU (5.91 MPa at -15 °C) and for WPU/40% Fe<sub>3</sub>O<sub>4</sub>-synthetic talc (134 MPa at -20.34 °C). Changes on  $T_g$  values with filler addition are associated with strong interaction filler/WPU [32].

### Morphological properties

Surface morphology of the samples was identified by SEM and AFM (Figs. S3, 7; Table 4). MEV and topography AFM images are also presented (Fig. S3). Surface structure changes occur with the increase of filler content. Yet, good filler dispersion



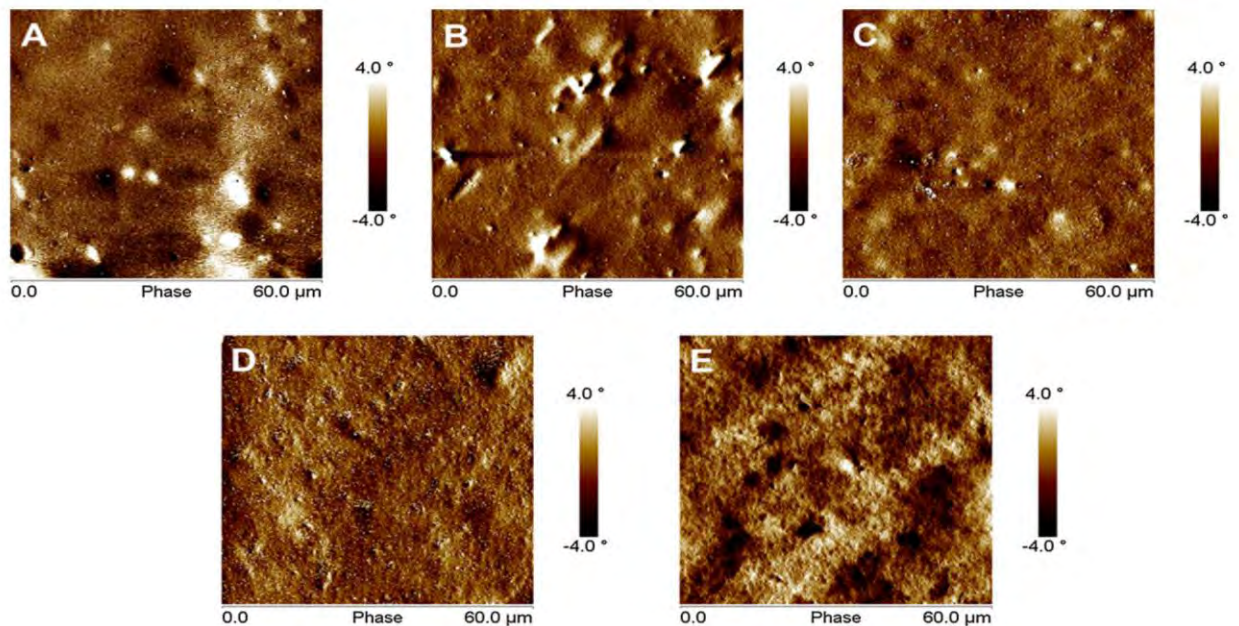


**Fig. 7** AFM phase images: **a** WPU pure, **b** WPU/0.5 wt%  $\text{Fe}_3\text{O}_4$ -synthetic talc, **c** WPU/5 wt%  $\text{Fe}_3\text{O}_4$ -synthetic talc, **d** WPU/30 wt%  $\text{Fe}_3\text{O}_4$ -synthetic talc, and **e** WPU/40 wt%  $\text{Fe}_3\text{O}_4$ -synthetic talc

**Table 4** Average roughness ( $R_a$ ), root-mean-square roughness ( $R_q$ ), and maximum height roughness ( $R_{\max}$ ) for WPU/ $\text{Fe}_3\text{O}_4$ -synthetic talc nanocomposites

Filler (%)	$R_a$ (nm)	$R_q$ (nm)	$R_{\max}$ (nm)
0.0	13.7	19.1	230.0
0.5	1.9	2.3	30.3
5.0	3.5	4.6	44.9
10.0	6.1	8.1	116.3
30.0	17.0	22.9	205.2
40.0	20.1	25.8	222.3

can be observed even at higher filler contents. Discontinuous darker and lighter regions can be seen in AFM images. Higher filler content fosters the rearrangement of soft and hard domains (Fig. S3). Polyurethane hard/hard and hard/soft domains interactions by hydrogen bonding are important at lower filler contents. Therefore, at higher filler content, polymer/filler and filler/filler interaction became more important [9]. These changes, mainly based on hydrogen bonds, are mainly responsible for changes in mechanical properties.

Small bright spots can be seen in AFM images (Fig. 7), which are probably  $\text{Fe}_3\text{O}_4$ -synthetic-talc nanoparticles present in the polymeric film surface [33].

Table 4 shows that for percentages of 0.5–10%/ $\text{Fe}_3\text{O}_4$ -synthetic talc, the roughness values were lower relative to neat WPU. In percentages of 30 and 40% of synthetic talc, the values of  $R_a$  and  $R_q$  are higher and  $R_{\max}$  lower when compared to pure WPU. In sample solvent-based PU/ $\text{Fe}_3\text{O}_4$ -synthetic talc, the addition of filler increases the roughness until 1% and above these values, it decreases [9]. Zhang et al. [18] described an increase in surface smoothness until the addition of 1%  $\text{Fe}_3\text{O}_4$  and an increase in roughness above this value indicating a



probable filler aggregation. In the case of WPU/Fe<sub>3</sub>O<sub>4</sub>-synthetic talc samples with higher filler values, agglomeration may also take place.

## Conclusions

A new way to obtain magnetic nanocomposites, using water-based environmentally and friendly materials, was presented. The hydrophilicity of Fe<sub>3</sub>O<sub>4</sub>-synthetic talc-nanofillers resulted in a good filler dispersion into the polyurethane matrix even at high filler content as supported by XRD and TEM analyses. NMR indicates the interaction of filler OH groups with the matrix. For all nanocomposites, one can see a typical ferromagnetic behavior below Curie temperature (about 120 K) and a superparamagnetic behavior above this temperature. The use of Fe<sub>3</sub>O<sub>4</sub>-synthetic talc for obtaining magnetic nanocomposites resulted in improved materials with superior mechanical properties.

**Acknowledgements** LS (No Proc.: BEX 6547/15-0) thanks CAPES, SE, and RL acknowledge CNPq for DT grant. We acknowledge LabNMR-CENIMAT at FCT-UNL and RNRMN for access to the facilities. RNRMN is supported with funds from the Foundation for Science and Technology. This work is also funded by FEDER funds through the COMPETE 2020 Programme and National Funds through FCT-Portuguese Foundation for Science and Technology under the Project Number POCI-01-0145-FEDER-007688, Reference UID/CTM/50025.

## References

1. Kirchberg S, Rudolph M, Ziegmann G, Peuker UA (2012) Nanocomposites based on technical polymers and sterically functionalized soft magnetic magnetite nanoparticles: synthesis, processing, and characterization. *J Nanomater* 2012:1–8
2. Mohammadi A, Barikani M, Lakouraj MM (2016) Biocompatible polyurethane/thiacalix[4]arenes functionalized Fe<sub>3</sub>O<sub>4</sub> magnetic nanocomposites: synthesis and properties. *Mater Sci Eng C Mater Biol Appl* 66:106–118
3. Yan F, Li J, Zhang J, Liu F, Yang W (2009) Preparation of Fe<sub>3</sub>O<sub>4</sub>/polystyrene composite particles from monolayer oleic acid modified Fe<sub>3</sub>O<sub>4</sub> nanoparticles via miniemulsion polymerization. *J Nanopart Res* 11:289–296
4. Balakrishnan S, Bonder MJ, Hadjipanayis GC (2009) Particle size effect on phase and magnetic properties of polymer-coated magnetic nanoparticles. *J Magn Magn Mater* 321:117–122
5. Giri SK, Pradhan GC, Das N (2014) Thermal, electrical and tensile properties of synthesized magnetite/polyurethane nanocomposites using magnetite nanoparticles derived from waste iron ore tailing. *J Polym Res* 21:446
6. Dallas P, Georgakilas V, Niarchos D, Komninou P, Kehagias T, Petridis D (2006) Synthesis, characterization and thermal properties of polymer/magnetite nanocomposites. *Nanotechnology* 17:2046–2053
7. Dumas A, Gardes E, Le Roux C, Martin F, Micoud P (2013) Process for preparing a magnetic talcous composition and magnetic talcous composition. PCT Int. Pat. Appl. WO 2013093376 A1 June 27 2013 Fr. Pat. Appl. FR 2984872 A1 June 28 2013
8. Dumas A, Le Roux C, Martin F, Micoud P (2013) Process for preparing a composition comprising synthetic mineral particles and composition. PCT Int. Pat. Appl. WO 2013004979 A1 Jan 10 2013 Fr. Pat. FR 2977580 B1 August 16 2013
9. dos Santos LM, Ligabue R, Dumas A, Le Roux C, Micoud P, Meunier J-F, Martin F, Einloft S (2015) New magnetic nanocomposites: polyurethane/Fe<sub>3</sub>O<sub>4</sub>-synthetic talc. *Eur Polym J* 69:38–49
10. Dias G, Prado MA, Carone C, Ligabue R, Dumas A, Martin F, Le Roux C, Micoud P, Einloft S (2015) Synthetic silico-metallic mineral particles (SSMMP) as nanofillers: comparing the effect of



- different hydrothermal treatments on the PU/SSMMP nanocomposites properties. *Polym Bull* 7:2991–3006
11. Dias G, Prado MA, Carone C, Ligabue R, Dumas A, Martin F, Le Roux C, Micoud P, Einloft S (2016) Comparing different synthetic talc as fillers for polyurethane nanocomposites. *Macromol Symp* 367:136–142
  12. Prado MA, Dias G, Carone C, Ligabue R, Dumas A, Martin F, Le Roux C, Micoud P, Einloft S (2015) Synthetic Ni-talc as filler for producing polyurethane nanocomposites. *J Appl Polym Sci* 132:41854
  13. Yousfi M, Livi S, Dumas A, Le Roux C, Crépin-Leblond J, Greenhill-Hooper M, Duchet-Rumeau J (2013) Use of new synthetic talc as reinforcing nanofillers for polypropylene and polyamide 6 systems: thermal and mechanical properties. *J Colloid Interf Sci* 403:29–42
  14. Yousfi M, Livi S, Dumas A, Crépin-Leblond J, Greenhill-Hooper M, Duchet-Rumeau J (2014) Compatibilization of polypropylene/polyamide 6 blends using new synthetic nanosized talc fillers: morphology, thermal and mechanical properties. *J Appl Polym Sci* 131:40453
  15. Dumas A, Claverie M, Slostowski C, Aubert G, Careme C, Le Roux C, Micoud P, Martin F, Aymonier C (2016) Fast-geomimicking using chemistry in supercritical water. *Angew Chem* 128:1–5
  16. Wang G, Ma G, Hou CA, Guan T, Ling L, Wang B (2014) Preparation and properties of waterborne polyurethane/nanosilica composites: a diol as extender with triethoxysilane group. *J Appl Polym Sci* 131(15):1–7
  17. Chen S, Chen S, Zhao G, Chen J (2015) Fabrication and properties of novel superparamagnetic, well-dispersed waterborne polyurethane/Ni-Zn ferrite nanocomposites. *Comp Sci Tech* 119:108–114
  18. Zhang S, Li Y, Peng L, Li Q, Chen S, Hou K (2013) Synthesis and characterization of novel waterborne polyurethane nanocomposites with magnetic and electrical properties. *Compos Part A* 55:94–101
  19. Soares RR, Carone C, Einloft S, Ligabue R, Monteiro WF (2014) Synthesis and characterization of waterborne polyurethane/ZnO composites. *Polym Bull* 71:829–838
  20. Dumas A, Martin F, Le Roux C, Micoud P, Petit S, Ferrage E, Brendlé J, Grauby O, Greenhill-Hooper M (2013) Phyllosilicates synthesis: a way of accessing edges contributions in NMR and FTIR spectroscopies. Example of synthetic talc. *Phys Chem Miner* 40:361–373
  21. Tang E, Cheng G, Ma X (2006) Preparation of nano-ZnO/PMMA composite particles via grafting of the copolymer onto the surface of zinc oxide nanoparticles. *Powder Technol* 161:209–214
  22. Da Silva V, Dos Santos LM, Subda S, Ligabue R, Seferin M, Carone C, Einloft S (2013) Synthesis and characterization of polyurethane/titanium dioxide nanocomposites obtained by in situ polymerization. *Polym Bull* 70:1819–1833
  23. Lippmaa E, Magi M, Samoson A, Tarmac M, Engelhardt G (1980) Structural studies of silicates by solid-state high-resolution  $^{29}\text{Si}$  NMR. *J Am Chem Soc* 102:4889–4893
  24. Wang T-L, Ou C-C, Yang C-H (2008) Synthesis and properties of organic/inorganic hybrid nanoparticles prepared using atom transfer radical polymerization. *J Appl Polym Sci* 109:3421–3430
  25. Sardon H, Irusta L, Santamaría P, Fernández-Berridi MJ (2012) Thermal and mechanical behaviour of self-curable waterborne hybrid polyurethanes functionalized with (3-aminopropyl)triethoxysilane (APTES). *J Polym Res* 19:545–546
  26. Jena KK, Sahoo S, Narayan R, Aminabhavi TM, Raju KVS N (2011) Novel hyperbranched waterborne polyurethane-urea/silica hybrid coatings and their characterizations. *Polym Int* 60:1504–1513
  27. Chesnel K, Trevino M, Cai Y, Hancock JM, Smith SJ, Harrison RG (2014) Particle size effects on the magnetic behaviour of 5 to 11 nm  $\text{Fe}_3\text{O}_4$  nanoparticles coated with oleic acid. *J Phys Conf Ser* 521:012004
  28. Mohapatra J, Nigam S, Gupta J, Mitra A, Aslam M, Bahadur D (2015) Enhancement of magnetic heating efficiency in size controlled  $\text{MFe}_2\text{O}_4$  (M=Mn, Fe, Co and Ni) nanoassemblies. *RSC Adv* 5:14311–14321
  29. Lei L, Xia Z, Zhang L, Zhang Y, Zhong L (2016) Preparation and properties of amino-functional reduced graphene oxide/waterborne polyurethane hybrid emulsions. *Prog Org Coat* 97:19–27
  30. Sabzi M, Mirabedini SM, Zohuriaan-Mehr J, Atai M (2009) Surface modification of  $\text{TiO}_2$  nanoparticles with silane coupling agent and investigation of its effect on the properties of polyurethane composite coating. *Prog Org Coat* 65:222–228
  31. Lorandi NP, Ornaghi MOHCH Jr (2016) Dynamic mechanical analysis (DMA) of polymeric composite materials. *Sci Cum Ind* 4:48–60

32. Serkis M, Špírková M, Hodan J, Kredatusová J (2016) Nanocomposites made from thermoplastic waterborne polyurethane and colloidal silica. The influence of nanosilica type and amount on the functional properties. *Prog Org Coat* 101:342–349
33. Gu X, Chen G, Zhao M, Watson SS, Nguyen T, Chin JW, Martin JW (2012) Critical role of particle/polymer interface in photostability of nano-filled polymeric coatings. *J Coat Technol Res* 9:251–267

## Supplementary information

### **Waterborne polyurethane/Fe<sub>3</sub>O<sub>4</sub>-synthetic talc composites:**

### **synthesis, characterization and magnetic properties**

Leonardo M dos Santos<sup>1</sup>, Rosane Ligabue<sup>1,2</sup>, Angela Dumas<sup>3</sup>, Christophe Le Roux<sup>3</sup>, Pierre Micoud<sup>3</sup>, Jean-François Meunier<sup>4</sup>, François Martin<sup>3</sup>, Marta Corvo<sup>5</sup>, Pedro Almeida<sup>5</sup>, Sandra Einloft<sup>1,2</sup>

1- Post-Graduation Program in Materials Engineering and Technology. Pontifical Catholic University of Rio Grande do Sul – PUCRS.

2- School of Chemistry. Pontifical Catholic University of Rio Grande do Sul – PUCRS.

3- ERT 1074 Géomatériaux – GET UMR 5563 CNRS - Université de Toulouse – Toulouse, France.

4-Laboratoire de Chimie de Coordination- Université de Toulouse – Toulouse, France.

5- CENIMAT/I3N, Research Centre in Materials/Institute for Nanostructures, Nanomodelling and Nanofabrication, Departamento de Ciências dos Materiais, Faculdade de Ciências e Tecnologia, Universidade Nova de Lisboa, 2829-516 Caparica, Portugal.

6- Área Departamental de Física, Instituto Superior de Engenharia de Lisboa, Instituto Politécnico de Lisboa, 1959-007 Lisbon, Portugal;

Correspondence to: Sandra Einloft (E-mail: [einloft@pucrs.br](mailto:einloft@pucrs.br))

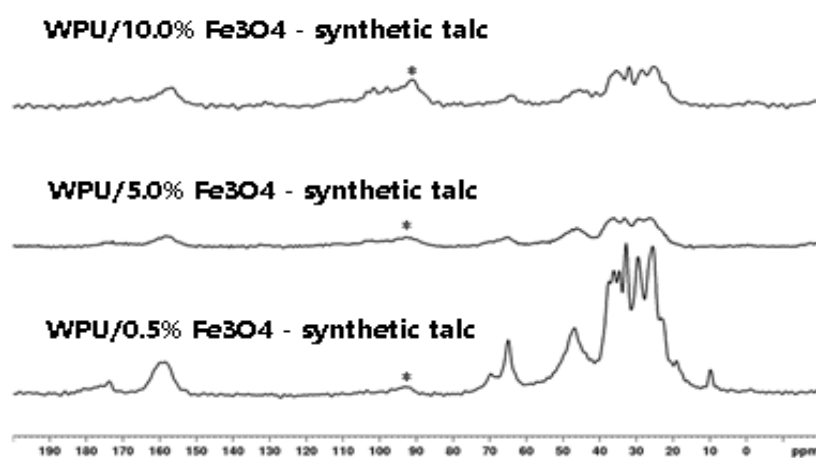
<sup>13</sup>C CPMAS NMR

Figure S1. <sup>13</sup>C CP/MAS NMR of WPU/0.5; 5.0 and 10.0% Fe<sub>3</sub>O<sub>4</sub> -synthetic talc acquired at room temperature and under 5 kHz MAS. Asterisks (\*) represent spinning sidebands.

Table S1. <sup>13</sup>C CP/MAS NMR assignments.

<sup>13</sup> C CPMAS NMR (ppm)	Assignment	Backbone
173	COO <sup>-</sup>	DMPA
160	C(O)ONH	Urethane
66	OCH <sub>2</sub>	Diol
45 - 20	CH and CH <sub>2</sub>	IPDI
10	CH <sub>3</sub>	IPDI



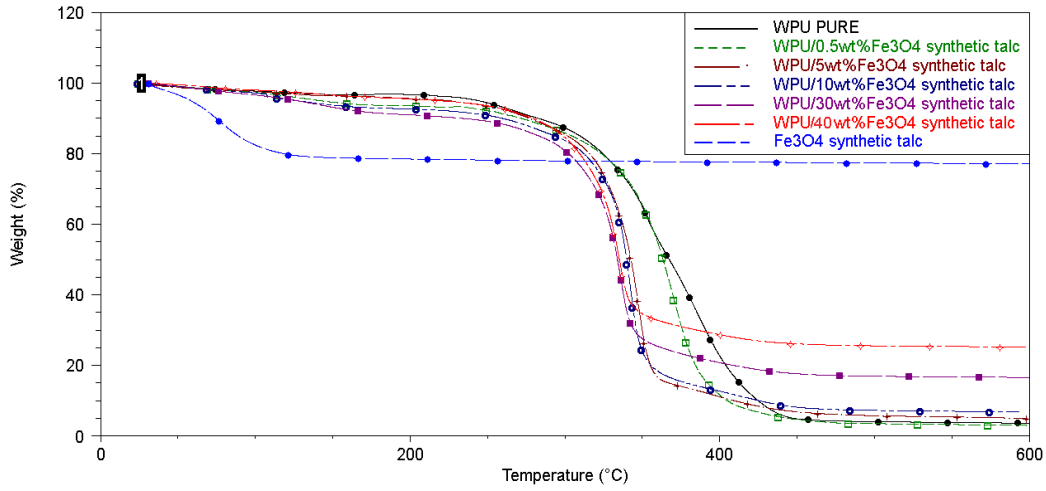


Figure S2. TGA curves for neat WPU and nanocomposites WPU/Fe<sub>3</sub>O<sub>4</sub>- synthetic talc.

Table S2. Magnetic properties of nanocomposites at different temperatures.

Property	WPU/ 0.5 wt.% Fe <sub>3</sub> O <sub>4</sub> -synthetic talc				WPU/ 5.0 wt.% Fe <sub>3</sub> O <sub>4</sub> -synthetic talc				WPU/ 10.0 wt.% Fe <sub>3</sub> O <sub>4</sub> -synthetic talc			
	2K	100K	200K	300K	2K	100K	200K	300K	2K	100K	200K	300K
Saturation magnetization (emu/g)	0.153	0.148	0.136	0.123	0.918	0.882	0.829	0.751	1.88	1.81	1.71	1.55
Remanent magnetization (emu/g)	0.0525	0.0081	0.0051	0.0051	0.287	0.0455	0.0477	0.032	0.583	0.2	0.097	0.065
Coercivity (Oe)	239	19	24	20	228	23	24	23	229	20	25	25
Property	WPU/ 30.0 wt.% Fe <sub>3</sub> O <sub>4</sub> -synthetic talc				WPU/ 40.0 wt.% Fe <sub>3</sub> O <sub>4</sub> -synthetic talc							
	2K	100K	200K	300K	2K	100K	200K	300K				
Saturation magnetization (emu/g)	5.26	5.08	4.79	4.32	7.4	7.15	6.74	6.14				
Remanent magnetization (emu/g)	1.6	0.25	0.27	0.185	2.27	0.371	0.394	0.26				
Coercivity (Oe)	225	20	27	25	225	26	25	23				

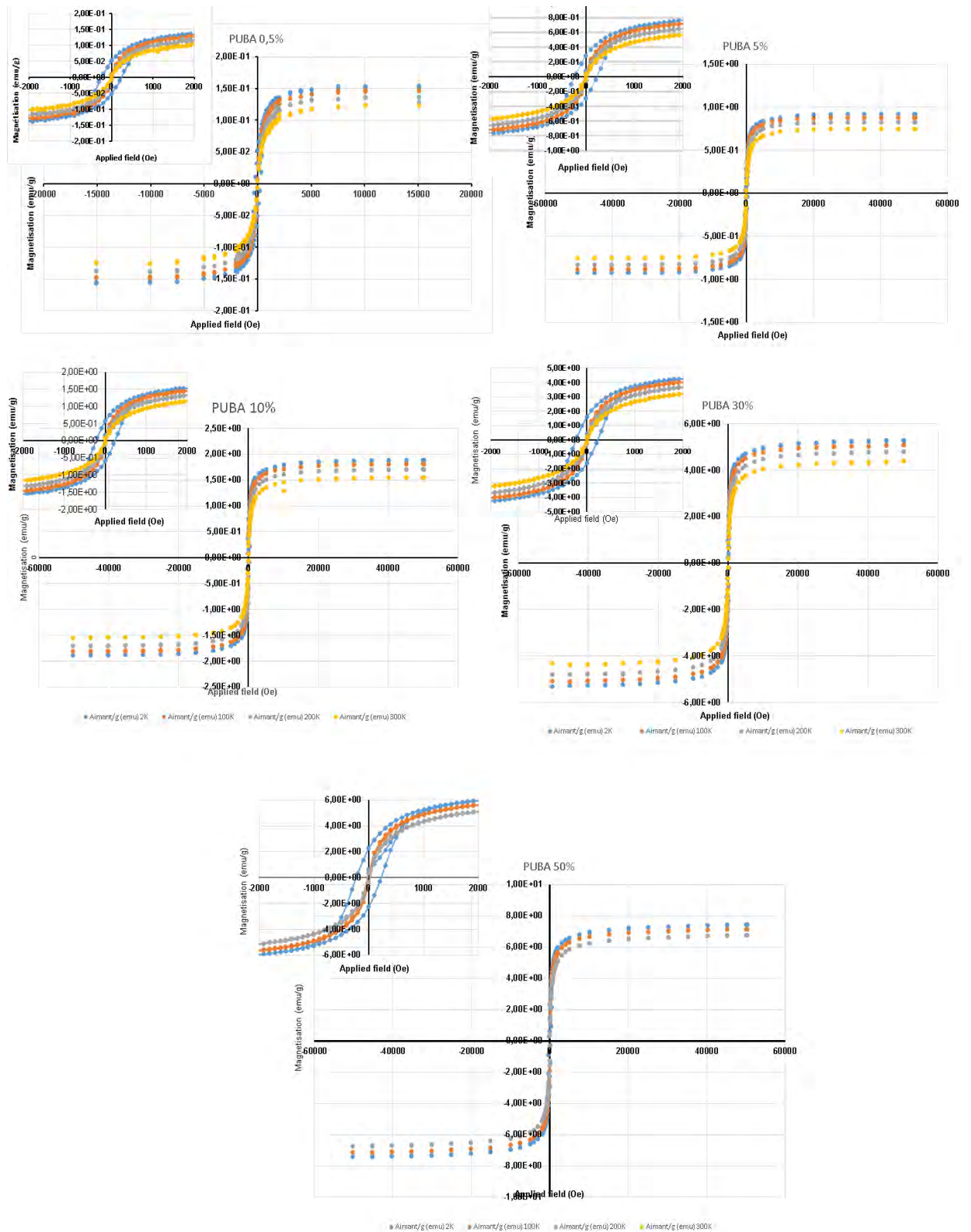


Figure S3. Magnetization curves for nanocomposites at different temperatures (2K, 100K, 200K and 300K).

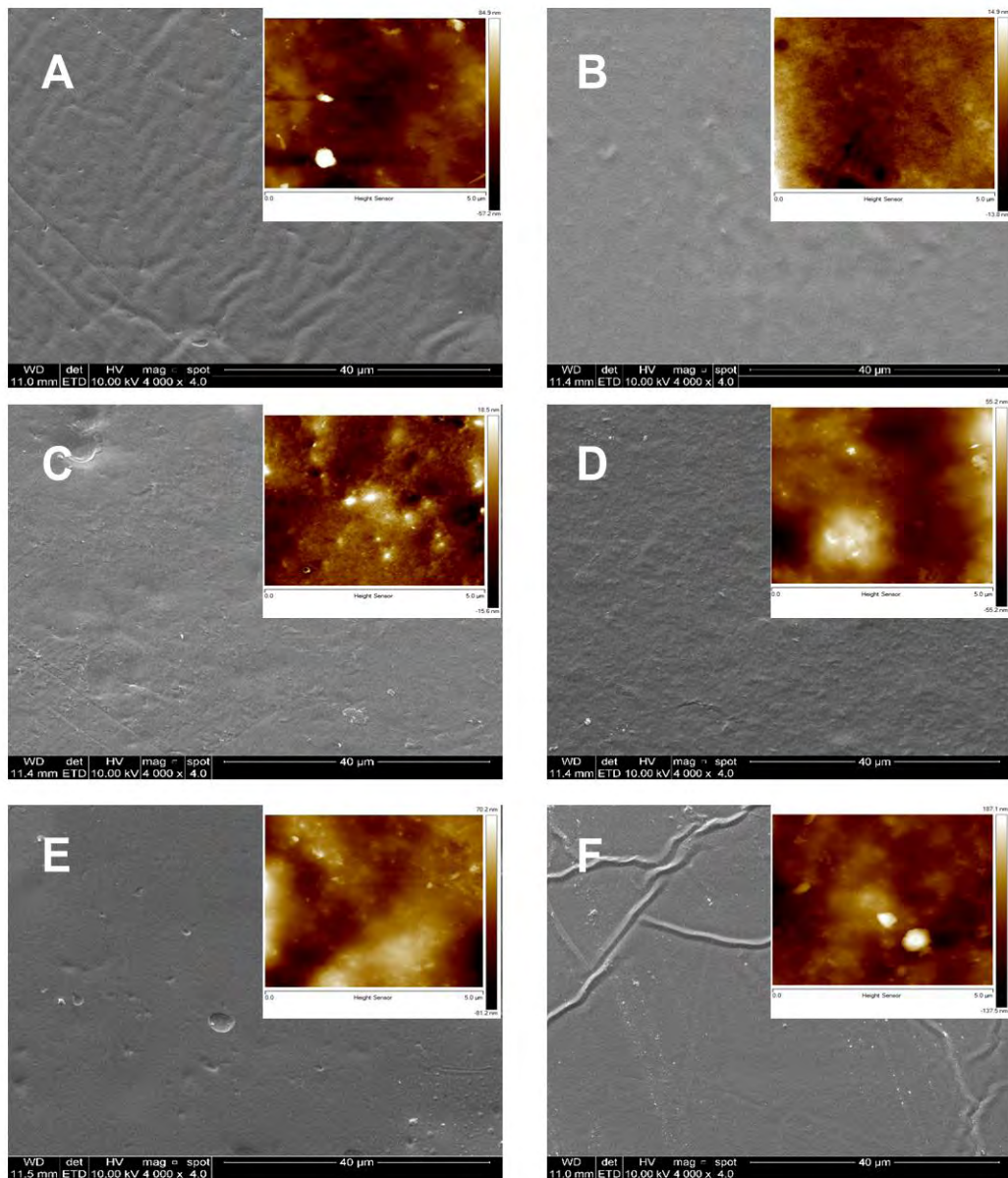


Figure S4. SEM micrographs (magnification 4000x) and AFM height sensor images (insert) (A)WPU pure, (B) WPU/0.5 wt.% Fe<sub>3</sub>O<sub>4</sub> -synthetic talc, (C) WPU/5 wt.% Fe<sub>3</sub>O<sub>4</sub> -synthetic talc, (D) WPU/10 wt.% Fe<sub>3</sub>O<sub>4</sub> -synthetic talc, (E) WPU/30 wt.% Fe<sub>3</sub>O<sub>4</sub> -synthetic talc and (F) WPU/40 wt.% Fe<sub>3</sub>O<sub>4</sub> -synthetic talc.

## 5. CONCLUSÕES

Os nanocompósitos de PU/  $\text{Fe}_3\text{O}_4$  – talco sintético obtidos por mistura física apresentaram uma distribuição homogênea da carga na matriz polimérica. Já para mistura física PUBA/  $\text{Fe}_3\text{O}_4$  – talco sintético foram obtidas distribuição homogênea até a porcentagem de PUBA/10%  $\text{Fe}_3\text{O}_4$  – talco sintético, para quantidades maiores de carga (30 e 40% de  $\text{Fe}_3\text{O}_4$  – talco sintético) observou-se a formação de agregados na matriz polimérica.

A adição de quantidades diferentes de  $\text{Fe}_3\text{O}_4$  – talco sintético interferem diminuindo proporcionalmente a intensidade das bandas características da matriz polimérica PU base solvente e PUBA base água visto por DRX. PU base solvente observa-se que a carga ficou esfoliada/intercalada na matriz. Já para o PUBA/  $\text{Fe}_3\text{O}_4$  – talco sintético a carga ficou intercalada, podendo ser visto em duas regiões de  $2\theta=10^\circ$  e  $2\theta=35^\circ$  correspondente a  $9.4 \text{ \AA}$  e  $3.13 \text{ \AA}$ , característico do  $\text{Fe}_3\text{O}_4$  – talco sintético.

As massas molares dos nanocompósitos PU/  $\text{Fe}_3\text{O}_4$  – talco sintético com até 3,0% foram superiores quando comparado ao PU puro (base solvente).

As decomposições térmicas dos nanocompósitos de PU base solvente e PUBA base água, ocorreram em uma única etapa, exceto o PUBA puro. Porém foi possível observar pequenas variações nas temperaturas inicial e final das curvas de degradação, que evidência uma certa interação da carga com o polímero. Os valores de teor de resíduo obtidos nas análises térmicas aumentaram com o aumento da concentração da carga. Para teores de carga até 10% os valores calculados estão de acordo com o resíduo obtido. Para valores mais altos o valor incorporado no nanocompósito foi mais baixo que o calculado. Estes resultados



indicam que existe um valor máximo de carga que pode ser incorporado, em torno de 26%.

Os ensaios de tensão-deformação para o PU base solvente mostraram que o material com adição de até 10% de  $\text{Fe}_3\text{O}_4$  – talco sintético, não apresentou uma variação significativa na resistência a deformação mecânica do material passando de 0,5 MPa (PU puro) para 0,9 MPa (10% de  $\text{Fe}_3\text{O}_4$  – talco. Os PUBA base água mostraram que os nanocompósitos até 40 % de  $\text{Fe}_3\text{O}_4$  – talco sintético, apresentaram uma melhora no seu módulo de Young, passando de 29 Mpa (PUBA puro) para 70Mpa (PUBA 40 % de  $\text{Fe}_3\text{O}_4$  – talco sintético) indicando um aumento na resistência a deformação mecânica.

As análises magnéticas mostraram que os nanocompósitos PU/  $\text{Fe}_3\text{O}_4$  – talco sintético tiveram comportamento de material ferromagnético de 0 a 300K. Diferentemente, os nanocompósitos PUBA/  $\text{Fe}_3\text{O}_4$  – talco sintético evidenciaram um comportamento de material ferromagnético abaixo da temperatura de Curie (120K) e paramagnético para temperaturas superiores.

Os espectros de  $^{29}\text{Si}$  MAS-RMN dos nanocompósitos PUBA/0,5; 5 e 10%  $\text{Fe}_3\text{O}_4$ -talco sintético mostram um único pico na região entre -110 a -115ppm que corresponde a bandas  $Q_4$ , indicando que não existem OH livres na superfície. Estes resultados corroboram a interação da carga com a matriz polimérica. A interação carga/matriz também foi evidenciada pelas análises de AFM e DRX.

## 6. REFERÊNCIAS BIBLIOGRÁFICAS

AKBARI, B.; Bagheri, R. Deformation behavior and mechanical properties of polystyrene/organoclay/SEBS. **Mechanics of Materials**. v.103, p. 11 – 17, 2016.

BAIN & COMPANY. Potencial de Diversidade da Indústria Química Brasileira. Relatório 4 – Poliuretanos e seus Intermediários. **Bain & Company**. Nov. 2014.

BARBOZA, E.M.; Delpech, M. C.; Garcia, M. E. F.; Pimenta, F. D. Avaliação das Propriedades de Barreira de Membranas Obtidas a partir de Dispersões Aquosas à Base de Poliuretanos e Argila. **Polímeros**. v. 24, p. 94-100, 2014.

BEUGUEL, Q.; Ville, J.; Crepin-Leblond, J.; Mederic, P.; Aubry, T. Comparative study of the structural and rheological properties of PA6 and PA12 based synthetic talc nanocomposites. **Polymer**. v.62, p.109 – 117, 2015.

CHATTOPADHYAY, D. K.; Raju, K. V. S. N. Structural engineering of polyurethane coatings for high performance applications. **Progress in Polymer Science**. v. 32, p. 352-418, 2007.

COUTINHO, F. M. B.; Delpech, M. C. Poliuretanos como materiais de Revestimento de Superfície. **Polímeros: Ciência e Tecnologia**. v.9, p. 41 – 48, 1999.

COUTINHO, F. M. B.; Delpech, M. C.; Alves, L. A.; Gomes, A. S. Síntese e Caracterização de Poliuretanos em Dispersão Aquosa à Base de Polibutadieno Líquido Hidroxilado e Diferentes Diisocianatos. **Polímeros: Ciência e Tecnologia**. v.12, p. 248 – 254, 2002.

DIAS, Guilherme; Prado, Manoela; Carone, Carlos; Ligabue, Rosane; Dumas, Angela; Martin, François; Le Roux, Christophe; Micoud, Pierre; Einloft, Sandra. Synthetic silico-metallic mineral particles (SSMMP) as nanofillers: comparing the effect of different hydrothermal treatments on the PU/SSMMP nanocomposites properties. **Polymer Bulletin**. v.72, p. 2991–3006, 2015.

DIAS, Guilherme; Prado, Manoela; Carone, Carlos; Ligabue, Rosane; Dumas, Angela; Martin, François; Le Roux, Christophe; Micoud, Pierre; Einloft, Sandra. Comparing different synthetic Talc as Fillers for Polyurethane Nanocomposites. **Macromolecular Symposia**. v.367, p. 136–142, 2016.

DODGE, J. Polyurethanes and Polyureas. In: Rogers, M. E.; Long, T. E. (Ed.). Synthetic Methods in Step-Growth Polymers. United States of America: **John Wiley & Sons**, 2003. p. 197-258.

<sup>a</sup>DUMAS, A.; Gardes, E.; Le Roux, C.; Martin, F.; Micoud, P. Process for preparing a magnetic talcous composition and magnetic talcous composition. PCT Int. Pat. Appl. WO 2013093376 A1 June 27 2013 Fr. Pat. Appl. FR 2984872 A1 June 28 2013.

<sup>b</sup>DUMAS, A; Martin, F; Ferrage, E; Micoud, P.; Le Roux,C; Petit, S. Synthetic talc advances: coming closer to nature, added value, and industrial requirements. **Applied Clay Science**. v.23, p.8-18, 2013.

<sup>c</sup>DUMAS, F; Martin, Le Roux,C; E; Micoud, P; Petit, S; Ferrage, E; Brendlé, J; Grauby, M.; Greenhill-Hopper, M. Phyllosilicates synthesis: a way of accessing edges contributions in NMR and FTIR spectroscopies. Example of synthetic talc. **Physical Chemistry Minerals**. v.40, p.361-373, 2013.

<sup>d</sup>DUMAS, A; Claverie, M; Slostowski, C; Aubert, G; Careme, C; R; Le Roux,C; Petit, S; Martin, F; Aymonier, C. Fast-Geomimicking using chemistry in supercritical water. **Angewandte chemie**. v.55, p. 9868 -9871, 2016.

ENGELS, H.W; Pirkl, H.G, Albers, R., Albach, R.W.; Krause, J.; Hoffmann, A.; Casselmann, H.; Dormish, J. Polyurethanes: Versatile materials and sustainable

problem solvers for today's challenges. **Angew. Chem. Int. Ed.**, 52, p. 9422–9441, 2013.

GU, X.; Chen, G.; Zhao, M.; Watson S. S.; Nguyen, T.; Chin, J. W.; Martin, J. W. Critical role of particle/polymer interface in photostability of nano-filled polymeric coatings. **Journal of Coatings Technology and Research**. v. 9, p. 251 – 267, 2012.

MARINHO, N. P.; Nascimento, E. M.; Nisgoski, S.; Magalhães, W.L.E.; Neto, S.C.; AZEVEDO, E.C. Caracterização física e térmica de compósito de poliuretano derivado de óleo de mamona associado com partículas de bambu. **Polímeros**. v.23, p. 201 – 203, 2013.

MITTAL, Vicas. Polymer Layered Silicate Nanocomposites: A Review. **Materials**. v. 2, p.992-1057, 2009.

MONTICELLI, O.; Bocchini, S.; Gardella, L.; Cavallo, D.; Cebe, P.; Germelli, G. Impact of synthetic talc on PLLA electrospun fibers. **European Polymer Journal**. v. 49, p.2572 – 2583, 2013.

PAIVA, L.B; Morales, A.R; Guimarães,T.R. Propriedades mecânicas de Nanocompósitos de polipropileno e montmorilonita organofílica. **Polímeros**. v.16, p. 136 – 140, 2006.

PAIVA, L.B; Morales, A.R; Diaz, F.R.V. Argilas organofílicas: Características, metodologia de preparação, compostos de intercalação e técnicas de caracterização. **Cerâmica**. v.54, p. 213-226, 2008.

PFISTER, D. P; Xia, Y; Larock R. C.Recent Advances in Vegetable Oil-Based Polyurethanes. **ChemSusChem**. v. 4, p. 703-717, 2011.



RIAZ, T.; Ahmad, A.; Saleemi, S.; Adrees, M.; Jamshed, F.; Hai, A. M.; Jamil, T. Synthesis and characterization of polyurethane-cellulose acetate blend membrane for chromium (IV) Removal. **Carbohydrate Polymers**. v. 153, p. 582 – 591, 2016.

SARDON H.; Irusta L.; Aguirresarobe R.H.; Fernández-Berridi M.J. Polymer/silica nanohybrids by means of tetraethoxysilane sol-gel condensation onto waterborne polyurethane particles. **Progress in Organic Coatings**. v.77, p.1436-1442, 2014.

SINHA RAY, S; Okamoto, M. Polymer/layered silicate nanocomposites: a review from preparation to processing. **Progress Polymer Science**. v. 28, p.1539–1641, 2003.

SOARES, Rafael; Carone, Carlos; Einloft, Sandra; Ligabue, Rosane; Monteiro, Wesley. Synthesis and characterization of waterborne polyurethane/ZnO composites. **Polymer Bulletin**, v. 71, p. 829-838, 2014.

TIARKS, F.; Landfester, K.; Antonietti, M. One step preparation of polyurethane dispersions by miniemulsion polyaddition. **Journal Polymer Science: Part A**. v.39, p. 2520 – 2524, 2001.

THOMAS, P. S.; Thamas, Sabu; Bandyopadhyay, Sri; Wurm, Andreas; Schick, Christoph. Polystyrene/calcium phosphate nanocomposites: Dynamic mechanical and differential scanning calorimetric studies. **Composites Science and Technology**. v. 68, p. 3220-3229, 2008.

WANG, G.; Ma, G.; Hou, C.; Guan, T.; Ling, L.; Wang, B. Preparation and properties of waterborne polyurethane/nanosilica composites: A diol as extender with Triethoxysilane group. **Journal of Applied Polymer Science**. v.131, p. 40526:1-7, 2014.

WANG, W.; Guo, Y.; Otaigbe, J.U. Synthesis and characterization of novel biodegradable and biocompatible poly(ester-urethane) thin films prepared by homogeneous solution polymerization. **Polymer**. v. 49, p. 4393 – 4398, 2008.

YEH, J-M.; Yao, C-T.; Hsieh, C-F.; Lin, L-H.; Chen, P-L.; Wu, J-C.; Yang, H-C.; Wu, C-P. Preparation, characterization and electrochemical corrosion studies on environmentally friendly waterborne polyurethane/Na<sup>+</sup> - MMT clay nanocomposite coatings. **European Polymer Journal**. v.11, p. 3046 – 3056, 2008.

YOUSFI M.; Livia S.; Dumas A.; Le Rouxd C.; Crépin-Leblond J.; Greenhill-Hooper M.; Duchet-Rumeau J. Use of new synthetic talc as reinforcing nanofillers for polypropylene and polyamide 6 systems: thermal and mechanical properties. **Journal of Colloid and Interface Science**, v.403, p. 29-42, 2013.

ZHANG, S.; Li, Y.; Peng, L.; Li, Q.; Chen, S.; Hou, K .Synthesis and characterization of novel waterborne polyurethane nanocomposites with magnetic and electrical properties. **Composites Part A**. v.55, p.94 – 101, 2013

ZHANG, X.; Xu, R; Wu, Zenggang; Zhou, Chixing. The synthesis and characterization of polyurethane/clay nanocomposites. **Polymer International**. v.52, p.790–794, 2003.

ZHOU, X.; Li, Y.; Fang, C.; Li, S.; Cheng, Y.; Lei, W.; Meng, X. Recent advances in Synthesis of Waterborne Polyurethane and their application in Water-Based ink: A Review. **Journal of Materials Science & Technology** v.31, p. 708-722, 2015.

ZILG, Carsten; Thomann, Ralf; Mülhaupt, Rolf; Finter, Jürgen. Polyurethane nanocomposites containing laminated anisotropic nanoparticles derived from organophilic layered silicates. **Advanced Materials**. v.11, p.49–52, 1999.